Central Lancashire Online Knowledge (CLoK)

Title	Taxonomy of protoplanetary discs observed with ALMA
Type	Article
URL	https://clok.uclan.ac.uk/id/eprint/40641/
DOI	https://doi.org/10.1093/mnras/stac152
Date	2022
Citation	Parker, Raeesa, Ward-Thompson, Derek and Kirk, Jason Matthew (2022) Taxonomy of protoplanetary discs observed with ALMA. Monthly Notices of the Royal Astronomical Society, 511 (2). pp. 2453-2490. ISSN 0035-8711
Creators	Parker, Raeesa, Ward-Thompson, Derek and Kirk, Jason Matthew

It is advisable to refer to the publisher's version if you intend to cite from the work.
https://doi.org/10.1093/mnras/stac152

For information about Research at UCLan please go to http://www.uclan.ac.uk/research/

Taxonomy of protoplanetary discs observed with ALMA

Raeesa Parker,★ Derek Ward-Thompson ® and Jason Kirk
Jeremiah Horrocks Institute, University of Central Lancashire, Preston PR1 2HE, UK

ABSTRACT

Many observations of protoplanetary discs studied with ALMA have revealed the complex substructure present in the discs. Rings and gaps in the dust continuum are now a common sight in many discs; however, their origins still remain unknown. We look at all protoplanetary disc images taken with ALMA from cycles 0 to 5 and find that 56 discs show clear substructure. We further study the 56 discs and classify the morphology seen according to four categories: Rim, Ring, Horseshoe, and Spiral. We calculate the ages of the host stars using stellar isochrones and investigate the relation between the morphology of the substructure seen in the protoplanetary discs and the age of the host stars. We find that there is no clear evolutionary sequence in the protoplanetary discs as the stars increase in age, although there is a slight tendency for spirals to appear in younger systems and horseshoes to be seen in more evolved systems. We also show that majority of the images of protoplanetary discs made by ALMA may not have had a sufficiently high resolution or sensitivity to resolve substructure in the disc. We show that angular resolution is important in detecting substructure within protoplanetary discs, with sensitivity distinguishing between the different types of substructure. We compare the substructure seen in protoplanetary discs at sub-mm to those seen in scattered light. We find that cavities are a common substructure seen in discs at both sub-mm wavelengths and in scattered light.

Key words: protoplanetary discs – stars: pre-main-sequence – stars: protostars.

1 INTRODUCTION

ALMA observations of protoplanetary discs have revealed a multitude of different complex substructures. These include horseshoe-like structures (Casassus et al. 2013), spiral arms (Pérez et al. 2016), inner cavities (van der Marel et al. 2015), and discs featuring bright, concentric dust rings (ALMA Partnership et al. 2015). There has also been an increase in the amount of theoretical work being undertaken in order to explain the origin of these substructures (Dong, Zhu & Whitney 2015a; Takahashi & Inutsuka 2016; Gonzalez, Laibe & Maddison 2017).

A common substructure seen in the protoplanetary discs observed with ALMA is a cavity of some sort. This could be in the form of the inner cavities seen in transition discs or the depletion of dust and gas in different regions of a protoplanetary disc. These cavities may be caused by photoevaporation (Hollenbach et al. 1994; Hardy et al. 2015), planet–disc interactions (Lin & Papaloizou 1979; Kley & Nelson 2012; Baruteau et al. 2014; Dong et al. 2015a), or gravitational instabilities (Lorén-Aguilar & Bate 2016; Takahashi & Inutsuka 2016). Comparisons between cavities seen in the dust and the gas may be used to determine if planets in the disc are responsible for the depletions (van der Marel et al. 2016a; Boehler et al. 2017, 2018; Dong et al. 2017; van der Marel, Williams & Bruderer 2018). Scattered light observations comparing the sizes of small and large grains may also be used to determine if planets are the origin of the inner cavities (de Juan Ovelar et al. 2013; Villenave et al. 2019).

Dead zones may also be responsible for the inner cavities seen in transition discs (Pinilla et al. 2016).

Spiral density waves can also be seen in some protoplanetary discs at submillimetre wavelengths (Pérez et al. 2016). These structures are thought to be excited by either planet–disc interactions (Dong et al. 2015a; Zhu et al. 2015), gravitational instabilities (Dong et al. 2015b), or a combination of both (Pohl et al. 2015).

The interaction of a planet with a disc is commonly thought to be the origin mechanism for forming ring-like structures seen in protoplanetary discs. Fedele et al. (2018) were able to show that multiple gaps in a disc may be formed by single or multiple planets. Additional methods to explain the formation of dust rings in protoplanetary discs have also been theorized. Fast pebble growth near condensation fronts (Zhang, Blake & Bergin 2015), secular gravitational instability (Takahashi & Inutsuka 2016), and aggregate sintering (Okuzumi et al. 2016) are just some of the mechanisms proposed.

Submillimetre observations of the discs surrounding HD142527 and IRS48 have revealed azimuthal dust concentrations in the disc (Casassus et al. 2013; van der Marel et al. 2013). It is thought that these pile-ups of large dust grains are formed due to a pressure maximum at the edge of a gap in the disc. This pressure maximum can develop in a number of ways including the gas disc becoming unstable due to the Rossby Wave Instability (Baruteau & Zhu 2016) or due to a binary companion (Ragusa et al. 2017). Embedded young protoplanets could also cause a pressure maximum to form. These planets are able to carve out a gap in the dust and gas components of a protoplanetary disc (Paardekooper & Mellema 2006), developing the pressure maximum, and large dust grains, which would otherwise radially migrate inwards, are trapped.

★ E-mail: rparker4@uclan.ac.uk

Substructures have been observed in the protoplanetary discs surrounding stars with a wide range of different stellar parameters. Previous works have mostly focused on individual objects, or surveys have been conducted on specific regions (targeting both uniform and structured discs). More recently, van der Marel et al. (2019) focused solely on stars surrounded by protoplanetary discs featuring rings, while the Disk Substructures at High Angular Resolution Project (DSHARP) looked at 20 nearby discs to characterize the range of substructures seen in the dust spatial distribution (Andrews et al. 2018b). Long et al. (2018) have also recently focused on discs in Taurus featuring substructure.

In this work, we study the different substructures found in 56 protoplanetary discs observed with ALMA. There are a range of substructures seen in the discs and the stars studied cover a wide parameter range of both intermediate- and low-mass stars. Our 56 discs were chosen from the complete sample of discs observed by ALMA thus far. This is discussed further in Section 2, where we also present our sample. We discuss any biases in our sample in Section 3. This is followed by Section 6.1, where the properties of our sample are both derived here and obtained from literature. We present a new morphology scheme to classify the substructure seen in protoplanetary discs in Section 5. The main results of this paper are then presented in Section 6 and discussed in Section 7. We finally conclude in Section 8.

2 DATA

The ALMA archive has been searched to find protoplanetary discs that feature different morphological structures seen in the millimetre dust continuum. The continuum product images of 793 targets from cycles 0 to 5 were looked at. The full sample of images we have looked at is shown in Table A1 in Appendix A. The project code for each observation can also be found in the table. The images obtained from the archive are of 793 unique systems, and feature both young pre-stellar discs and older debris discs.

Protoplanetary discs that are spatially resolved and show clear substructure in millimetre dust were chosen. We confirm that the discs are resolved by comparing the beam size of the observations to the disc size. In order to be classified as having substructure, the discs had to feature either a cavity or gap of some sort or a pile-up of dust grains. We are interested in asymmetric substructure that may be seen in the dust continuum of the mm-dust disc. We have chosen to exclude debris discs from our sample, including the well-studied discs surrounding HR4796A, HD107146, and HD181327. This was done as they are much older than the discs in our sample and the ALMA Archive is much less complete for these older discs (see Section 6.2). Similarly, we have excluded young, embedded discs such as Elias 2-24 and HL Tau as they may still be surrounded by an envelope. If no previous observations have found an object to be embedded, we discard it if its age is determined to be less than 0.5 Myr. These young objects are discarded as the ALMA Archive is much less complete for these discs. We have only obtained the final, calibrated continuum products of each observation and any images that have undergone further processing will be discussed in Section 5.1 below.

An absence of substructure may be seen in many of the discs due to a number of reasons. First, many objects observed by ALMA, unless explicitly targetted, have only been observed once. The detection of substructure can depend upon the observational waveband, resolution, and sensitivity. Therefore, many discs may feature substructure, but this has not been detected due to the incorrect

conditions under which the observations were conducted. This is discussed further in Section 3.

Thus, we have a large sample of protoplanetary discs observed by ALMA, during cycles 0 to 5, that currently shows resolvable substructure. We acknowledge that our sample is not complete with regards to all protoplanetary discs featuring substructure, as some discs in the archive may have substructure that remains unresolved. It is, however, a large enough sample from which conclusions can be drawn.

The sample that we are left with consists of 56 protoplanetary discs across the first six cycles of ALMA observations. The observations for each disc were conducted at either Band 6 or Band 7 (1.3 or 0.8 mm, respectively) with three exceptions. Observations of 2MASS J16152023−3255051 (hereafter J16152023) and HD36112 were conducted at Band 9 (0.4 mm), while observations of HD163296 were conducted at Band 8 (0.6 mm). The complete sample of discs is shown in Table 1.

The continuum product files available on the ALMA Archive are often of a lower quality than the final published data. We compare the product files to the published data on each source and find that the quality of the data, with regards to the final rms and recovered total flux, improves by less than an order of magnitude. No additional substructure is revealed between the archive product files and the published data. Therefore, additional processing has not been done in order to improve the quality of the product files as this is not needed for the analysis conducted in this work.

The archival ALMA observations were taken at a range of resolutions; all sub-arcsecond. We further discuss the detectability of substructure in Section 3.1. The smallest angular scale we can resolve in our sample is in the DM Tau disc, with a resolution of 0.02 arcsec (2.9 au at 145 pc), while we can only resolve down to 0.77 arcsec (123.6 pc at 160 pc) in the disc of 2MASS J16230923−2417047. Also, the discs are located at a range of distances and the observations were conducted with varying sensitivities. As a result, any statement on the detectability of substructure based on flux would be meaningless.

3 OBSERVATIONAL BIASES OF ALMA

The analysis conducted in this work is subjected to several observational and selection biases. We discuss this further in the sections below.

3.1 Angular resolution

The angular resolutions of the discs studied in this work are shown in Table 2. These discs were observed with a higher resolution than the majority of the ALMA discs (see Table A1 for the angular resolution of all the ALMA protoplanetary discs observed during cycles 0–5). We have plotted a histogram of the angular resolutions with which the individual protoplanetary discs in our sample were observed (see Table A1). This is shown in Fig. 1.

We have looked at 793 protoplanetary discs, of which we have identified 56 that show substructure. As discussed above, we have omitted known young, embedded discs as well as debris discs. The majority of the discs we have classified here (46/56 ≃ 80 per cent) were observed with a resolution higher than 0.22 arcsec. This limit is indicated by the red dashed line on Fig. 1. From the complete sample of ALMA discs looked at, 171 discs were observed with a resolution of 0.22 arcsec or better. Therefore, ∼27 per cent of the discs observed with ALMA with a resolution 0.22 arcsec or greater have resolvable substructure.

Table 1. Literature properties of the sample studied in this work. The references correspond to the luminosity and temperature, respectively. All distances have been obtained from *Gaia* DR2 (Gaia Collaboration 2018) with the exceptions of 2MASS J05052286+2531312 and RY Tau which were obtained from Kenyon, Gómez & Whitney (2008) and (Garufi et al. 2019), respectively (see the text for details). Stellar masses are calculated in Section 4.1.

ID #	Name	Luminosity ($L_\odot$)	Effective temperature (K)	Distance (pc)	Star-forming region	Reference
1	AA Tau	0.8 ± 0.3	4000 ± 400	137.2 ± 2.4	Taurus	(1)(2)
2	AB Auriga	89.6 ± 35.7	9800 ± 980	162.9 ± 1.5	Taurus	(3)(4)
3	AS 209	1.4 ± 0.7	4300 ± 300	121.0 ± 0.9	Ophiuchus	(5)
4	CI Tau	0.8 ± 0.3	4100 ± 190	158.7 ± 1.2	Taurus	(5)
5	CQ Tau	10.0 ± 7.6	6900 ± 640	163.1 ± 2.2	Taurus	(5)
6	CS Cha	1.9 ± 0.2	4800 ± 480	176.0 ± 2.0	Chamaeleon	(6)
7	DM Tau	0.2 ± 0.0	3700 ± 170	145.1 ± 1.1	Taurus	(5)
8	DoAr25	1.0 ± 0.4	4300 ± 300	138.5 ± 1.5	Upper Scorpius	(5)
9	DoAr44	1.8 ± 0.8	4800 ± 220	145.9 ± 1.0	Ophiuchus	(5)
10	DS Tau	0.3 ± 0.1	3800 ± 380	159.0 ± 1.0	Taurus	(7)
11	Elias 2-27	0.9 ± 0.3	3700 ± 370	118.5 ± 13.1	Upper Scorpius	(8)
12	EM* SR 21A	12.9 ± 5.9	5800 ± 400	138.4 ± 1.1	Ophiuchus	(5)
13	EM* SR 24S	3.8 ± 1.8	5000 ± 350	114.4 ± 4.5	Ophiuchus	(5)
14	EM* SR 4	1.2 ± 0.5	5100 ± 190	134.6 ± 0.8	Upper Scorpius	(5)
15	GG Tau	1.8 ± 2.0	4000 ± 400	150.3 ± 24.2	Taurus	(9)(10)
16	GM Auriga	1.6 ± 0.4	4800 ± 220	159.6 ± 2.1	Taurus	(5)
17	GO Tau	0.7 ± 0.1	3800 ± 110	144.0 ± 3.0	Taurus	(5)
18	GW Lup	0.3 ± 0.2	3600 ± 170	155.9 ± 1.3	Lupus	(5)
19	HD 100453	6.2 ± 2.6	7300 ± 250	104.2 ± 0.4	Lower Centaurus Crux	(11)
20	HD 100546	36.5 ± 7.2	10400 ± 600	110.0 ± 0.6	Chamaeleon	(12)
21	HD 142527	20.6 ± 8.2	6600 ± 100	157.3 ± 1.2	Lupus	(13)
22	HD 142666	9.5 ± 6.5	7500 ± 250	148.3 ± 1.2	Upper Scorpius	(11)
23	HD 143006	3.8 ± 1.3	5600 ± 260	166.1 ± 4.0	Upper Scorpius	(14)
24	HD 163296	17.0 ± 11.7	9300 ± 650	101.5 ± 1.2	Upper Scorpius	(5)
25	HD 169142	9.5 ± 2.0	8400 ± 820	114.0 ± 0.8	Lupus	(15)
26	HD 34282	10.7 ± 8.9	9500 ± 250	311.6 ± 4.6	Orion	(11)
27	HD 36112	9.8 ± 4.5	7600 ± 500	160.2 ± 1.7	Taurus	(5)
28	HD 97048	42.9 ± 12.0	10000 ± 1000	184.8 ± 1.3	Chamaeleon	(12)
29	IM Lup	2.6 ± 1.1	4400 ± 200	158.5 ± 1.3	Lupus	(5)
30	IP Tau	0.4 ± 0.2	3900 ± 90	130.0 ± 2.0	Taurus	(5)
31	LkCa15	1.1 ± 0.4	4400 ± 300	158.9 ± 1.2	Taurus	(5)
32	2MASS J05052286+2531312	0.1 ± 0.1	3600 ± 360	140.0 ± 14.0	Taurus	(6)
33	2MASS J16042165−2130284	0.6 ± 0.2	4900 ± 340	150.1 ± 1.3	Upper Scorpius	(5)
34	2MASS J16152023−3255051	0.9 ± 0.4	4400 ± 300	157.7 ± 0.9	Lupus	(5)
35	2MASS J16230923−2417047	1.0 ± 0.1	6000 ± 600	160.5 ± 1.4	Ophiuchus	(5)
36	MWC 480	17.4 ± 2.0	8500 ± 850	162.0 ± 2.0	Taurus	(7)
37	PDS 70	0.8 ± 0.7	4400 ± 440	113.4 ± 0.5	Lupus	(16)
38	PDS 99	1.1 ± 0.1	4200 ± 420	155.0 ± 2.0	Corona Australis SFR	(6)
39	RU Lup	1.5 ± 0.7	4100 ± 190	159.6 ± 1.7	Lupus	(5)
40	RXJ1842.9-3532	0.8 ± 0.1	4800 ± 480	154.0 ± 1.0	Corona Australis SFR	(6)
41	RXJ1852.3-3700	0.6 ± 0.1	4800 ± 480	146.0 ± 1.0	Corona Australis SFR	(6)
42	RY Lup	1.9 ± 0.9	4900 ± 230	159.1 ± 1.8	Lupus	(5)
43	RY Tau	6.0 ± 4.0	5100 ± 510	443.1 ± 47.0	Taurus	(17)
44	SAO 206462	7.2 ± 3.3	6600 ± 460	178.9 ± 1.2	Lupus	(5)
45	SZ 111	0.2 ± 0.1	3700 ± 170	158.3 ± 0.8	Lupus	(5)
46	SZ 129	0.4 ± 0.2	4100 ± 190	161.7 ± 1.3	Lupus	(5)
47	SZ 91	0.2 ± 0.1	3700 ± 170	159.1 ± 1.6	Lupus	(5)
48	T Cha	1.3 ± 0.1	5600 ± 560	110.0 ± 1.0	Chamaeleon	(6)
49	TW Hya	0.3 ± 0.2	4100 ± 280	60.1 ± 0.2	TW Hydrae Association	(5)
50	UX Tau	1.9 ± 0.8	4900 ± 230	139.4 ± 1.9	Taurus	(5)
51	V1094 Sco	1.7 ± 0.2	4200 ± 420	150.0 ± 1.0	Upper Scorpius	(18)
52	V1247 Ori	14.3 ± 2.1	7300 ± 780	398.4 ± 10.1	Orion	(19)
53	V4046 Sgr	0.5 ± 0.1	4100 ± 410	72.0 ± 1.0	Beta Pic	(6)
54	V892 Tau	38.0 ± 18.0	12000 ± 1200	117.4 ± 1.6	Taurus	(20)(21)
55	WaOph6	2.9 ± 1.3	4200 ± 290	123.9 ± 0.7	Ophiuchus	(5)
56	WSB 60	0.2 ± 0.1	3400 ± 100	137.0 ± 4.0	Ophiuchus	(5)

Note. The distance measurement for RY Tau has been obtained from Garufi et al. (2019). See the text for further details. References: (1) Grosso et al. (2007), (2) Schneider et al. (2015), (3) Monnier et al. (2006), (4) Isella, Testi & Natta (2006), (5) Andrews et al. (2018a), (6) Francis & van der Marel (2020), (7) Long et al. (2018), (8) Isella, Carpenter & Sargent (2009), (9) White et al. (1999), (10) Dutrey et al. (2016), (11) Fairlamb et al. (2015), (12) van den Ancker et al. (1997), (13) Mendigutía et al. (2014), (14) Andrews et al. (2018b), (15) Fedele et al. (2017), (16) Metchev, Hillenbrand & Meyer (2004), (17) Bertout, Siess & Cabrit (2007), (18) van Terwisga et al. (2018), (19) Kraus et al. (2013), (20) Berrilli et al. (1992), (21) Manoj et al. (2006).

Table 2. The values derived in this work. Columns 3 and 4 show the stellar ages and masses derived using the stellar tracks from Siess et al. (2000) and Baraffe et al. (2015). Column 5 shows the classification assigned to the protoplanetary disc. The radius of the disc that contains 68 per cent of the total disc flux is shown in Column 6. Columns 7 and 8 show the spatial resolution and continuum sensitivity for each ALMA observation, while column 9 shows the ALMA project code.

ID #	Name	Age (Myr)	Stellar mass ($M_\odot$)	Classification	$R_{68 \text{ per cent } F}$ (au)	Spatial resolution (arcsec)	Sensitivity (μJy beam^{-1})	ALMA Project code
1	AA Tau	1.5 ± 0.8	0.8 ± 0.2	Rim	55 ± 5	0.19	58	2015.1.01017.S
2	AB Auriga	3.0 ± 0.5	2.7 ± 0.6	Horseshoe	163 ± 8	0.14	51	2012.1.00303.S
3	AS 209	1.5 ± 0.9	0.9 ± 0.2	Rings	97 ± 4	0.15	41	2015.1.00486.S
4	CI Tau	2.0 ± 1.0	0.8 ± 0.2	Rings	127 ± 5	0.07	52	2017.A.00014.S
5	CQ Tau	10.0 ± 4.9	1.7 ± 0.4	Rim	60 ± 8	0.21	31	2013.1.00498.S
6	CS Cha	4.0 ± 3.0	1.4 ± 0.2	Rim	46 ± 3	0.03	33	2017.1.00969.S
7	DM Tau	5.0 ± 3.0	0.6 ± 0.2	Rim	29 ± 1	0.02	17	2017.1.01460.S
8	DoAr25	2.5 ± 1.0	1.0 ± 0.2	Rings	97 ± 5	0.03	18	2016.1.00484.L
9	DoAr44	3.0 ± 1.0	1.4 ± 0.3	Rim	54 ± 7	0.23	64	2012.1.00158.S
10	DS Tau	4.0 ± 1.0	0.7 ± 0.1	Rim	59 ± 2	0.09	44	2016.1.01164.S
11	Elias 2-27	0.5 ± 0.1	0.5 ± 0.1	Spirals	59 ± 7	0.2	39	2013.1.00498.S
12	EM∗ SR 21A	4.0 ± 1.2	2.2 ± 0.4	Rim	62 ± 10	0.23	64	2012.1.00158.S
13	EM∗ SR 24S	4.0 ± 1.7	1.9 ± 0.4	Rim	26 ± 1	0.14	23	2013.1.00091.S
14	EM∗ SR 4	12.0 ± 6.0	1.2 ± 0.2	Rim	24 ± 1	0.02	15	2016.1.00484.L
15	GG Tau	0.9 ± 0.2	0.6 ± 0.1	Rim	225 ± 36	0.14	93	2013.1.00105.S
16	GM Auriga	8.0 ± 5.0	1.4 ± 0.3	Rings	61 ± 4	0.02	15	2017.1.01151.S
17	GO Tau	1.0 ± 0.5	0.5 ± 0.1	Rings	96 ± 10	0.1	45	2016.1.01164.S
18	GW Lup	2.0 ± 1.5	0.4 ± 0.1	Rings	47 ± 2	0.02	18	2016.1.00484.L
19	HD 100453	13.0 ± 3.1	1.7 ± 0.3	Rim	31 ± 1	0.03	25	2017.1.01424.S
20	HD 100546	20.0 ± 4.0	2.5 ± 0.5	Rim	29 ± 2	0.03	57	2015.1.00806.S
21	HD 142527	6.0 ± 1.0	1.9 ± 0.4	Horseshoe	186 ± 10	0.14	60	2012.1.00631.S
22	HD 142666	10.3 ± 8.5	1.7 ± 0.3	Rings	37 ± 1	0.2	34	2013.1.00498.S.
23	HD 143006	10.0 ± 2.0	1.5 ± 0.3	Rings	68 ± 8	0.4	62	2015.1.00964.S
24	HD 163296	4.0 ± 1.0	2.1 ± 0.4	Rings	56 ± 11	0.17	138	2015.1.00847.S
25	HD 169142	8.0 ± 0.5	1.9 ± 0.4	Rings	52 ± 3	0.13	37	2012.1.00799.S
26	HD 34282	7.0 ± 2.0	2.1 ± 0.4	Horseshoe	187 ± 14	0.14	87	2013.1.00658.S
27	HD 36112	10.0 ± 5.0	1.9 ± 0.5	Rim	80 ± 4	0.03	87	2017.1.00492.S
28	HD 97048	5.4 ± 0.4	2.5 ± 0.5	Rim	139 ± 43	0.03	31	2016.1.00826.S
29	IM Lup	0.8 ± 0.2	1.0 ± 0.2	Spirals	87 ± 4	0.39	79	2013.1.00226.S
30	IP Tau	3.0 ± 1.5	0.6 ± 0.1	Rim	26 ± 2	0.09	75	2016.1.01164.S
31	LkCa15	3.0 ± 2.0	1.1 ± 0.2	Rim	79 ± 5	0.17	68	2012.1.00870.S
32	2MASS J05052286+2531312	12.0 ± 10.0	0.6 ± 0.1	Rim	42 ± 4	0.47	45	2016.1.01164.S
33	2MASS J16042165−2130284	20.0 ± 8.0	1.0 ± 0.2	Rim	98 ± 5	0.16	46	2015.1.00888.S
34	2MASS J16152023−3255051	6.0 ± 4.0	1.0 ± 0.2	Spirals	63 ± 3	0.22	925	2011.0.00724.S
35	2MASS J16230923−2417047	30.0 ± 6.0	1.1 ± 0.2	Rim	32 ± 5	0.13	261	2013.1.00157.S
36	MWC 480	9.0 ± 1.0	2.2 ± 0.4	Rim	50 ± 4	0.11	45	2016.1.01164.S
37	PDS 70	5.0 ± 4.0	1.1 ± 0.2	Rim	68 ± 2	0.08	30	2017.A.00006.S
38	PDS 99	2.0 ± 1.0	0.8 ± 0.2	Rim	62 ± 5	0.24	24	2015.1.01301.S
39	RU Lup	0.6 ± 0.1	0.7 ± 0.1	Rings	37 ± 2	0.02	16	2016.1.00484.L
40	RXJ1842.9-3532	13.0 ± 4.0	1.0 ± 0.2	Rim	71 ± 3	0.14	48	2015.1.01083.S
41	RXJ1852.3-3700	17.0 ± 4.0	1.1 ± 0.2	Rim	47 ± 2	0.14	60	2015.1.01083.S
42	RY Lup	4.0 ± 2.0	1.4 ± 0.3	Rim	72 ± 4	0.14	27	2017.1.00449.S
43	RY Tau	3.0 ± 1.0	2.2 ± 0.5	Rim	133 ± 14	0.02	44	2017.1.01460.S
44	SAO 206462	14.0 ± 5.5	1.5 ± 0.3	Horseshoe	120 ± 21	0.35	108	2012.1.00870.S
45	SZ 111	5.0 ± 3.0	0.5 ± 0.1	Rim	52 ± 8	0.28	236	2013.1.00220.S
46	SZ 129	6.0 ± 6.0	0.3 ± 0.1	Rings	36 ± 1	0.02	15	2016.1.00484.L
47	SZ 91	5.0 ± 3.0	0.6 ± 0.1	Rim	80 ± 7	0.13	69	2013.1.00663.S
48	T Cha	20.0 ± 4.0	1.2 ± 0.2	Rim	44 ± 2	0.13	90	2012.1.00182.S
49	TW Hya	10.0 ± 5.0	0.8 ± 0.2	Rings	36 ± 0	0.04	11	2017.1.00520.S
50	UX Tau	6.5 ± 3.5	1.5 ± 0.3	Rim	42 ± 4	0.14	93	2013.1.00105.S
51	V1094 Sco	0.8 ± 0.3	0.8 ± 0.2	Rings	135 ± 5	0.24	61	2016.1.01239.S
52	V1247 Ori	9.0 ± 0.9	1.8 ± 0.3	Rings	131 ± 17	0.01	42	2015.1.00986.S
53	V4046 Sgr	4.0 ± 2.0	0.8 ± 0.2	Rings	37 ± 3	0.54	27	2017.1.01167.S
54	V892 Tau	10.0 ± 0.0	2.7 ± 0.5	Rim	35 ± 2	0.14	51	2013.1.00498.S
55	WaOph6	0.5 ± 0.1	0.8 ± 0.2	Spirals	50 ± 1	0.03	25	2016.1.00484.L
56	WSB 60	2.0 ± 1.0	0.3 ± 0.1	Rim	36 ± 5	0.1	36	2016.1.01042.S
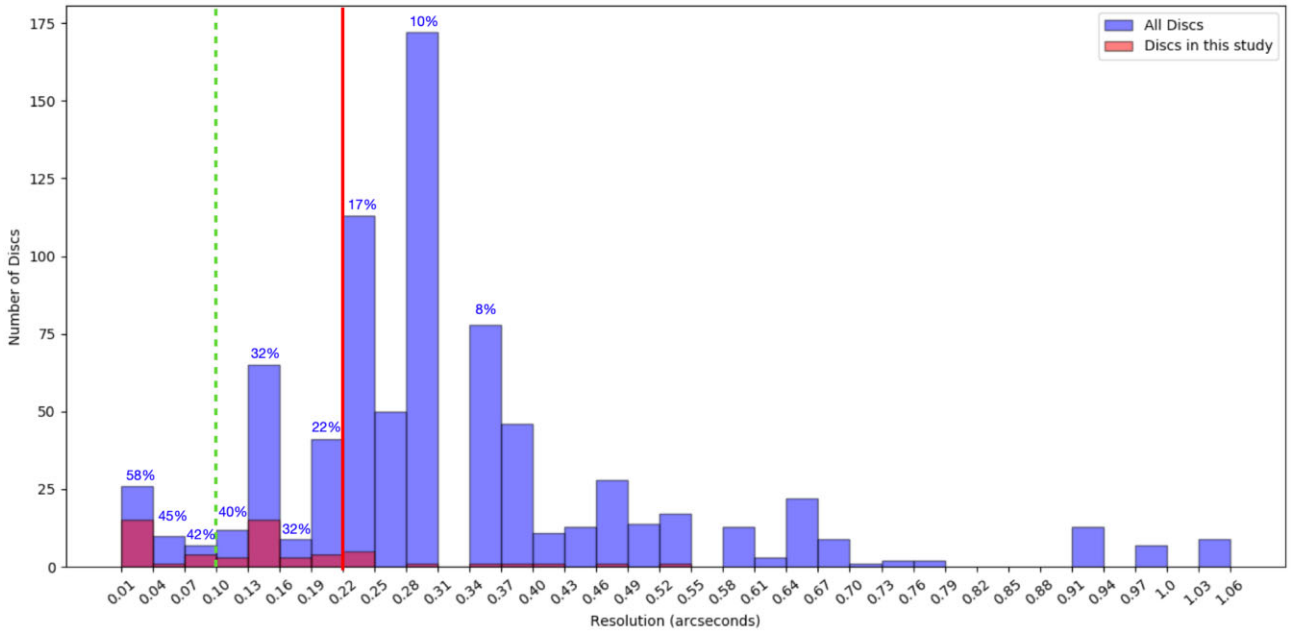
Figure 1. The resolutions of the entire sample of protoplanetary discs we have looked at in the ALMA Archive. Details of the discs can be found in Table A1. The discs have been binned with resolutions of 0.03 arcsec. The red, solid line indicates the resolution limit below which the majority of the discs featuring substructure were observed at (46/56 ≃ 80 per cent). The green, dashed line indicates a resolution limit of 0.1 arcsec, below which is considered 'high resolution' with ALMA. We have highlighted, in pink, the discs identified as containing substructure and studied in this work. The percentages above each bin indicate the fraction of discs showing substructure at each resolution and greater.

Cieza et al. (2019) conduct a survey of the discs within Ophiuchus using ALMA at a resolution of 0.2 arcsec. Observations were able to resolve 60 protoplanetary discs, of which 12 showed substructure (eight clear, and four probable detections). This is 20 per cent of their resolved discs, which agrees with the finding here that ∼27 per cent of discs show substructure when observed at a resolution limit of 0.22 arcsec.

A resolution of 0.22 arcsec is still considered relatively moderate with ALMA. Studies explicitly targeting transition discs and discs with known substructure aim for resolutions of ≈0.1 arcsec or better. A total of 52 protoplanetary discs observed with ALMA at a resolution of 0.1 arcsec or better have been looked at in this work. This limit is shown as the green line on the histogram (Fig. 1). Of these 52 discs, 22 have been shown to have substructure and have been classified here. This is approximately 42 per cent of the discs.

Long et al. (2019) studied 32 protoplanetary discs in Taurus with ALMA using a resolution of ≈0.12 arcsec. They found that just under half of the discs showed dust gaps and rings. In agreement with the 42 per cent we have found here for the same resolution limit. The DSHARP project, however, has found that all the discs they observe at a very high resolution of ≈0.035 arcsec feature substructure. It should be noted, however, that the DSHARP project was a targeted survey and only looked at discs that had previously showed substructure. For a resolution limit of ≲0.04 arcsec, we find that the fraction of discs showing substructure increases to 60 per cent.

3.2 Sensitivity

The continuum sensitivities of the discs studied in this work are shown in Table 2, with Table A1 showing the sensitivity of all the ALMA protoplanetary discs observed during cycles 0–5. A histogram of the sensitivities used to observe the discs in this work has been plotted in Fig. 2.

The majority of our discs (53/56 ≃85 per cent) that show substructure were observed with a sensitivity greater than 140 μJy beam^{-1}. A second histogram showing the discs with sensitivities greater than this can be seen in Fig. 2. From the complete sample of ALMA discs looked at, 308 discs were observed with a sensitivity of 140 μJy beam^{-1} or greater. Therefore, substructure can be seen in ∼17 per cent of the discs observed with ALMA when observed with a sensitivity of 140 μJy beam^{-1} or greater. This value agrees with the work of Cieza et al. (2019), who find that 20 per cent of their discs show substructure when observed with a sensitivity of 150 μJy beam^{-1}.

The 32 protoplanetary discs observed by Long et al. (2019) had an average sensitivity of 50 μJy beam^{-1}. We have indicated this sensitivity limit on Fig. 2 with a pink dashed line. The number of discs showing substructure below this limit is 31; this is ∼25 per cent out of a total of 126 discs observed by ALMA. Long et al. (2019) were able to detect substructure in just under half of their discs.

Similar to the effect of increasing the resolution, increasing the sensitivity limit to 20 μJy beam^{-1} results in 8 out of 23 discs featuring substructure (∼35 per cent). This limit is indicated by the blue, solid line on Fig. 2. At an average sensitivity limit of 17 μJy beam^{-1}, the DSHARP project was able to detect substructure in all the discs they observed (Andrews et al. 2018b).

3.3 Selection biases

We have studied 56 protoplanetary discs that cover a wide parameter space. Both low- and intermediate-mass stars have been looked at, with a wide range of ages, temperatures, and luminosities. A plot of the relation between the stellar masses of our sample and their
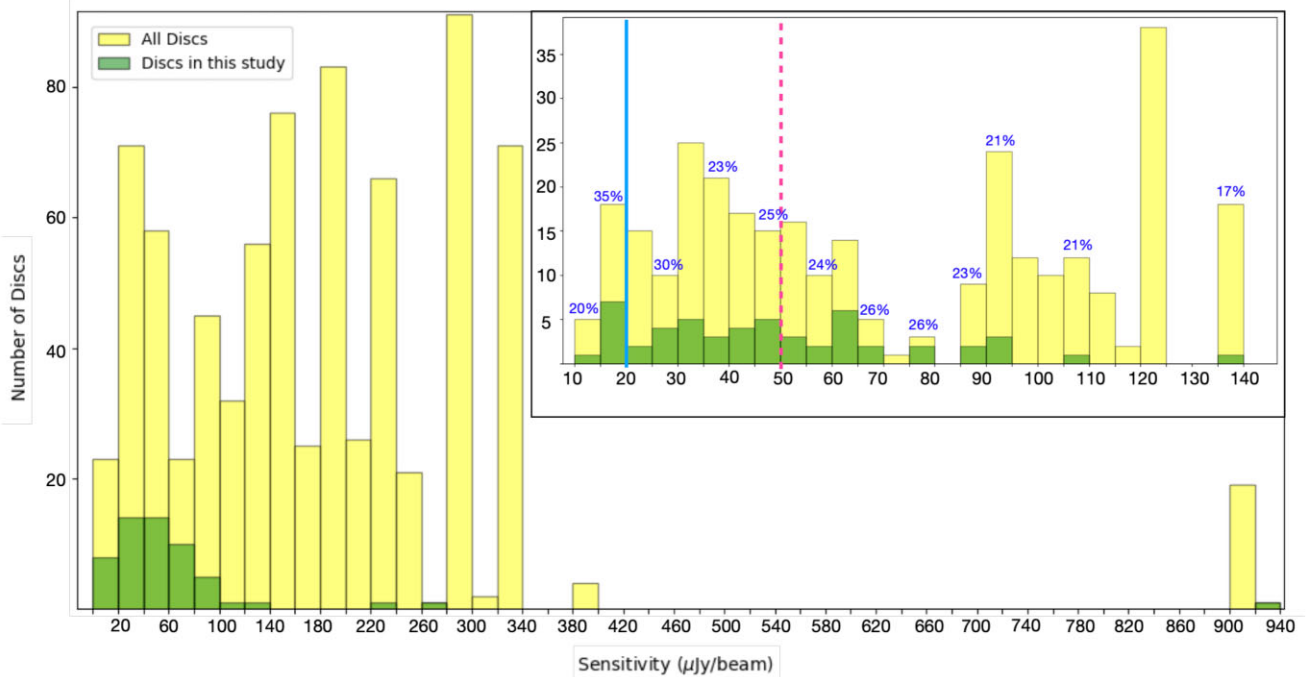
Figure 2. The continuum sensitivities of the entire sample of protoplanetary discs we have looked at in the ALMA Archive. Details of the discs can be found in Table A1. The discs have been binned with sensitivities of 20 μJy beam^{-1}. The graph insert shows a zoomed-in version of the original figure binned to 10 μJy beam^{-1}. The pink dashed, and blue solid lines indicate the mean sensitivities of the discs observed by Long et al. (2019) and Andrews et al. (2018b), respectively. The percentages above each bin indicate the fraction of discs showing substructure at each sensitivity and greater.

corresponding age has been made in order to determine if there are any observational biases in our sample (see Fig. 3).

There is a lack of old low-mass stars that show protoplanetary substructure as well as significantly fewer old high-mass stars. Although old low-mass stars have been previously observed (Barenfeld et al. 2016), deep, high-resolution observations have not been conducted with ALMA. This may indicate why there is a lack of old low-mass stars in our sample.

We also see that there are significantly fewer young, high-mass stars in our sample. This could be attributed to the fact that high-mass stars evolve on a much quicker time-scale than low-mass stars. They can evolve to the post pre-main-sequence (PMS) phase while still being embedded and actively accreting (Beuther et al. 2007). Therefore, imaging a protoplanetary disc around a high-mass star would be problematic.

Our sample contains more low-mass stars than intermediate-mass stars. However, it is known that low-mass stars are more common than intermediate- and high-mass stars, as would be expected from a standard Salpeter-like initial mass function (Salpeter 1955; Kroupa 2001; Chabrier 2003). Therefore, any results showing the commonalty of substructures around low-mass stars compared to high-mass stars may be a selection bias.

3.4 Comparison to full ALMA sample

A total of 793 protoplanetary discs were looked at in this work. Omitting young, embedded discs, as well as debris discs, we have identified 56 discs that show some kind of substructure, which is around 7 per cent of all discs. This is in contrast to Long et al. (2019) and work by the DSHARP project (Andrews et al. 2018b), who find that at least 50 per cent of the discs studied show substructure. As discussed in Section 3.1 above, this is due to the majority of ALMA

observations being conducted at lower resolutions than studied in these works.

The 793 protoplanetary discs studied here mainly surround Class I, II, and III young stellar objects. However, the protoplanetary disc surveys conducted by ALMA thus far have focused mainly on Class II discs from several star-forming regions. These include Chamaeleon I (Pascucci et al. 2016), Lupus (Ansdell et al. 2016, 2018), Ophiuchus (Cox et al. 2017; Cieza et al. 2019), the Orion Nebula Cluster (Eisner et al. 2018), σ Ori (Ansdell et al. 2017), Taurus (Akeson & Jensen 2014; Akeson et al. 2019; Long et al. 2018, 2019), and Upper Scorpius (Barenfeld et al. 2016).

Although these surveys focused on Class II protoplanetary discs, the star-forming regions have a range of ages. Therefore, the Class II discs in the ALMA archive are at different evolutionary stages. The sample of 56 discs studied here is representative of that. We have young stellar objects from 11 different star-forming regions, with a range of ages (see Table A1 in Appendix A). Also, there is a diverse range of calculated ages for the young stellar objects, the youngest being Wa Oph 6 (0.5 ± 0.1 Myr) and the oldest being J160230923 (30.0 ± 5.0 Myr). Therefore, we have studied systems with a comparable range of Class II evolutionary states as that found in the ALMA Archive.

4 PROPERTIES OF SAMPLE

A literature search has been conducted to obtain the temperature and luminosity of each host star. The luminosities have been scaled to the *Gaia* DR2 distances (Gaia Collaboration 2018). Where the error is not given in the literature for the temperature, we make an estimate of the uncertainty. The typical error on the quoted values is 6 per cent, therefore we use this and make a conservative estimated error of 10 per cent for temperatures without an uncertainty value. No *Gaia*
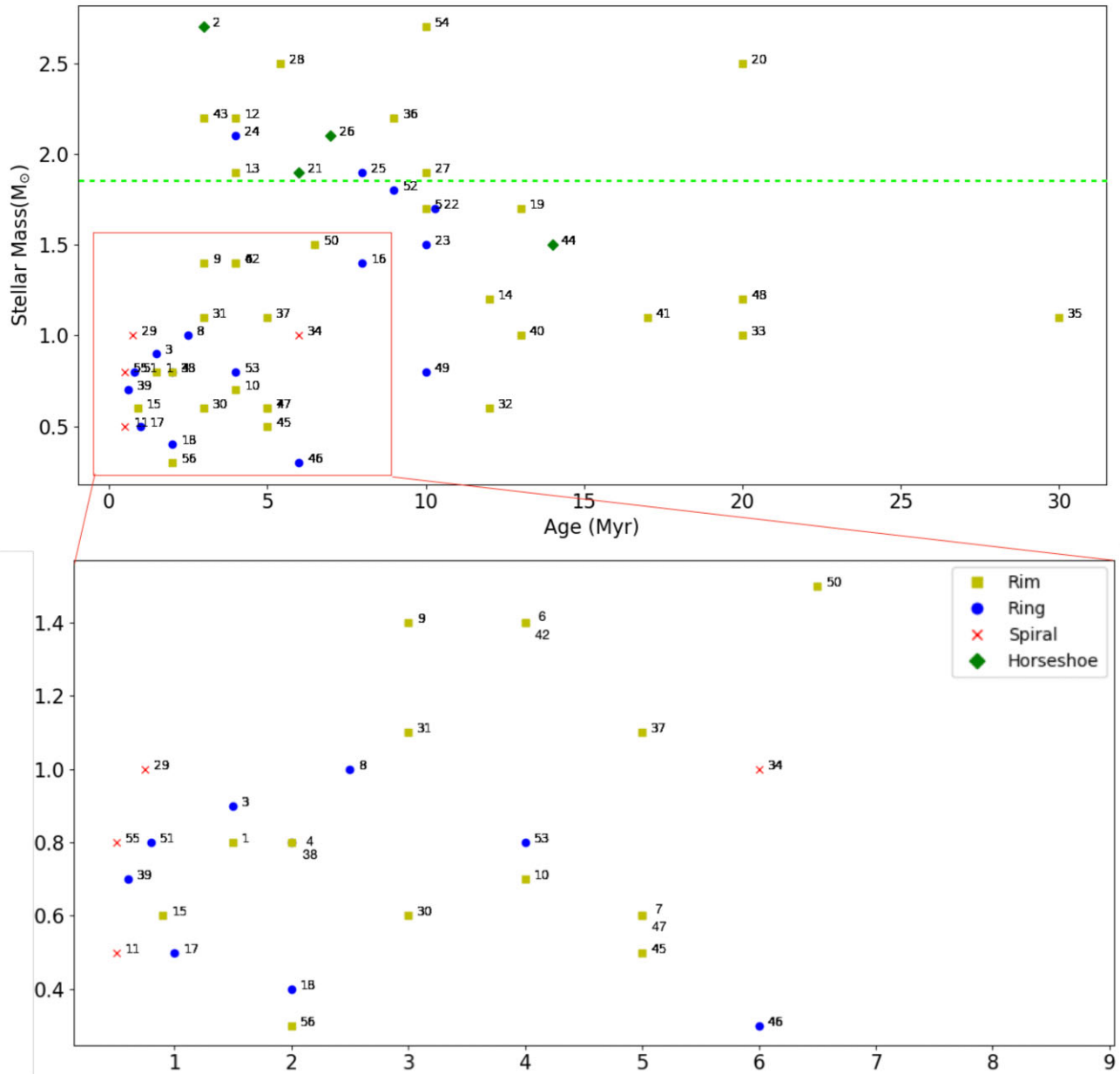
Figure 3. Stellar mass with age. The coloured markers indicate the category assigned to each protoplanetary disc in Section 5. The green dashed line indicates the limit between low-mass and intermediate-mass, as defined in Section 6.1.

DR2 distances were available for 2MASS J05052286+2531312. We make a distance estimate of 140.0 ± 14.0 pc for this object based on its location in the Taurus molecular cloud. We have assumed a conservative error estimate of 10 per cent for this distance.

An HR diagram of the sample has been plotted in Fig. 4. It is evident in the diagram that our sample uniformly covers both stellar luminosity and temperature. The zero-age main sequence (ZAMS) has also been plotted on the HR Diagram (ZAMS from Siess, Dufour & Forestini 2000). The discs have been plotting with different symbols according to the classification they have been given in this work. This will be discussed further in Section 5.

The 56 host stars have luminosities spanning from 0.1 to $90L_\odot$ and temperatures from 3400 to 12 000 K, covering a wide parameter range of low- and intermediate-mass stars. We refer to host stars with mass $M < 1.8M_\odot$ as low-mass objects. Intermediate objects are defined as those with mass $1.8 < M_\odot < 8$, while objects with mass greater than $8M_\odot$ are referred to as high-mass objects. The lower mass limit of $1.8M_\odot$ for the intermediate stars comes from Simon et al. (2002). The lower mass limit for high-mass stars ($8M_\odot$) originates from the minimum mass required to produce a Type II supernova (Zinnecker & Yorke 2007). The stars in our sample are located in a number of different star-forming regions (SFR), at a range of distances.

The *Gaia* DR2 distances agree to within 20 per cent of the previous literature values for the majority of sources. The DR2 distance to HD169142 was determined to be 114.0 pc, compared to its previous distance of 145.0 pc (Manoj et al. 2006). Other examples include
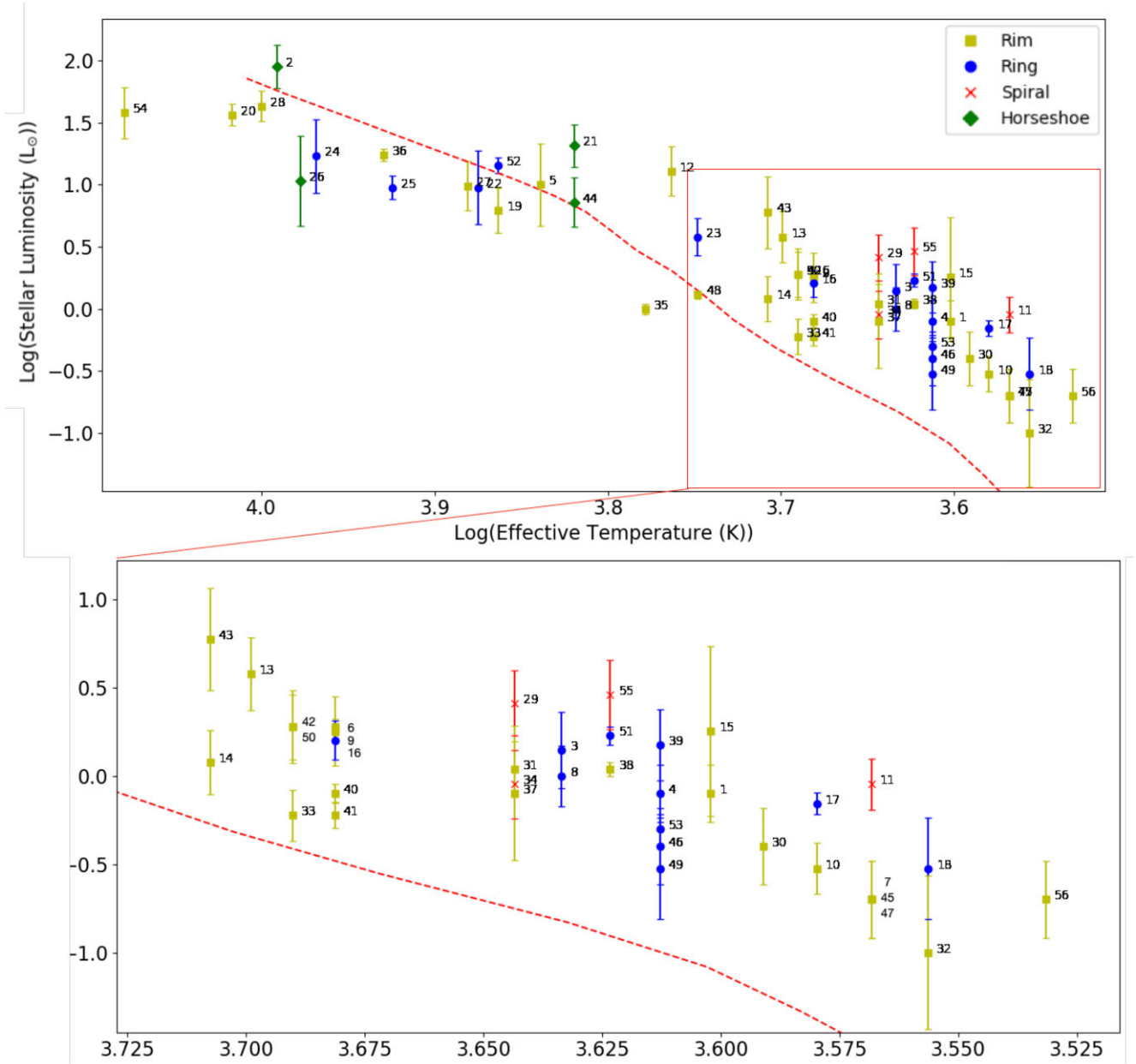
Figure 4. An HR diagram of the sources in our sample. The red dashed line marks the ZAMS using the model of Siess et al. (2000). The discs have been labelled and their identities can be found in Table 1. The coloured markers indicate the category assigned to each protoplanetary disc (see Section 5).

SZ111, which changed from 200.0 to 158.3 pc, and CQ Tau, 100 to 163 pc. The estimated distance to the Class II T-Tauri star RY Tau has changed drastically, from 140 pc (Agra-Amboage et al. 2009) to 177 pc in *Gaia* DR1 to 443.1 ± 47.0 pc in *Gaia* DR2 (Gaia Collaboration 2018). This discrepancy was discussed by Garufi et al. (2019). Therefore, we adopt their value of 133^{+55}_{-30} pc obtained from HIPPARCOS data (ESA 1997) The majority of the discs observed with ALMA are located in well-surveyed star-forming regions and have distances less than ∼200 pc.

All but eight systems in our sample are single-star systems. UX Tau A and HD100453 both have companions orbiting at a radius >100 au and are surrounded by a circumprimary disc (Tanii et al. 2012; Wagner et al. 2018). Circumbinary discs surround HD142527, CS Cha, DS Tau, V4046 Sgr, V892 Tau, and GG Tau (with GG Tau A being a triple-star system, Di Folco et al. 2014) (Smith et al. 2005;

Fukagawa et al. 2006; Guenther et al. 2007; Rodriguez et al. 2010; Akeson & Jensen 2014). With such a limited sample of multiple star systems, we have not investigated trends relating to disc morphology and multiplicity.

4.1 Determining stellar ages and masses

Individual stellar ages and masses were determined for the host stars using the new luminosities and the models of Siess et al. (2000) and Baraffe et al. (2015). The models of Baraffe et al. (2015) are only applicable for stars <1.4 M$_\odot$, therefore we use the models of Siess et al. (2000) for any star with a mass larger than this. Evolutionary tracks were plotted on to the HR diagram (Fig. 4) and the stellar mass and ages were interpolated. Errors on the ages and masses are derived using the associated luminosity error for each star. For

reference, we show the HR diagrams with plotted evolutionary tracks in Appendix B.

The derived ages are given in Table 2. It should be noted that this method of determining the ages and masses of PMS stars is quite uncertain. This is due to the luminosities of some stars having large errors, resulting in a large uncertainty range for the ages and masses. Therefore, the derived values from this method are only an estimate and should be treated with caution. The estimates of the stellar ages are later used to order the protoplanetary discs according to age (see Section 6).

We compare the ages derived here to the estimated age of the star-forming region each star belongs to. We find that the ages we have derived generally agree with the estimated ages of the star-forming region within 3σ. The ages of the star-forming regions can be found in Table B1. We find that the derived ages of the objects that do not agree with the age of the star-forming region ar either very young or very old objects. Therefore, the stellar isochrones may be underestimating or overestimating the ages for these stars.

4.2 Determining disc radii

For a quantitative analysis of the structure of the protoplanetary discs, we calculate the dust disc radii. As the observations were taken with different resolutions and sensitivities, we calculate the radius containing 68 per cent of the total flux for each disc (see Tripathi et al. 2017 for a more detailed explanation of this method). The radius of each disc can be found in Table 2. This method for determining the effective radius of the disc has previously been utilized in a number of works. We compare our derived radii to literature values of the radii containing 68 per cent of the total flux for the discs where this has been calculated. We find that the radii calculated here agree with the literature values within 3σ (Tripathi et al. 2017; Ansdell et al. 2018; Long et al. 2019). We make use of the derived radii in Sections 6.2 and 6.3.

5 CLASSIFYING PROTOPLANETARY DISCS

Garufi et al. (2018) studied the appearance of protoplanetary discs (in morphology and spatial extent) in scattered light. Stellar and disc properties were calculated and related to seven categories defined in the study: Ring, Spiral, Giant, Rim, Inclined, Faint, and Small discs. Following a similar approach, we classify our discs into four categories based upon their appearance and morphology. The characteristics of the four categories are outlined below and summarized in Fig. 5.

Rings: Protoplanetary discs that feature bright, concentric rings have been classified as ringed discs. Between the rings are gaps devoid of gas and/or dust. A minimum of two concentric rings need to be seen in order for a disc to be classified as ringed. Examples of these discs that have been observed with ALMA include GM Auriga (Macías et al. 2018) and HD169142 (Fedele et al. 2017). These discs may also feature a central cavity, as can be seen in GM Auriga.

Rims: The majority of the discs that have been studied in this work feature a single bright rim at the edge of a large disc cavity. These rims have been seen in both intermediate-mass and low-mass young stellar objects including DM Tau, LkCa15, and 2MASS J16042165–2130284 – hereafter J16042165 (Pinilla et al. 2018). Disc rims can also be seen in protoplanetary discs that have been classified as ring or horseshoe. However since the rim is not the most prominent feature, these discs have been sorted in other categories. Furthermore, rims can be seen in some discs as such at the present angular resolution. As we will discuss later in the paper, further observation of rim discs
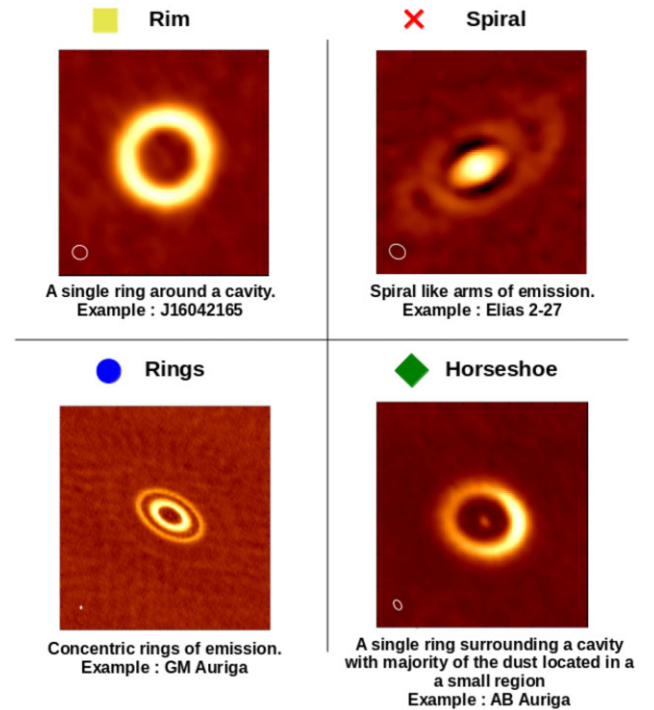
Figure 5. Examples of protoplanetary discs from each category defined in this work. More detail about each category is given in the text.

may place them in alternate categories. Since we are only focusing on the continuum emission from the protoplanetary disc, the cavity needs to be void of only dust in order to be classified as a rim.

Horseshoe: Horseshoe-shaped discs are similar to rim discs; a single ring of dust surrounding a large cavity. However, the majority of the dust in horseshoe discs is located in a small region of one side of the disc. An example of a system containing a horseshoe-shaped protoplanetary disc is HD142527 (Casassus et al. 2015), where the dust in the protoplanetary disc resembles a crescent or horseshoe shape.

Spiral: Discs which feature spiral-like arms of continuum emission are classified as spiral discs. This structure has rarely been seen in protoplanetary discs as of yet, the first being Elias 2-27 (Pérez et al. 2016).

All of our chosen discs are resolved and show substructure, therefore we have omitted the Faint category of discs used by Garufi et al. (2018). We have also not used the Small disc category as all of our discs have a radius larger than 20 au. Garufi et al. (2018) define discs that show faint arm-like structures on large scales as Giant. These structures are only seen in discs with a radial extent $\gg$100 au. The structures seen in these discs are faint and could even be attributed to broken rings rather than spiral arms. Therefore, we have removed the Giant category and introduced the Horseshoe category which has been outlined above.

The discs have been classified based on the most prominent morphological feature seen in the sub-mm dust emission. Some discs like CQ Tau could be defined as either a horseshoe disc or a rim disc. We have chosen to classify this disc as a rim disc since this is the most prominent feature. RY Lup also appears to have a horseshoe-like morphology. However this disc is nearly edge on with an inclination angle of $\approx$70 deg (Langlois et al. 2018). Therefore, the horseshoe-like morphology may just be an observational effect. Therefore, we have placed this disc in the Rim category. We strongly
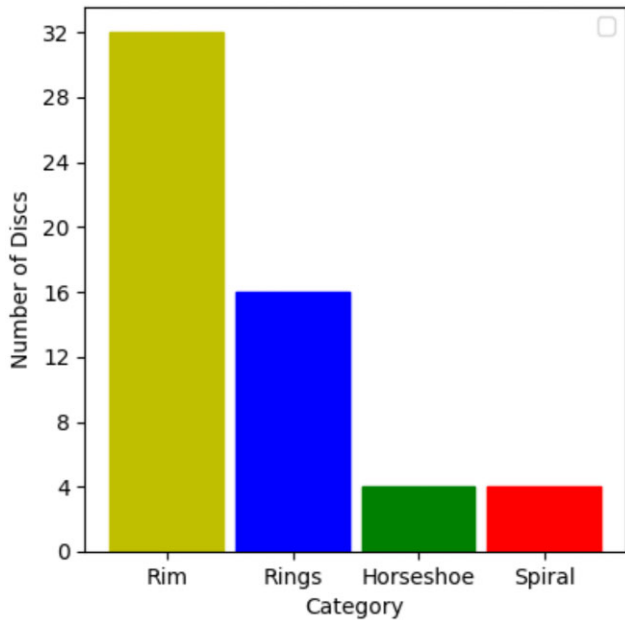
Figure 6. 56 protoplanetary discs have been studied in our sample. Rim and Ringed protoplanetary discs are the most common discs that have been observed with ALMA. Horseshoe and Spiral discs are the least common types.

acknowledge that some discs can fit into multiple classifications. The classification for each source can be found in Table 2.

5.1 Unsharp Masking Filtering

ALMA observations of Elias 2-27 by Pérez et al. (2016) revealed spiral density waves in the protoplanetary disc. The technique of Unsharp Masking Filtering was performed on the images in order to remove the large-scale disc emission and highlight the spiral structure of the disc. The observations of Elias 2-27 from Pérez et al. (2016) were obtained from the ALMA Archive and the original observation was smoothed with a 2D Gaussian of 0.33 arcsec full width at half-maximum (FWHM). This image was then scaled by a factor of 0.87 before subtracting it from the original image.

We applied a similar process to the ALMA observations of J16152023 and Wa Oph 6 as faint spiral substructure could be seen. The Filtering was applied to J16152023 and Wa Oph 6 in order to highlight the spiral structures that can be seen in the disc. These discs were smoothed with a Gaussian of FWHM 0.33 arcsec; J16152023 was scaled by a factor of 0.87, while Wa Oph 6 was scaled by 0.67. The Filtering was performed in order to bring out the fainter structures of the disc; this then allowed us to better classify these protoplanetary discs. No other science was performed using these filtered images

6 RESULTS

6.1 Prevalence of each substructure

The number of discs in each category can be seen in Fig. 6. Of the 56 discs studied in this sample, Rim discs appear to be the most populous category in our sample featuring 32 discs. 16 discs have been classified as having rings. Horseshoe and Spiral discs are least populous, with four discs in each category. Although the majority of our sample have been classified as a Rim disc, it should be noted

that cavities are the easiest substructure to be detected with ALMA. And as a result, the large number of Rim discs may be a selection effect due to extensive interest in them. This is further discussed in Section 7.1.1 below. While horseshoe-shaped discs have been placed in their own category, they all feature a single ring of emission on the edge of a large cavity and could also be classified as Rim discs. This would increase the number of Rim discs to 36, more than 60 per cent of our sample, intensifying the notion that the presence of a Rim seems to be a common feature in the current population of protoplanetary discs observed at mm-wavelengths.

We now investigate the properties of the host stars of each disc category. From Fig. 4 we can see that Horseshoe-shaped discs are most commonly found around intermediate-mass stars. These stars are all Herbig Ae/Be type stars, with their high effective temperatures ($T_{\rm eff} > 6000$ K). The lack of Horseshoe-shaped protoplanetary discs around low-mass stars may indicate that the formation mechanism responsible for forming a pile-up of dust grains on one side of the disc preferentially occurs in higher mass stars (van der Marel et al. 2021).

Spiral discs surround just four host stars in our sample. All systems in this category are single-star systems and are Class II T-Tauri-type stars with stellar masses $\leq 1.0 M_{\odot}$. Due to the small number of both Horseshoe and Spiral discs, we cannot make any real conclusions about the characteristics of the host stars that these discs surround.

6.2 Structure versus age

To study whether the morphological structures seen in protoplanetary discs evolve with age, we have ordered the discs studied in this work according to age. We have used the ages derived in Section 4.1 using the evolutionary tracks from Siess et al. (2000) and Baraffe et al. (2015). Figs C1, C2, C3, and C4 in Appendix C show the Rim, Ring, Horseshoe, and Spiral discs ordered according to age. Images have been scaled to 500×500 au. Stars with a † symbol in the lower left corner have been scaled to 1000×1000 au. This has been done to enable us to compare the spatial extent of the discs.

6.2.1 Rims and ring

The Rim discs, ordered by age, can be seen in Fig. C1. The ages of the stars surrounded by a Rim protoplanetary disc vary quite widely. The youngest disc is a T-Tauri star with an age of 0.9 ± 0.2 Myr, while J16230923 is the oldest disc with an age of 30.0 ± 6.0 Myr. Furthermore, from Fig. 3, we can see that all of the discs with an age greater than 10 Myr (except one Horseshoe disc) are surrounded by a Rim. Therefore, a Rim appears to be a long-lasting structure of a protoplanetary disc, whereas a Spiral or Ring is a shorter lived structure. The intermediate-mass stars with Rims appear in the later stages of the evolutionary plot. However, this may simply be an observational bias as there are very little observations of old low-mass stars.

Fig. C2 shows the Ring discs ordered by age. There does not appear to be a correlation between the age of the system and the radial extent of the disc. RU Lup is the youngest Ring disc we have classified, while HD 142666 is the oldest. Each low-mass star is scaled to 500×500 au, therefore we can see that the radial extent of the disc does not depend on the age of the system.

The spatial extent of the Rim and Ring discs does not appear to be correlated with age. We test this quantitatively by plotting the disc radius against the derived stellar age (values in Table 2). This plot is shown in Fig. 7. The discs plotted do not feature a spiral or horseshoe
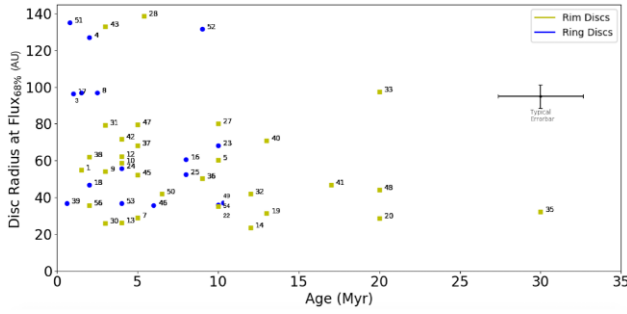
Figure 7. The radii of the protoplanetary discs containing 68 per cent of the total flux against the stellar age. The yellow markers indicate the Rim discs and the blue markers indicate the Ring discs.

Figure 8. The radii of the protoplanetary discs containing 68 per cent of the total flux against the stellar mass. The yellow markers indicate the Rim discs and the blue markers indicate the Ring discs.

morphology as we have a low number of these discs. We have also omitted the circumbinary discs.

We fit the relation of the disc radius to age using the Bayesian linear regression method of Kelly (2007), *linmix*. This method of regression takes into account errors on both axes, as well as intrinsic scatter.

We find a negative trend relating the disc radius to the age of the system with a slope of -1.3 ± 1.0 for the Rim discs. However, we have a large dispersion of 2.7 ± 2.3 dex, indicating that this relationship may not be significant. This high dispersion may be due to the large errors associated with the calculated ages. We confirm this by calculating a Pearson correlation coefficient for the trend. We find a slightly negative relationship with an R-value of -0.22. We measure a p-value of 0.24, indicating that this slight negative trend may not be statistically significant.
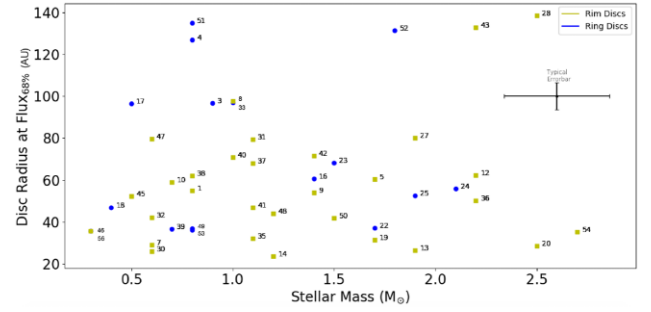
The same analysis is performed for the Ring discs and we find a slightly negative trend with a slope of -2.1 ± 4.0 and a high dispersion of 3.2 ± 3.0 dex. This negative correlation, however, has an R-value of -0.33, with a p-value of 0.21, thus indicating that this negative trend is not statistically significant. Therefore, we conclude that there is no correlation between the radial extent of the ring discs and the age of the system.

The results presented here agree with the work done by van der Marel et al. (2019) who showed that there was no correlation between the radius of the disc and the age of the system.

6.2.2 Horseshoe

Fig. C3 shows the Horseshoe discs arranged according to age. There is a wide range of ages for the protoplanetary discs that feature a Horseshoe morphology. AB Auriga, the youngest star, has an age of 3.0 ± 0.5 Myr, while the oldest disc, SAO 206462, is 14.0 ± 5.5 Myr old. Therefore, the horseshoe-like morphology may be caused by a mechanism that occurs in the later evolutionary stage of a protoplanetary disc. However, due to our small sample and a lack of young intermediate stars observed with ALMA at a high resolution, we cannot make any definitive conclusions about this.

There appears to be no variation in the morphological structure of the discs as they get older. It can be seen that the radius of the disc is not correlated with the age of the star. The radii of the discs surrounding the intermediate-mass stars AB Auriga, HD142527, HD34282, and SAO206462 are 163 ± 16, 186 ± 27, 187 ± 28, and 120 ± 62, respectively. However, our sample only features four protoplanetary discs with a horseshoe morphology, therefore any conclusions may be due to small number statistics.

We do not make use of the derived radii for the Horseshoe and Spiral discs as we only have four discs in each category; an insufficient sample to derive meaningful relationships.

6.3 Structure versus mass

We have also investigated whether the substructures seen in a protoplanetary disc are dependant on stellar mass. The stellar masses have been calculated in Section 4.1 and can be found in Table 1. Figs C5, C6, C7, and C8 can be found in Appendix C and show the Rim, Ring, Horseshoe, and Spiral discs ordered according to stellar mass. The images of the low-mass stars have been scaled to 500×500 au, while the stars with a † symbol have been scaled to 1000×1000 au. This again was done to enable us to compare the spatial extents of the discs.

By looking at Figs C5, C6, C7, and C8, we can see that there is no correlation between the mass of the host star and the outer radius of the protoplanetary disc. This is true for both the low- and intermediate-mass stars of our sample. Our sample covers host stars with a wide range of stellar masses: from ~ 0.3 to >3.0 M$_\odot$ for the stars surrounded by a rim disc, ~ 0.3 to 4.0 M$_\odot$ for the Ring protoplanetary discs, ~ 1.5 to $2.7 M_\odot$ for the horseshoe-shaped protoplanetary discs, and ~ 0.5 to 1.0 M$_\odot$ for the stars surrounded by a spiral-shaped protoplanetary disc.

We confirm this by following the same method adopted when studying the relation between the radius of the disc and the age of the system in Section 6.2 above. A graph relating the mass of the star and the radius of the disc can be seen in Fig. 8. The values for the derived disc radii and stellar masses can be found in Tables 2 and 1, respectively. We have not examined trends for the Horseshoe and Spiral discs as we only have a small sample of discs. We have also omitted the circumbinary discs.

We find positive trends relating the mass of the star to the outer radius of the disc for both the Rim and Ring discs. However, the large errors associated with the determination of the stellar mass make these trends uncertain. The Rim discs have a slope of 5.3 ± 10.9 with a large dispersion of 2.8 ± 2.3 dex. We confirm that this is a weak relationship by calculating a correlation coefficient for the trend. We find an R-value of 0.24 with a p-value of 0.21 for the trend relating the stellar mass of the system to the radius of the disc. The trend relating the radius to the stellar mass of the Ring discs has a large dispersion of 3.2 ± 3.0 dex. We calculate a correlation coefficient of 0.03 for this trend with a p-value of 0.92. This is strong evidence for there being no correlation between the outer radius of the Ring discs and the stellar mass. This is in agreement with the result found by van der Marel et al. (2019).

Table 3. The discs observed by ALMA using a high enough resolution and sensitivity to justify there being undetected substructure. See the text for further details. The IDs correspond to the IDs of the discs listed in Table A1. Distances have been obtained from *Gaia* DR2 unless otherwise stated (Gaia Collaboration 2018).

ID #	Name[†]	Distance (arcsec)	Spatial resolution (pc)	Sensitivity (μJy beam^{-1})	ALMA Project code	Reason for not included in sample
14	V∗ Z CMa	233 ± 48	0.05	20	2016.1.00110.S	No substructure detected
50	2MASS J18191220−2047297	1900∗	0.03	22	2015.1.00480.S	No substructure detected
53	IRAS 13481−6124	3600∗	0.03	30	2016.1.01504.S	No substructure detected
132	V∗ HP Cha[††]	196∗∗	0.02	16	2017.1.01460.S	Substructure detected but too young
265	V∗ GW Ori[††]	402 ± 11	0.10	18	2017.1.00286.S	Substructure detected but too young
386	[JJK2008] SMM J162740−24431	133∗∗	0.10	48	2016.1.01042.S	No substructure detected
391	IRAS 16285−2355[††]	133∗∗	0.02	16	2015.1.01512.S	Substructure detected but too young
471	HH 520	450∗∗	0.07	34	2017.1.01478.S	No substructure present
491	2MASS J17112317−2724315 [††]	130∗∗	0.03	17	2016.1.01186.S	Substructure detected but too young
532	V∗ DG Tau	121 ± 2	0.02	12	2015.1.01268.S	No substructure detected
612	V∗ V1213 Tau	140∗∗	0.02	13	2017.1.01701.S	No substructure detected- Edge-on disc
613	V∗ HL Tau[††]	140∗∗	0.09	36	2013.1.00355.S	Substructure detected but too young
656	HD 98800	50∗∗	0.10	33	2016.1.01042.S	No substructure detected
659	V∗ CE Ant	34 ± 1	0.10	33	2015.1.01015.S	No substructure detected
768	Elia 2-20[††]	138 ± 4	0.02	15	2016.1.00484.L	Substructure detected – too young
792	GSS 26	140∗∗	0.10	48	2016.1.01042.S	No substructure detected

Notes.

[†]The name of each object given here can be queried in data bases such as *SIMBAD*. An alternative name for each object may have been used on the ALMA Archive, in which case the project code should also be used to find the object.

[††]These observations show substructure but were discarded from our sample due to our selection criteria (see Section 2). These discs all have ages less than 0.5 Myr – see the text for further details.

∗These sources have no associated *Gaia* distances and their distance was obtained from literature measurements – see the text for details.

∗∗These sources have no associated *Gaia* distance, nor individual distance estimate. Therefore, we approximate the distance by using the distance to its association.

7 DISCUSSION

7.1 The detectability of substructures

We previously introduced the resolution bias of our sample in Section 3.1. Our finding that ∼27 per cent of discs show substructure when observed with a resolution limit of 0.22 arcsec agrees with Cieza et al. (2019). These authors find that 20 per cent of their discs show substructure for the same resolution limit.

Furthermore, we were able to show that just less than half of the discs observed by ALMA show substructure when observed with a resolution limit of ≈0.12 arcsec, in agreement with Long et al. (2019). Higher resolution observations of protoplanetary discs are needed in order to bring the frequency of discs showing substructure in line with the results of the DSHARP project, where 60 per cent of discs showed substructure when observed with very high resolutions of ≈0.035 arcsec.

Similarly, only 25 per cent of discs observed by ALMA show substructure when observed with a sensitivity limit of 50 μJy beam^{-1} or greater. This increases to 35 per cent when the sensitivity increases to 20 μJy beam^{-1} or greater. Both Long et al. (2019) and Andrews et al. (2018b) were able to find a higher proportion of discs to show substructure when using these sensitivity limits (≤50 per cent and 100 per cent, respectively). Therefore, the fraction of discs showing substructure here is smaller than is expected for these sensitivity limits. This could imply that other factors, such as the resolution, may be affecting our ability to detect substructure in the discs even though our sensitivities are high enough.

We look at the 738 discs that do not show substructure – or showed substructure but were not included during our sample selection (see Section 2) – to determine the number of discs that are bright and extended enough to justify substructure that is undetected. We use our previous resolution and sensitivity limits of 0.1 arcsec and

50 μJy beam^{-1}, where Long et al. (2019) were able to show that just under half of the discs in their sample show substructure. We find that 98 discs meet the sensitivity limit, while 30 discs meet the resolution limit. Of these objects, 16 discs are both bright and extended enough within our limits to show substructure. These discs are shown below in Table 3.

Six of these 16 discs showed substructure, but were removed from our sample due to having ages less than 0.5 Myr. These objects are V∗ HP Cha, V∗ GW Ori, IRAS 16285−2355, 2MASS J17112317−2724315, V∗ HL Tau, and Elias 2-20 (Welch et al. 2000; Brooke et al. 2007; Fang et al. 2014; Soderblom et al. 2014; Czekala et al. 2017; Segura-Cox et al. 2020). Furthermore, two discs were removed from our sample due to their large distances. Objects 2MASS J18191220−2047297 and IRAS 13481−6124 have distances of 1900 and 3600 pc, respectively (Busfield et al. 2006; Maud et al. 2015). Therefore, currently, no substructure can be detected in their discs regardless of how high the resolution and sensitivity are. The object V∗ V1213 Tau is an edge-on protoplanetary disc, therefore we are unable to detect substructure in the disc (Burrows et al. 1996; Stapelfeldt et al. 1999).

We show the continuum product images of the remaining seven discs that have been observed with a sufficiently high resolution and sensitivity to warrant substructure in Fig. 9. Reobservation of these discs at higher resolution and sensitivities may result in detection of substructure.

The resolution and sensitivity used to observe protoplanetary discs may also affect the type of substructure that is detected. We plot the resolution of the observations used to detect our sample against the sensitivities in Fig. 10. We find that the majority of discs featuring rings are detected when the sensitivity is below ∼60 μJy beam^{-1}, regardless of the resolution used. Rim discs, on the other hand, span a wide resolution and sensitivity range. However, below 20 μJy beam^{-1}, five ring discs are detected compared to
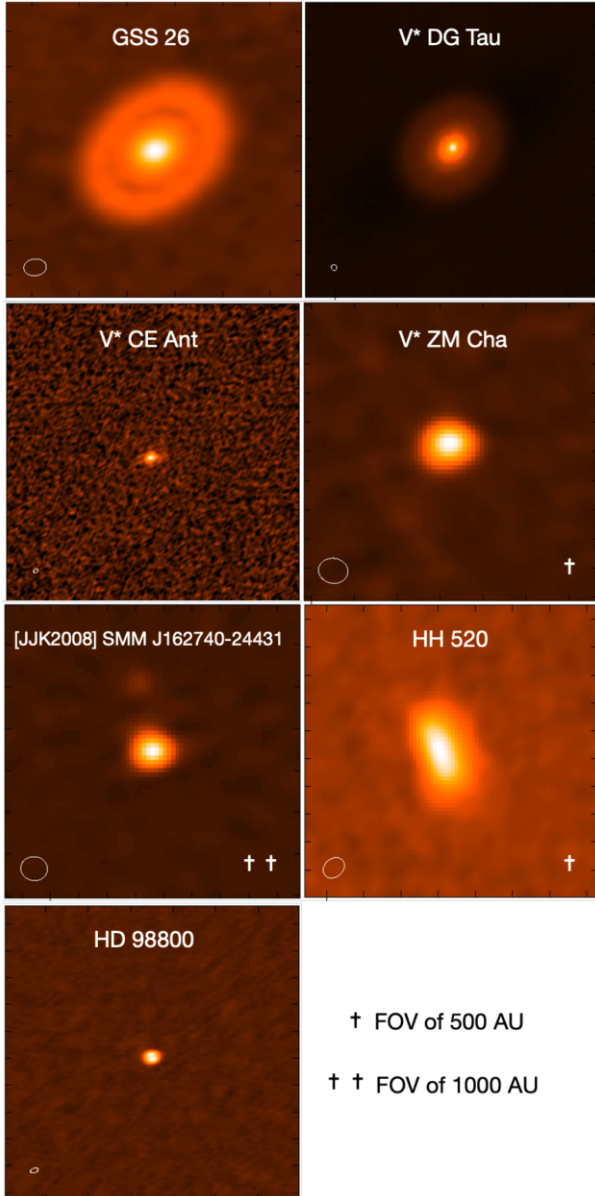
Figure 9. The protoplanetary discs observed with a high enough resolution and sensitivity to hint at unresolved substructure. The images show a field of view of 250 × 250 au unless otherwise stated. The beam of the observations are shown in the bottom left corner.
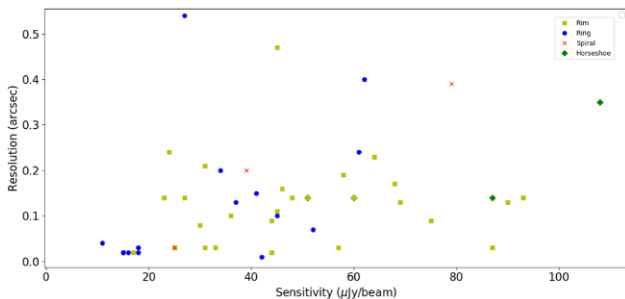
Figure 10. A plot of the angular resolutions and sensitivities of the observations of the discs in our sample. We have omitted the four protoplanetary discs with sensitivities greater than 120 μJy beam^{-1}.

only one rim disc. Thus, additionally, supporting the notion that increasing the resolution and sensitivity of observations may cause discs to be reclassified from Rim to Rings. Therefore, although angular resolution may play a vital role in detecting substructure in protoplanetary discs (as we have shown in Section 3.1), the sensitivity of the observations is key in determining the type of substructure present in the disc.

7.1.1 The observability of rims

32 discs in our sample have been classified as having a Rim; a single ring of dust surrounding a large cavity devoid of dust and/or gas. It is clear from Fig. 4 that the hosts stars that are surrounded by a Rim disc cover both stellar temperature and luminosity quite uniformly. There are somewhat more Rim discs around low-mass stars than around intermediate-mass stars (24 low-mass stars and eight intermediate-mass stars). However, due to the nature of our classification scheme, all four of the high-mass Horseshoe discs could also be classified as Rim discs. Therefore, a single ring of emission on the edge of a large cavity appears to be a very common feature seen in protoplanetary discs regardless of temperature or luminosity.

There are numerous ways to form a rim of dust around a star and this may explain why they are a frequent substructure seen in protoplanetary discs. A planet present in a disc would cause a pressure maximum to form. As dust radially migrates inwards from the outer regions of the disc it hits this pressure maximum. This would cause a pile-up of dust grains to form in a ring around the orbit of the forming protoplanet (Paardekooper & Mellema 2006; Fouchet et al.2007).

In order to detect if a rim has been formed due to a planetary companion, observations of CO isotopologues can be made. Gas gaps have previously been shown to have been carved out by a planetary or substellar companion (Bruderer et al. 2014; van der Marel et al. 2015, 2016b; Dong et al. 2017; Boehler et al. 2017, 2018) In recent work, Ubeira Gabellini et al. (2019) were able to show that depressions in both continuum and CO isotopologue ring maps could be caused by an embedded planet within the disc.

A rim can also form in the disc due to photoevaporation. UV radiation from the central star can heat up the surface of the disc. This can cause the dust to evaporate and eventually leave the disc as a photoevaporative wind, thus forming a cavity (Hollenbach et al. 1994; Hardy et al. 2015) A rim can then be seen at the outer edge of the cavity. A rim, as the outer edge of a cavity, can also form in a protoplanetary disc due to condensation fronts (Zhang et al. 2015), aggregate sintering (Okuzumi et al. 2016), and the inner edge of a dead zone (Flock et al. 2015; Béthune, Lesur & Ferreira 2016).

The populous nature of rings, however, may be due to a selection bias. Transition discs have explicitly been targeted by ALMA, both in individual projects as well as part of surveys (e.g. DSHARP, Andrews et al. 2018b). This is because rim discs are easily detected, even at the lower resolutions and sensitivities. More complex substructure, such as spiral and horseshoes, may only be detected at higher resolutions and sensitivities.

This resolution dependence has recently been demonstrated in ALMA observations of LkCa15 by Facchini et al. (2020). In previous works, and here, it has been classified as a rim surrounding a cavity. However, ALMA observations with a resolution ~0.04 arcsec of were able to resolve multiple rings in the disc. In addition to this, Francis & van der Marel (2020) were able to show that the cavities of transition discs are often not void of dust. Therefore, there may be unresolved dust rings in some of the discs classified as being Rim discs in this work. Further high-resolution observations may reveal that Rings are the most populous substructure seen in protoplanetary

discs and not a single rim of emission. Likewise, high-resolution observations would also increase the number of discs that are known to have resolvable substructure.

7.1.2 Observing horseshoes

Recent work by van der Marel et al. (2021) has shown that the diversity in asymmetric and non-asymmetric dust structures in protoplanetary discs is linked to the local gas surface density at the location of pressure bumps. Asymmetric structures such as horseshoes may only be detected if the local gas surface density is sufficiently low. The upcoming ngVLA may be able to trace the dust at these low gas density locations using centimetre wavelengths, thus increasing the population of discs showing asymmetric structures. The increased resolution capabilities of the ngVLA may also resolve new substructures and increase the population of discs showing substructures to greater than 60 per cent, as shown by the DSHARP project (Andrews et al. 2018b).

7.1.3 The observability of rings

The low-mass stars that feature protoplanetary rings have a wide range of ages; from 0.6 Myr for RU Lup to 10.3 Myr for HD 142666. The spread of ages imply that rings can form very early in the evolution of the disc and are long-lasting substructures or that they can form at a range of evolutionary stages.

Recent observations of HL Tau, Elias 2-24, and GY 91 revealed protoplanetary discs with multiple rings and gaps (ALMA Partnership et al. 2015; Dipierro et al. 2018; Sheehan & Eisner 2018). These young stellar objects all have ages less than 1 Myr. Therefore, planet formation is thought to begin very early in the evolution of the disc. As the protoplanets grow in mass and size, they are able to carve gaps in the dust and gas of the protoplanetary disc forming rings. Mamajek (2009) showed that planet formation could end between 2 and 3 Myr as half of the protoplanetary discs in their sample disappeared by this time. The majority of the low-mass discs in our sample have derived ages greater than 2 Myr (in part due to the removal of young, embedded discs from the sample), meaning that it is possible for their gaps and rings to have been formed by planets. In order to confirm this, similarly to rim discs, additional CO isotopologue observations could be carried out to determine the origin of the dust rings. However, the gas gaps in ring discs are harder to constrain, as discussed by Isella et al. (2016).

Other mechanisms, such as the accumulation and growth of material at various ice lines (Zhang et al. 2015), may be responsible for the ringed substructure. However, this method was recently put into question by Huang et al. (2018) and van der Marel et al. (2019) who showed that the gap radii in ringed protoplanetary discs do not correspond with common ice lines. The analysis conducted in this work cannot determine the precise origins of the protoplanetary rings seen.

7.2 Comparisons to scattered light observations

Observations of protoplanetary discs have previously been made at a number of different wavelengths, including optical, near-infrared, and sub-mm. These different wavelengths probe different regions of the protoplanetary disc. Observations at near-infrared wavelengths trace the smallest dust grains (typically μm-sized) in the innermost parts and surface of the protoplanetary disc. At these wavelengths the dust is optically thick. As the observing wavelength approaches mm/sub-mm, the dust in the mid-plane of the disc begins to become

Table 4. The discs studied in both this work at mm-wavelengths and by Garufi et al. (2018) in scattered light.

ID #	Name	Classification at mm wavelength	Classification in scattered light
2	AB Auriga	Horseshoe	Spiral
3	AS 209	Rings	Rings
5	CQ Tau	Rim	Spiral
9	DoAr44	Rim	Rim
12	EM∗SR21A	Rim	Rings
15	GG Tau	Rim	Rim
16	GM Auriga	Rings	Rim
19	HD 100453	Rim	Spiral
20	HD 100546	Rim	Spiral
21	HD 142527	Horseshoe	Spiral
23	HD 143006	Rings	Rings
24	HD 163296	Rings	Rings
25	HD 169142	Rings	Rings
26	HD 34282	Horseshoe	Spiral
27	HD 36112	Rim	Spiral
28	HD 97048	Rim	Rings
29	IM Lup	Spiral	Rings
31	LkCa15	Rim	Rim
33	J16042165−2130284	Rim	Rim
34	J16152023−3255051	Spiral	Rings
37	PDS 70	Rim	Rim
41	RXJ1852.3-3700	Rim	Rings
44	SAO 206462	Horseshoe	Spiral
47	SZ 91	Rim	Rim
49	TW Hya	Rings	Rings
50	UX Tau	Rim	Rim
52	V1247 Ori	Rings	Spiral
53	V4046 Sgr	Rings	Rings

optically thin. The largest dust grains lie in the mid-plane of the disc and this is where the majority of the disc mass lies.

Substructures can be seen in protoplanetary discs in both mm and polarized scattered light observations. Garufi et al. (2018) studied the morphology of 58 protoplanetary discs in scattered light and classified them into the following categories: Rim, Rings, Spirals, Faint, Giant, Inclined, and Small. Our sample has 36 protoplanetary discs in common with the sample studied by Garufi et al. (2018). Five discs have been classified as Spiral, five discs as Giant, five as Faint, six as Rim, 11 as Rings, three as Inclined, and one as small.

We have discarded the Faint, Giant, Small, and Inclined categories as they are not morphological structures and have reclassified these discs according to our classification. The scattered light observation of RU Lup, Sz111, CI Tau, MWC 480, and GW Lup were classified as Faint in Garufi et al. (2018), while HD142666, T Cha, and RY Lup were classified as Inclined and CS Cha as Small. Since there is no clear substructure in the these discs and they do not fit in any of our classification categories, we have discarded them from the common sample, leaving 28 discs for comparison. Following the characteristics outlined in Section 5, three of the five discs classified as Giant by Garufi et al. (2018) have been classified as Spiral discs (AB Auriga, HD142527, and HD100546). These three discs are all intermediate-mass stars. The remaining two low-mass stars have been classified as Rim discs (GG Tau A and GM Auriga). The common sample and their classifications, including the newly reclassified Giant discs, can be found in Table 4.

Fig. 11 compares the morphology seen in scattered light with the morphology seen in sub-mm for the 27 protoplanetary discs. The
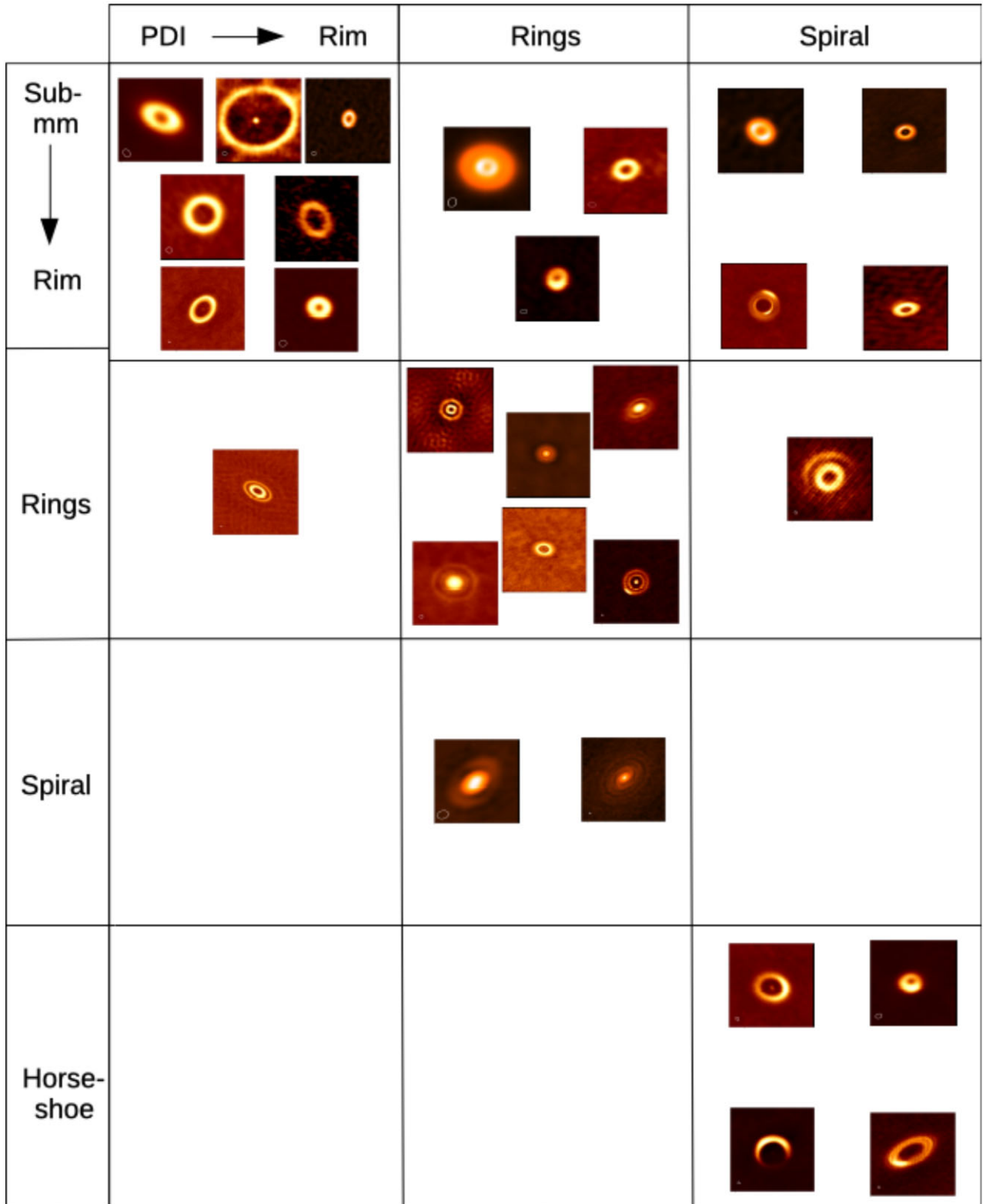
Figure 11. A comparison between the morphology seen in protoplanetary discs at sub-mm continuum and near-IR polarized differential imaging. The columns show the morphology seen in scattered light and the rows show the morphology seen in sub-mm continuum.

columns indicate the morphology assigned by Garufi et al. (2018) and the rows indicate the morphologies assigned in this work.

All of the discs showing a Horseshoe-shaped morphology in sub-mm continuum emission have a Spiral morphology in scattered light. The disc surrounding SAO206462 was shown to have a mass of $\sim$0.002 M$_\odot$ (Pérez et al. 2014), while the disc masses of AB Auriga, HD142527, and HD100546 have been shown to be 0.01 M$_\odot$ (Tang et al. 2012), 0.1 M$_\odot$ (Perez et al. 2015), and $\sim$0.03 M$_\odot$ (Kama et al. 2016), respectively. The wide range of disc masses may indicate that disc mass plays little role in the type of morphology seen in discs in both sub-mm and scattered light.

Spiral substructure seen in scattered light observations has previously been seen in a number of protoplanetary discs (Grady et al. 2001, 2013; Fukagawa et al. 2004; Casassus et al. 2012; Muto et al. 2012; Wagner et al. 2015; Akiyama et al. 2016; Ohta et al. 2016; Canovas et al. 2018). The submillimetre counterpart observations to these discs, however, show large cavities and axisymmetric substructure (Isella et al. 2013; van der Marel et al. 2013; Ansdell et al. 2016; Kraus et al. 2017; Tang et al. 2017; Cazzoletti et al. 2018; Dong et al. 2018; Ohashi et al. 2018; Pineda et al. 2019). The mm images shown here of IM Lup and J16152023 both feature a spiral-like morphology, however rings were seen in scattered light observations rather than large cavities and axisymmetric substructures. This agrees with the results found by Avenhaus et al. (2018) and Huang et al. (2018) for these two discs.

The nine discs shown here with a spiral-like morphology in scattered light were found to be relatively old (Garufi et al. 2018). The host stars had ages between $\approx$3 and $\approx$12 Myr and are at the very late stage of their PMS lifetime. Also, the lack of young stars featuring a Spiral disc led to the conclusion that the formation of spiral arms in μm-sized dust discs may only occur in the latter phases of their PMS lifetime. This contrasts with the results found in this work. The four Spiral discs in this work are at an early stage of their PMS lifetime and have ages $\lesssim$6 Myr. Therefore, the mechanism responsible for forming spiral arms in the sub-mm dust of a protoplanetary disc happens during the earliest stages of its evolution around low-mass stars. This discrepancy may suggest that there are different mechanisms forming the spiral arms seen in scattered light and those seen in the sub-mm.

14 discs have been classified as Rim discs in the sub-mm, 10 of them being low-mass stars and four being intermediate-mass stars. Seven low-mass stars have been shown to have Rims in both sub-mm and scattered light. EM∗SR21 and HD97048 are both intermediate-mass stars that show a Rim in sub-mm but have a ringed protoplanetary disc in scattered light. Both EM∗SR21 and HD97048 have relatively young ages. Recent work by Muro-Arena et al. (2020) and van der Marel et al. (2021) has shown that the structure within these discs may be more complex and it may be possible for multiple rings to be present. Observations at a higher resolution would need to be conducted in order to confirm the structure within the disc.

All the discs in our sample (56 discs) show some sort of cavity or gap. 65 per cent of the discs studied by Garufi et al. (2018) showed some sort of cavity in scattered light indicating that they are a common occurrence in both sub-mm and scattered light. The discs that showed a cavity in sub-mm and not scattered light were classified by Garufi et al. (2018) as either Faint or Inclined. The lack of a cavity may contribute to the faintness of the discs in scattered light, while the absence of a cavity in the Inclined discs may be an observational bias (Garufi et al. 2018). The high number of discs that exhibit a cavity in both scattered light and sub-mm shows that cavities are a common feature found in protoplanetary discs across a range of star type and evolutionary stage. However, it should be

noted that there may be a bias in both samples. The sample by Garufi et al. (2018) may contain many transition discs as they are bright due to their cavity wall. Likewise, the sample presented here may be biased towards transition discs as they are easiest to find at low resolution.

Eight discs classified as Rings in sub-mm have been studied in scattered light, six of which surround low-mass stars and two surrounding intermediate stars. Rings in scatted light are seen in six of the protoplanetary discs as well as in the sub-mm. The two systems that do not show rings in scattered light are GM Auriga and V1247 Ori, both low-mass stars. The discs around these stars were shown to have a Rim and Spiral morphology, respectively. The rings seen in protoplanetary discs in scattered light and in the sub-mm can form with similar mechanisms, such as the interaction of the disc with a companion (Lin & Papaloizou 1979; Kley & Nelson 2012; Pinilla, Benisty & Birnstiel 2012; de Juan Ovelar et al. 2013).

8 CONCLUSIONS

We have studied the morphology of the substructure seen in protoplanetary discs. We have classified 56 discs with visible structure in the ALMA Archive cycles 0 to 6. These discs, observed in the sub-mm continuum, were placed into four categories: Rim, Ring, Horseshoe, and Spiral. By calculating the age of the host stars we are able to study the evolution of the substructures seen in protoplanetary discs over a range of ages. The sub-mm images studied in this work were then compared to scattered light observations of protoplanetary discs studied by Garufi et al. (2018). We have reached the following conclusions in this work:

(i) We find that 27 per cent of 798 discs observed with ALMA during cycles 0–5 show substructure when observed with a moderate resolution of at least $\sim$0.22 arcsec. Using a higher resolution of $\sim$0.1 arcsec, 42 per cent of the discs observed show clear substructure. The fraction of discs showing substructure increases to 60 per cent when observed with a very high resolution of $\lesssim$0.04 arcsec. Therefore, many of the discs observed with ALMA thus far may have substructure that remains unresolved due to the relatively low resolutions used.

(ii) When looking at the 798 discs observed with ALMA during cycles 0–5, we find that 31 (or 25 per cent) show substructure when observed with a moderate sensitivity of 50 μJy beam^{-1}. A higher sensitivity of 20 μJy beam^{-1} results in 35 per cent of the discs showing substructure. This low proportion indicates that many of the discs observed by ALMA thus far may feature substructure that remains undetected due to relatively low sensitivities used.

(iii) We have shown that angular resolution is key in detecting substructures within protoplanetary discs, with sensitivity playing a vital role in determining the type of substructure present in the disc.

(iv) The protoplanetary discs studied here show substructure surrounds Class II young stellar objects with a range of ages. This is representative of the full sample of discs observed by ALMA thus far, where the majority of the systems observed have been Class II young stellar objects. The discs studied here, however, were observed with much higher resolutions than the majority of the discs in the ALMA Archive. Therefore, they are not representative of many discs which were observed at significantly lower resolutions.

(v) In our sample the most populous substructure seen is a rim of sub-mm dust surrounding a large cavity. A rim of some sort is found for over half of the discs in our sample and they appear around stars with a range of ages, temperatures, and luminosities. This type of substructure, however, is the easiest to detect and have been explicitly

targeted by ALMA. None the less, it confirms that cavities and gaps are a common feature in protoplanetary discs.

(vi) The second most common substructure seen in our protoplanetary discs is a ringed disc. As the majority of the discs observed with ALMA thus far were not observed using sufficiently high resolution, a Ring disc may be the most common substructure seen in protoplanetary discs.

(vii) A distinctive horseshoe-shaped protoplanetary disc has only been seen in a few systems. These systems contain relatively old, intermediate-mass stars.

(viii) All discs showing a horseshoe morphology in the sub-mm continuum images show a spiral-like morphology in scattered light.

(ix) Low-mass stars that have been classified as Rim discs in the sub-mm have also been classified as Rim in scattered light. The occurrence of a single rim of emission around a large cavity seems to be a common substructure found in both scattered light and sub-mm continuum emission.

(x) The substructures seen in ALMA images of protoplanetary discs mostly do not seem to follow an evolutionary sequence nor do they depend on the mass of the star.

In future work we will compare the images with theoretical predictions.

ACKNOWLEDGEMENTS

DATA AVAILABILITY

The data underlying this article are available in the ALMA Archive, at https://almascience.nrao.edu/aq/. The project codes for the data have been provided in the Acknowledgements section above.

REFERENCES

Agra-Amboage V., Dougados C., Cabrit S., Garcia P. J. V., Ferruit P., 2009, A&A, 493, 1029
Akeson R. L., Jensen E. L. N., 2014, ApJ, 784, 62
Akeson R. L., Jensen E. L. N., Carpenter J., Ricci L., Laos S., Nogueira N. F., Suen-Lewis E. M., 2019, ApJ, 872, 158
Akiyama E. et al., 2016, AJ, 152, 222
Alcalá J. M. et al., 2017, A&A, 600, A20
ALMA Partnership et al., 2015, ApJ, 808, L3
Andrews S. M. et al., 2018b, ApJ, 869, L41
Andrews S. M., Terrell M., Tripathi A., Ansdell M., Williams J. P., Wilner D. J., 2018a, ApJ, 865, 157
Ansdell M. et al., 2016, ApJ, 828, 46
Ansdell M. et al., 2018, ApJ, 859, 21
Ansdell M., Williams J. P., Manara C. F., Miotello A., Facchini S., van der Marel N., Testi L., van Dishoeck E. F., 2017, AJ, 153, 240
Avenhaus H. et al., 2018, ApJ, 863, 44
Baraffe I., Homeier D., Allard F., Chabrier G., 2015, A&A, 577, A42
Barenfeld S. A., Carpenter J. M., Ricci L., Isella A., 2016, ApJ, 827, 142
Baruteau C. et al., 2014, in Beuther H., Klessen R. S., Dullemond C. P., Henning T., eds, Protostars and Planets VI. University of Arizona Press, Tucson, p. 667
Baruteau C., Zhu Z., 2016, MNRAS, 458, 3927
Bell C. P. M., Mamajek E. E., Naylor T., 2015, MNRAS, 454, 593
Berrilli F., Corciulo G., Ingrosso G., Lorenzetti D., Nisini B., Strafella F., 1992, ApJ, 398, 254
Bertout C., Siess L., Cabrit S., 2007, A&A, 473, L21
Béthune W., Lesur G., Ferreira J., 2016, A&A, 589, A87
Beuther H., Churchwell E. B., McKee C. F., Tan J. C., 2007, in Reipurth B., Jewitt D., Keil K., eds, Protostars and Planets V. University of Arizona Press, Tucson, p. 165
Boehler Y. et al., 2018, ApJ, 853, 162
Boehler Y., Weaver E., Isella A., Ricci L., Grady C., Carpenter J., Perez L., 2017, ApJ, 840, 60
Brooke T. Y. et al., 2007, ApJ, 655, 364
Bruderer S., van der Marel N., van Dishoeck E. F., van Kempen T. A., 2014, A&A, 562, A26

Burrows C. J. et al., 1996, ApJ, 473, 437
Busfield A. L., Purcell C. R., Hoare M. G., Lumsden S. L., Moore T. J. T., Oudmaijer R. D., 2006, MNRAS, 366, 1096
Caballero J. A., Solano E., 2008, A&A, 485, 931
Canovas H. et al., 2018, A&A, 610, A13
Casassus S. et al., 2013, Nature, 493, 191
Casassus S. et al., 2015, ApJ, 812, 126
Casassus S., Perez M. S., Jordán A., Ménard F., Cuadra J., Schreiber M. R., Hales A. S., Ercolano B., 2012, ApJ, 754, L31
Cazzoletti P. et al., 2018, A&A, 619, A161
Chabrier G., 2003, ApJ, 586, L133
Cieza L. A. et al., 2019, MNRAS, 482, 698
Cox E. G. et al., 2017, ApJ, 851, 83
Czekala I. et al., 2017, ApJ, 851, 132
Da Rio N., Robberto M., Soderblom D. R., Panagia N., Hillenbrand L. A., Palla F., Stassun K. G., 2010, ApJ, 722, 1092
de Juan Ovelar M., Min M., Dominik C., Thalmann C., Pinilla P., Benisty M., Birnstiel T., 2013, A&A, 560, A111
Di Folco E. et al., 2014, A&A, 565, L2
Dipierro G. et al., 2018, MNRAS, 475, 5296
Dong R. et al., 2017, ApJ, 836, 201
Dong R. et al., 2018, ApJ, 860, 124
Dong R., Zhu Z., Whitney B., 2015a, ApJ, 809, 93
Dong R., Hall C., Rice K., Chiang E., 2015b, ApJ, 812, L32
Dutrey A., Di Folco E., Beck T., Guilloteau S., 2016, A&A Rev., 24, 5
Eisner J. A. et al., 2018, ApJ, 860, 77
ESA, 1997, The Hipparcos and Tycho catalogues. Astrometric and photometric star catalogues derived from the ESA Hipparcos Space Astrometry Mission, ESA SP Series vol no: 1200. ESA Publications Division, Noordwijk, Netherlands
Facchini S. et al., 2020, A&A, 639, A121
Fairlamb J. R., Oudmaijer R. D., Mendigutía I., Ilee J. D., van den Ancker M. E., 2015, MNRAS, 453, 976
Fang M., Sicilia-Aguilar A., Roccatagliata V., Fedele D., Henning T., Eiroa C., Müller A., 2014, A&A, 570, A118
Fedele D. et al., 2017, A&A, 600, A72
Fedele D. et al., 2018, A&A, 610, A24
Flock M., Ruge J. P., Dzyurkevich N., Henning T., Klahr H., Wolf S., 2015, A&A, 574, A68
Fontani F., Beltrán M. T., Brand J., Cesaroni R., Testi L., Molinari S., Walmsley C. M., 2005, A&A, 432, 921
Fouchet L., Maddison S. T., Gonzalez J. F., Murray J. R., 2007, A&A, 474, 1037
Francis L., van der Marel N., 2020, ApJ, 892, 111
Fukagawa M. et al., 2004, ApJ, 605, L53
Fukagawa M., Tamura M., Itoh Y., Kudo T., Imaeda Y., Oasa Y., Hayashi S. S., Hayashi M., 2006, ApJ, 636, L153
Gaia Collaboration, 2016, A&A, 595, A2
Gaia Collaboration, 2018, A&A, 616, A1
Garufi A. et al., 2018, A&A, 620, A94
Garufi A. et al., 2019, A&A, 628, A68
Gonzalez J. F., Laibe G., Maddison S. T., 2017, MNRAS, 467, 1984
Grady C. A. et al., 2001, AJ, 122, 3396
Grady C. A. et al., 2013, ApJ, 762, 48
Grosso N., Bouvier J., Montmerle T., Fernández M., Grankin K., Zapatero Osorio M. R., 2007, A&A, 475, 607
Guenther E. W., Esposito M., Mundt R., Covino E., Alcalá J. M., Cusano F., Stecklum B., 2007, A&A, 467, 1147
Hardy A. et al., 2015, A&A, 583, A66
Hollenbach D., Johnstone D., Lizano S., Shu F., 1994, ApJ, 428, 654
Huang J. et al., 2018, ApJ, 869, L42
Isella A. et al., 2016, Phys. Rev. Lett., 117, 251101
Isella A., Testi L., Natta A., 2006, A&A, 451, 951
Isella A., Carpenter J. M., Sargent A. I., 2009, ApJ, 701, 260
Isella A., Pérez L. M., Carpenter J. M., Ricci L., Andrews S., Rosenfeld K., 2013, ApJ, 775, 30
James D. J., Melo C., Santos N. C., Bouvier J., 2006, A&A, 446, 971
Kama M. et al., 2016, A&A, 592, A83

Kelly B. C., 2007, ApJ, 665, 1489
Kenyon S. J., Gómez M., Whitney B. A., 2008, in Reipurth B., ed., Handbook of Star Forming Regions, Vol. 4, p. 405
Kley W., Nelson R. P., 2012, ARA&A, 50, 211
Kraus S. et al., 2013, ApJ, 768, 80
Kraus S. et al., 2017, ApJ, 848, L11
Kraus A. L., Hillenbrand L. A., 2009, ApJ, 704, 531
Kroupa P., 2001, MNRAS, 322, 231
Langlois M. et al., 2018, A&A, 614, A88
Lin D. N. C., Papaloizou J., 1979, MNRAS, 188, 191
Long F. et al., 2018, ApJ, 869, 17
Long F. et al., 2019, ApJ, 882, 49
Lorén-Aguilar P., Bate M. R., 2016, MNRAS, 457, L54
Luhman K. L., 2007, ApJS, 173, 104
Macías E. et al., 2018, ApJ, 865, 37
Mamajek E. E., 2009, in Usuda T., Tamura M., Ishii M., eds, AIP Conf. Proc. Vol. 1158, Exoplanets and Disks: Their Formation and Diversity. Am. Inst. Phys., New York, p. 3
Mamajek E. E., Bell C. P. M., 2014, MNRAS, 445, 2169
Manoj P., Bhatt H. C., Maheswar G., Muneer S., 2006, ApJ, 653, 657
Maud L. T., Moore T. J. T., Lumsden S. L., Mottram J. C., Urquhart J. S., Hoare M. G., 2015, MNRAS, 453, 645
Mendigutía I., Fairlamb J., Montesinos B., Oudmaijer R. D., Najita J. R., Brittain S. D., van den Ancker M. E., 2014, ApJ, 790, 21
Metchev S. A., Hillenbrand L. A., Meyer M. R., 2004, ApJ, 600, 435
Monnier J. D. et al., 2006, ApJ, 647, 444
Muro-Arena G. A. et al., 2020, A&A, 636, L4
Muto T. et al., 2012, ApJ, 748, L22
Ohashi S. et al., 2018, ApJ, 864, 81
Ohta Y. et al., 2016, PASJ, 68, 53
Okuzumi S., Momose M., Sirono S.-I., Kobayashi H., Tanaka H., 2016, ApJ, 821, 82
Paardekooper S. J., Mellema G., 2006, A&A, 453, 1129
Pascucci I. et al., 2016, ApJ, 831, 125
Perez S. et al., 2015, ApJ, 798, 85
Pérez L. M. et al., 2016, Science, 353, 1519
Pérez L. M., Isella A., Carpenter J. M., Chandler C. J., 2014, ApJ, 783, L13
Pineda J. E. et al., 2019, ApJ, 871, 48
Pinilla P. et al., 2018, ApJ, 859, 32
Pinilla P., Benisty M., Birnstiel T., 2012, A&A, 545, A81
Pinilla P., Flock M., Ovelar M. D. J., Birnstiel T., 2016, A&A, 596, A81
Pohl A., Pinilla P., Benisty M., Ataiee S., Juhász A., Dullemond C. P., Van Boekel R., Henning T., 2015, MNRAS, 453, 1768
Preibisch T., Mamajek E., 2008, in Reipurth B., ed., Handbook of Star Forming Regions, Volume II, 5, p. 235
Ragusa E., Dipierro G., Lodato G., Laibe G., Price D. J., 2017, MNRAS, 464, 1449
Rodriguez D. R., Kastner J. H., Wilner D., Qi C., 2010, ApJ, 720, 1684
Salpeter E. E., 1955, ApJ, 121, 161
Schneider P. C., France K., Günther H. M., Herczeg G., Robrade J., Bouvier J., McJunkin M., Schmitt J. H. M. M., 2015, A&A, 584, A51
Segura-Cox D. M. et al., 2020, Nature, 586, 228
Sheehan P. D., Eisner J. A., 2018, ApJ, 857, 18
Siess L., Dufour E., Forestini M., 2000, A&A, 358, 593
Simon T., Ayres T. R., Redfield S., Linsky J. L., 2002, ApJ, 579, 800
Smith K. W., Balega Y. Y., Duschl W. J., Hofmann K. H., Lachaume R., Preibisch T., Schertl D., Weigelt G., 2005, A&A, 431, 307
Soderblom D. R., Hillenbrand L. A., Jeffries R. D., Mamajek E. E., Naylor T., 2014, in Beuther H., Klessen R. S., Dullemond C. P., Henning T., eds, Protostars and Planets VI. University of Arizona Press, Tucson, p. 219
Stapelfeldt K. R. et al., 1999, ApJ, 516, L95
Takahashi S. Z., Inutsuka S.-I., 2016, AJ, 152, 184
Tang Y. W., Guilloteau S., Piétu V., Dutrey A., Ohashi N., Ho P. T. P., 2012, A&A, 547, A84
Tang Y.-W. et al., 2017, ApJ, 840, 32
Tanii R. et al., 2012, PASJ, 64, 124

Tripathi A., Andrews S. M., Birnstiel T., Wilner D. J., 2017, ApJ, 845, 44

Ubeira Gabellini M. G. et al., 2019, MNRAS, 486, 4638

van den Ancker M. E., The P. S., Tjin A Djie H. R. E., Catala C., de Winter D., Blondel P. F. C., Waters L. B. F. M., 1997, A&A, 324, L33

van der Marel N. et al., 2013, Science, 340, 1199

van der Marel N. et al., 2021, AJ, 161, 33

van der Marel N., van Dishoeck E. F., Bruderer S., Pérez L., Isella A., 2015, A&A, 579, A106

van der Marel N., van Dishoeck E. F., Bruderer S., Pinilla P., van Kempen T., Perez L., Isella A., 2016a, in Kastner J. H., Stelzer B., Metchev S. A., eds, Young Stars & Planets Near the Sun, vol. 314, p. 139

van der Marel N., van Dishoeck E. F., Bruderer S., Andrews S. M., Pontoppidan K. M., Herczeg G. J., van Kempen T., Miotello A., 2016b, A&A, 585, A58

van der Marel N., Williams J. P., Bruderer S., 2018, ApJ, 867, L14

van der Marel N., Dong R., di Francesco J., Williams J. P., Tobin J., 2019, ApJ, 872, 112

van Leeuwen F., 2007, A&A, 474, 653

van Terwisga S. E. et al., 2018, A&A, 616, A88

Villenave M. et al., 2019, A&A, 624, A7

Wagner K. et al., 2018, ApJ, 854, 130

Wagner K., Apai D., Kasper M., Robberto M., 2015, ApJ, 813, L2

Welch W. J., Hartmann L., Helfer T., Briceño C., 2000, ApJ, 540, 362

White R. J., Ghez A. M., Reid I. N., Schultz G., 1999, ApJ, 520, 811

Wilking B. A., Gagné M., Allen L. E., 2008, in Reipurth B., ed., Handbook of Star Forming Regions, Volume II, p. 351

Zhang K., Blake G. A., Bergin E. A., 2015, ApJ, 806, L7

Zhu Z., Dong R., Stone J. M., Rafikov R. R., 2015, ApJ, 813, 88

Zinnecker H., Yorke H. W., 2007, ARA&A, 45, 481

SUPPORTING INFORMATION

Supplementary data are available at *MNRAS* online.

suppl_data

Please note: Oxford University Press is not responsible for the content or functionality of any supporting materials supplied by the authors. Any queries (other than missing material) should be directed to the corresponding author for the article.

APPENDIX A: COMPLETE LIST OF STUDIED PROTOPLANETARY DISCS

Table A1 shows the complete list of images we have looked at in our search for protoplanetary discs featuring substructure. Only continuum observations were looked at as we are interested in substructure present in the dust populations of the discs. The complete version of Table A1 can be found online.

Table A1. The complete sample of the ALMA images we have looked at in our search for protoplanetary rings with substructure. We have listed major star-forming regions only. All distances have been obtained from *Gaia* DR2 (Gaia Collaboration 2018), unless otherwise stated.

ID #	Name[†]	Distance (pc)	Star-forming region	Resolution (arcsec)	Sensitivity (μJy beam^{-1})	ALMA project code
1	$*$ q01 Eri	17 ± 1	-	0.42	46	2015.1.00307.S
2	$*$ tau Cet	4 ± 1	-	0.99	23	2013.1.00588.S
3	LSPM J0343+1958	21 ± 1	-	0.54	120	2015.1.00783.S
4	Wolf 219	19 ± 1	-	0.54	120	2015.1.00783.S
5	LP 413-40	182 ± 3	-	0.54	120	2015.1.00783.S
6	HZ 10	34 ± 1	-	0.54	120	2015.1.00783.S
7	2MASS J04215810+2826300	631 ± 60	-	0.14	51	2013.1.00498.S
8	UCAC2 40978291	1404 ± 105	-	0.64	150	2012.1.00350.S
9	[XCR2012] TrES J043145+285909	484 ± 9	-	0.64	150	2012.1.00350.S
10	2MASS J05382310−0236269	1247 ± 113	-	0.24	281	2015.1.00089.S
11	[HHM2007] 852	908 ± 210	-	0.24	281	2015.1.00089.S
12	HD 38858	15 ± 1	-	0.63	33	2015.1.00307.S
13	HD 44627	50 ± 1	-	0.15	31	2015.1.01210.S
14	V$*$ Z CMa[††]	233 ± 48	-	0.05	20	2016.1.00110.S
15	HD 54341	101 ± 1	-	0.52	30	2015.1.00716.S
16	HD 61005	36 ± 1	-	0.45	23	2015.1.00633.S
17	HD 305539	3106 ± 289	-	0.02	63	2015.1.01323.S
18	HD 98922	691 ± 16	-	0.68	109	2015.1.01600.S
19	HD 107146	27 ± 1	-	0.35	30	2016.1.00104.S
20	$*$ 61 Vir	9 ± 1	-	0.63	30	2013.1.00359.S
21	LAWD 50	60 ± 1	-	0.69	43	2015.1.00783.S
22	V$*$ QS Vir	50 ± 1	-	0.69	43	2015.1.00783.S
23	PG 1350-090	20 ± 1	-	0.69	43	2015.1.00783.S
24	SDSS J135523.91+085645.4	642 ± 71	-	0.66	24	2016.1.01055.S
25	EC 14012-1446	60 ± 1	-	0.69	43	2015.1.00783.S
26	SDSS J141134.70+102839.7	753 ± 395	-	0.66	23	2016.1.01055.S
27	V$*$ GK Vir	475 ± 28	-	0.66	22	2016.1.01055.S
28	LBQS 1437-0053	519 ± 32	-	0.66	22	2016.1.01055.S
29	HD 131488	155 ± 2	-	0.52	33	2015.1.01243.S
30	$*$ g Lup	17 ± 1	-	0.48	43	2015.1.00307.S
31	2MASS J15430227−3444059	18519 ± 89163	-	0.28	250	2013.1.00220.S
32	V$*$ NN Ser	522 ± 27	-	0.99	32	2016.1.01055.S
33	THA 15-8	2304 ± 287	-	0.28	250	2013.1.00220.S
34	THA 15-9	2257 ± 204	-	0.28	250	2013.1.00220.S
35	IRAS 15563−4146	5988 ± 3980	-	0.28	236	2013.1.00220.S
36	2MASS J16070863−3947219	4762 ± 658	-	0.28	250	2013.1.00220.S
37	HD 164249	50 ± 1	-	0.20	45	2013.1.01147.S
38	HD 319139	72 ± 1	-	0.54	27	2011.0.00084.S
39	HD 169142	114 ± 1	-	0.13	37	2012.1.00799S
40	HD 172555	28 ± 1	-	0.20	39	2013.1.01147.S
41	HD 181327	48 ± 1	-	0.13	180	2013.1.00025.S
42	HD 202628	24 ± 1	-	0.64	14	2016.1.00515.S
43	HD 207129	16 ± 1	-	0.49	43	2015.1.00307.S
44	NGC 7293	201 ± 3	-	0.24	33	2015.1.00762.S
45	$*$ kap And	50 ± 1	-	0.14	40	2015.1.01210.S
46	V$*$ RW Aur	$65 \pm 15.5*$	-	0.15	22	2015.1.01506.S
47	$*$ bet Leo	$11 \pm 0.1*$	-	0.48	49	2015.1.00676.S
48	EM$*$ AS 220	$237 \pm 24.2*$	-	0.51	99	2015.1.01600.S
49	$*$ alf PsA	$8 \pm 0.1*$	-	0.38	100	2011.0.00191.S
50	2MASS J18191220−2047297[††]	$1900*$	-	0.03	22	2015.1.00480.S
51	GAL 035.03+00.35	$3490*$	-	0.38	136	2011.0.00275.S
52	MSX5C G023.0126-00.4177	$4590*$	-	0.15	25	2015.1.00615.S
53	IRAS 13481−6124[††]	$3600*$	-	0.03	30	2016.1.01504.S
54	2MASS J15354856−2958551	-	-	0.28	187	2013.1.00395.S
55	WRAY 16-23	$900*$	-	0.66	15	2016.1.01055.S
56	Parsamian 21	$400*$	-	0.14	21	2015.1.01067.S
57	hd97048	185 ± 1	-	0.03	31	2016.1.00826.S
58	HD 142527	157 ± 1	-	0.14	60	2012.1.00631.S
59	2MASS J18572247−3734427	2309 ± 288	-	0.26	148	2015.1.01058.S
60	2MASS J18593428−3721410	1575 ± 201	-	0.26	148	2015.1.01058.S
61	HD 14082B	40 ± 1	βP	0.21	53	2013.1.01147.S
62	HD 15115	49 ± 1	βP	0.45	26	2015.1.00633.S
63	BD+30 397	41 ± 1	β Pic Moving Group	0.21	51	2013.1.01147.S
64	$*$ 51 Eri	30 ± 1	β Pic Moving Group	0.15	19	2016.1.00358.S
65	$*$ bet Pic	20 ± 1	β Pic Moving Group	0.49	106	2011.0.00087.S
66	$*$ eta Tel	47 ± 1	β Pic Moving Group	0.15	62	2013.1.01147.S
67	V$*$ PZ Tel	47 ± 1	β Pic Moving Group	0.17	41	2015.1.01210.S
68	WRAY 15-1880	154 ± 1	Corona Australis	0.14	48	2015.1.01083.S
69	2MASS J18521730−3700119	146 ± 1	Corona Australis	0.14	60	2015.1.01083.S
70	2MASS J18563974−3707205	159 ± 5	Corona Australis	0.26	148	2015.1.01058.S

Table A1 – *continued*

ID #	Name†	Distance (pc)	Star-forming region	Resolution (arcsec)	Sensitivity (μJy beam⁻¹)	ALMA project code
71	2MASS J18564024−3655203	149 ± 3	Corona Australis	0.26	148	2015.1.01058.S
72	2MASSW J1858509−370631	155 ± 8	Corona Australis	0.26	148	2015.1.01058.S
73	2MASS J19002906−3656036	155 ± 9	Corona Australis	0.64	152	2011.0.00733.S
74	2MASS J19005804−3645048	153 ± 1	Corona Australis	0.60	181	2011.0.00733.S
75	2MASS J19005974−3647109	144 ± 6	Corona Australis	0.26	148	2015.1.01058.S
76	2MASS J19011149−3645337	154 ± 5	Corona Australis	0.26	148	2015.1.01058.S
77	V∗ V667 CrA	156 ± 3	Corona Australis	0.26	148	2015.1.01058.S
78	2MASS J19011893−3658282	149 ± 5	Corona Australis	0.26	148	2015.1.01058.S
79	2MASS J19012901−3701484	153 ± 2	Corona Australis	0.64	152	2011.0.00733.S
80	HD 176386	159 ± 2	Corona Australis	0.26	148	2015.1.01058.S
81	V∗ TY CrA	136 ± 3	Corona Australis	0.26	148	2015.1.01058.S
82	2MASS J19015374−3700339	147 ± 6	Corona Australis	0.26	148	2015.1.01058.S
83	V∗ DG CrA	157 ± 5	Corona Australis	0.26	148	2015.1.01058.S
84	2MASS J19021201−3703093	159 ± 4	Corona Australis	0.26	148	2015.1.01058.S
85	2MASS J19021667−3645493	155 ± 3	Corona Australis	0.26	148	2015.1.01058.S
86	SSTgbs J1902330−365821	139 ± 4	Corona Australis	0.26	148	2015.1.01058.S
87	*ISO*-CrA 177	282 ± 39	Corona Australis	0.26	148	2015.1.01058.S
88	VSST 10	164 ± 8	Corona Australis	0.26	148	2015.1.01058.S
89	2MASS J19032429−3715076	148 ± 35	Corona Australis	0.26	148	2015.1.01058.S
90	2MASS J19032547−3655051	154 ± 4	Corona Australis	0.26	148	2015.1.01058.S
91	V∗ V721 CrA	155 ± 2	Corona Australis	0.24	24	2015.1.01301.S
92	2MASS J18570785−3654041	148∗∗	Corona Australis	0.26	148	2015.1.01058.S
93	[QZM2013] MM3	148∗∗	Corona Australis	0.38	136	2011.0.00275.S
94	[WGL92] iras 10	148∗∗	Corona Australis	0.26	148	2015.1.01058.S
95	[LEM2005b] CrA 444b	148∗∗	Corona Australis	0.26	148	2015.1.01058.S
96	V∗ S CrA	148∗∗	Corona Australis	0.26	148	2015.1.01058.S
97	HH 730A	148∗∗	Corona Australis	0.26	148	2015.1.01058.S
98	2MASS J19013232−3658030	148∗∗	Corona Australis	0.26	148	2015.1.01058.S
99	2MASS J19013385−3657448	148∗∗	Corona Australis	0.26	148	2015.1.01058.S
100	MHO 2008	148∗∗	Corona Australis	0.26	148	2015.1.01058.S
101	2MASS J19014041−3651422	148∗∗	Corona Australis	0.26	148	2015.1.01058.S
102	2MASS J19015180−3710478	148∗∗	Corona Australis	0.26	148	2015.1.01058.S
103	AX 1858.4-3700	148∗∗	Corona Australis	0.26	148	2015.1.01058.S
104	2MASS J19015173−3655143	148∗∗	Corona Australis	0.26	148	2015.1.01058.S
105	2MASS J19015112−3654122	148∗∗	Corona Australis	0.26	148	2015.1.01058.S
106	[SHK2011b] 9	148∗∗	Corona Australis	0.26	148	2015.1.01058.S
107	V∗ T CrA	148∗∗	Corona Australis	0.26	148	2015.1.01058.S
108	2MASS J19020410−3657013	148∗∗	Corona Australis	0.26	148	2015.1.01058.S
109	2MASS J19020682−3658411	148∗∗	Corona Australis	0.26	148	2015.1.01058.S
110	2MASS J19021464−3700328	148∗∗	Corona Australis	0.26	148	2015.1.01058.S
111	2MASS J19022708−3658132	148∗∗	Corona Australis	0.26	148	2015.1.01058.S
112	2MASS J19031185−3709020	148∗∗	Corona Australis	0.60	181	2011.0.00733.S
113	2MASS J19041725−3659030	148∗∗	Corona Australis	0.26	148	2015.1.01058.S
114	V∗ DX Cha	108 ± 1	Chamaeleon	0.20	70	2013.1.00592.S
115	IRAS 12535−7623	160 ± 11	Chamaeleon	0.21	123	2013.1.00708.S
116	SZ 49	195 ± 2	Chamaeleon	0.21	123	2013.1.00708.S
117	SZ 50	147 ± 13	Chamaeleon	0.21	123	2013.1.00708.S
118	V∗ SX Cha	196∗∗	Chamaeleon	0.35	911	2013.1.00437.S
119	SZ 4	196∗∗	Chamaeleon	0.35	911	2013.1.00437.S
120	CHXR 9C	196∗∗	Chamaeleon	0.37	215	2013.1.01075.S
121	HH 48	196∗∗	Chamaeleon	0.28	180	2016.1.00460.S
122	Hn 4	196∗∗	Chamaeleon	0.37	215	2013.1.01075.S
123	CHXR 15	196∗∗	Chamaeleon	0.37	215	2013.1.01075.S
124	2MASS J11062942−7724586	196∗∗	Chamaeleon	0.35	320	2013.1.00437.S
125	[CCE98] 2-21	196∗∗	Chamaeleon	0.35	320	2013.1.00437.S
126	HH 927	196∗∗	Chamaeleon	0.37	215	2013.1.01075.S
127	V∗ VV Cha	196∗∗	Chamaeleon	0.35	911	2013.1.00437.S
128	V∗ HK Cha	196∗∗	Chamaeleon	0.35	320	2013.1.00437.S
129	Glass H	196∗∗	Chamaeleon	0.37	215	2013.1.01075.S
130	V∗ VW Cha	196∗∗	Chamaeleon	0.35	320	2013.1.00437.S
131	ESO-HA 562	196∗∗	Chamaeleon	0.35	320	2013.1.00437.S
132	V∗ HP Cha††	196∗∗	Chamaeleon	0.02	16	2017.1.01460.S
133	2MASS J11082570−7716396	196∗∗∗	Chamaeleon	0.35	320	2013.1.00437.S
134	V∗ HU Cha	196∗∗	Chamaeleon	0.35	320	2013.1.00437.S
135	V∗ HX Cha	196∗∗	Chamaeleon	0.35	320	2013.1.00437.S
136	V∗ WX Cha	196∗∗	Chamaeleon	0.35	320	2013.1.00437.S
137	OTS 44	196∗∗	Chamaeleon	0.61	17	2015.1.00243.S
138	Glass Q	196∗∗	Chamaeleon	0.35	320	2013.1.00437.S
139	ESO-HA 569	196∗∗	Chamaeleon	0.35	320	2013.1.00437.S
140	CHX 18	196∗∗	Chamaeleon	0.37	215	2013.1.01075.S
141	2MASS J11160287−7624533	196∗∗	Chamaeleon	0.35	911	2013.1.00437.S

Table A1 – *continued*

ID #	Name†	Distance (pc)	Star-forming region	Resolution (arcsec)	Sensitivity (μJy beam^{-1})	ALMA project code
142	2MASS J11175211−7629392	196**	Chamaeleon	0.37	320	2013.1.00437.S
143	CHXR 68	196**	Chamaeleon	0.37	215	2013.1.01075.S
144	IRAS F11171−7919	209**	Chamaeleon	0.37	320	2013.1.00437.S
145	2MASS J12534285−7715114	209**	Chamaeleon	0.21	123	2013.1.00708.S
146	2MASS J12580676−7709094	209**	Chamaeleon	0.21	123	2013.1.00708.S
147	SSTc2d J130529.0-774140	209**	Chamaeleon	0.21	123	2013.1.00708.S
148	V∗ BK Cha	209**	Chamaeleon	0.21	123	2013.1.00708.S
149	SZ 62	209**	Chamaeleon	0.21	123	2013.1.00708.S
150	2MASS J10533978-7712338	192 ± 4	Chamaeleon	0.35	911	2013.1.00437.S
151	2MASS J10561638-7630530	196 ± 4	Chamaeleon	0.37	320	2013.1.00437.S
152	V∗ SY Cha	183 ± 1	Chamaeleon	0.35	911	2013.1.00437.S
153	2MASS J10580597-7711501	187 ± 4	Chamaeleon	0.35	320	2013.1.00437.S
154	V∗ SZ Cha	190 ± 1	Chamaeleon	0.35	320	2013.1.00437.S
155	V∗ TW Cha	185 ± 1	Chamaeleon	0.35	911	2013.1.00437.S
156	Hen 3-545	187 ± 1	Chamaeleon	0.35	911	2013.1.00437.S
157	Ass Cha T 1-6	192 ± 2	Chamaeleon	0.37	320	2013.1.00437.S
158	V∗ CS Cha	176 ± 1	Chamaeleon	0.03	33	2017.1.00969.S
159	Hn 1	195 ± 6	Chamaeleon	0.35	320	2013.1.00437.S
160	Ass Cha T 1-8	182 ± 2	Chamaeleon	0.35	320	2013.1.00437.S
161	CHSM 1715	192 ± 3	Chamaeleon	0.37	320	2013.1.00437.S
162	V∗ CT Cha	192 ± 1	Chamaeleon	0.35	911	2013.1.00437.S
163	BYB 18	193 ± 3	Chamaeleon	0.37	320	2013.1.00437.S
164	SZ 13	194 ± 3	Chamaeleon	0.35	911	2013.1.00437.S
165	2MASS J11062554-7633418	209 ± 5	Chamaeleon	0.37	320	2013.1.00437.S
166	CHXR 73	191 ± 6	Chamaeleon	0.37	215	2013.1.01075.S
167	CHSM 7869	187 ± 7	Chamaeleon	0.37	320	2013.1.00437.S
168	*ISO*-ChaI 79	205 ± 22	Chamaeleon	0.35	320	2013.1.00437.S
169	Hn 5	195 ± 2	Chamaeleon	0.35	320	2013.1.00437.S
170	V∗ UX Cha	185 ± 1	Chamaeleon	0.35	320	2013.1.00437.S
171	V∗ UY Cha	190 ± 2	Chamaeleon	0.35	320	2013.1.00437.S
172	2MASS J11065939-7530559	196 ± 4	Chamaeleon	0.37	320	2013.1.00437.S
173	V∗ UZ Cha	196 ± 1	Chamaeleon	0.35	320	2013.1.00437.S
174	CHSM 9484	199 ± 4	Chamaeleon	0.35	320	2013.1.00437.S
175	[CCE98] 1-46	173 ± 7	Chamaeleon	0.35	911	2013.1.00437.S
176	[NC98] Cha HA 9	199 ± 12	Chamaeleon	0.35	320	2013.1.00437.S
177	V∗ DI Cha	191 ± 1	Chamaeleon	0.35	320	2013.1.00437.S
178	CHXR 76	189 ± 3	Chamaeleon	0.42	122	2012.1.00350.S
179	Ass Cha T 1-15	195 ± 2	Chamaeleon	0.35	320	2013.1.00437.S
180	2MASS J11074656-7615174	194 ± 7	Chamaeleon	0.37	320	2013.1.00437.S
181	SZ 23	184 ± 2	Chamaeleon	0.35	320	2013.1.00437.S
182	Ass Cha T 1-16	163 ± 8	Chamaeleon	0.35	320	2013.1.00437.S
183	V∗ HM Cha	187 ± 12	Chamaeleon	0.35	320	2013.1.00437.S
184	CHXR 30A	253 ± 26	Chamaeleon	0.35	320	2013.1.00437.S
185	*ISO*-ChaI 138	186 ± 7	Chamaeleon	0.35	320	2013.1.00437.S
186	*ISO*-ChaI 143	193 ± 5	Chamaeleon	0.35	320	2013.1.00437.S
187	*ISO*-ChaI 147	200 ± 8	Chamaeleon	0.35	320	2013.1.00437.S
188	V∗ HQ Cha	179 ± 4	Chamaeleon	0.35	320	2013.1.00437.S
189	Ass Cha T 1-20	188 ± 2	Chamaeleon	0.35	320	2013.1.00437.S
190	SZ 28	193 ± 3	Chamaeleon	0.35	320	2013.1.00437.S
191	V∗ PU Car	188 ± 1	Chamaeleon	0.35	911	2013.1.00437.S
192	V∗ VY Cha	186 ± 2	Chamaeleon	0.35	911	2013.1.00437.S
193	V∗ HS Cha	195 ± 4	Chamaeleon	0.35	320	2013.1.00437.S
194	NAME Sz 30A	197 ± 5	Chamaeleon	0.37	215	2013.1.01075.S
195	V∗ HV Cha	203 ± 8	Chamaeleon	0.35	320	2013.1.00437.S
196	V∗ VZ Cha	192 ± 1	Chamaeleon	0.35	320	2013.1.00437.S
197	HJM C 7-1	188 ± 6	Chamaeleon	0.35	320	2013.1.00437.S
198	HJM C 1-24	195 ± 3	Chamaeleon	0.35	320	2013.1.00437.S
199	BYB 43	193 ± 5	Chamaeleon	0.35	320	2013.1.00437.S
200	HD 97300	193 ± 1	Chamaeleon	0.37	215	2013.1.01075.S
201	*ISO*-ChaI 220	186 ± 16	Chamaeleon	0.35	320	2013.1.00437.S
202	*ISO*-ChaI 217	240 ± 13	Chamaeleon	0.35	320	2013.1.00437.S
203	Ass Cha T 1-23	202 ± 6	Chamaeleon	0.35	320	2013.1.00437.S
204	V∗ WW Cha	192 ± 1	Chamaeleon	0.35	320	2013.1.00437.S
205	V∗ FN Cha	195 ± 1	Chamaeleon	0.35	320	2013.1.00437.S
206	HJM C 1-4	201 ± 3	Chamaeleon	0.35	320	2013.1.00437.S
207	2MASS J11100785-7727480	200 ± 13	Chamaeleon	0.35	320	2013.1.00437.S
208	V∗ WY Cha	180 ± 9	Chamaeleon	0.35	911	2013.1.00437.S
209	HJM C 1-8	195 ± 2	Chamaeleon	0.35	320	2013.1.00437.S
210	*ISO*-ChaI 252	204 ± 12	Chamaeleon	0.35	320	2013.1.00437.S
211	Ass Cha T 1-27	185 ± 1	Chamaeleon	0.35	320	2013.1.00437.S
212	V∗ IK Cha	196 ± 11	Chamaeleon	0.35	320	2013.1.00437.S

Table A1 – *continued*

ID #	Name[†]	Distance (pc)	Star-forming region	Resolution (arcsec)	Sensitivity (μJy beam^{-1})	ALMA project code
213	V* WZ Cha	195 ± 1	Chamaeleon	0.35	911	2013.1.00437.S
214	HJM C 2-5	140 ± 14	Chamaeleon	0.35	320	2013.1.00437.S
215	V* XX Cha	191 ± 1	Chamaeleon	0.35	911	2013.1.00437.S
216	CHX 18N	193 ± 1	Chamaeleon	0.35	911	2013.1.00437.S
217	V* IM Cha	185 ± 4	Chamaeleon	0.37	320	2013.1.00437.S
218	SZ 40	193 ± 2	Chamaeleon	0.35	320	2013.1.00437.S
219	SZ 41	194 ± 1	Chamaeleon	0.35	320	2013.1.00437.S
220	V* CV Cha	193 ± 1	Chamaeleon	0.35	320	2013.1.00437.S
221	V* CW Cha	196 ± 2	Chamaeleon	0.35	320	2013.1.00437.S
222	Ass Cha T 2-54	202 ± 17	Chamaeleon	0.42	122	2012.1.00350.S
223	HJM E 2-9	191 ± 2	Chamaeleon	0.35	320	2013.1.00437.S
224	Hn 18	190 ± 2	Chamaeleon	0.35	911	2013.1.00437.S
225	Hn 21W	189 ± 3	Chamaeleon	0.37	320	2013.1.00437.S
226	Hn 21	189 ± 3	Chamaeleon	0.37	215	2013.1.01075.S
227	BYB 53	194 ± 7	Chamaeleon	0.37	215	2013.1.01075.S
228	Ass Cha T 1-32	188 ± 1	Chamaeleon	0.35	911	2013.1.00437.S
229	2MASS J11241186-7630425	185 ± 2	Chamaeleon	0.37	320	2013.1.00437.S
230	[FLG2003] eps Cha 17	181 ± 18	Chamaeleon	0.37	320	2013.1.00437.S
231	V* T Cha	110 ± 1	Chamaeleon	0.13	90	2012.2.00182.S
232	V* DK Cha	244 ± 22	Chamaeleon	0.21	123	2013.1.00708.S
233	NAME Sz 46N	196 ± 2	Chamaeleon	0.21	123	2013.1.00708.S
234	2MASS J13005927-7714027	220 ± 10	Chamaeleon	0.21	123	2013.1.00708.S
235	SZ 51	199 ± 1	Chamaeleon	0.21	123	2013.1.00708.S
236	V* CM Cha	194 ± 1	Chamaeleon	0.21	123	2013.1.00708.S
237	2MASS J13022287-7734494	205 ± 4	Chamaeleon	0.21	123	2013.1.00708.S
238	SZ 52	204 ± 3	Chamaeleon	0.21	123	2013.1.00708.S
239	Hn 22	199 ± 1	Chamaeleon	0.21	123	2013.1.00708.S
240	Hn 24	197 ± 1	Chamaeleon	0.21	123	2013.1.00708.S
241	Hn 25	197 ± 3	Chamaeleon	0.21	123	2013.1.00708.S
242	SZ 53	197 ± 2	Chamaeleon	0.21	123	2013.1.00708.S
243	Hen 3-854	197 ± 1	Chamaeleon	0.21	123	2013.1.00708.S
244	2MASS J13052169-7738102	202 ± 5	Chamaeleon	0.21	123	2013.1.00708.S
245	SZ 56	191 ± 2	Chamaeleon	0.21	123	2013.1.00708.S
246	SZ 58	186 ± 2	Chamaeleon	0.21	123	2013.1.00708.S
247	2MASS J13071806-7740529	199 ± 5	Chamaeleon	0.21	123	2013.1.00708.S
248	Hn 26	198 ± 3	Chamaeleon	0.21	123	2013.1.00708.S
249	V* BM Cha	202 ± 2	Chamaeleon	0.21	123	2013.1.00708.S
250	2MASS J13082714-7743232	205 ± 6	Chamaeleon	0.21	123	2013.1.00708.S
251	SZ 63	202 ± 1	Chamaeleon	0.21	123	2013.1.00708.S
252	Cl* Trumpler 14 VBF 125	3000**	Carina Nebula	0.02	63	2015.1.01323.S
253	[SBM2003] J104405.4-592940	3000**	Carina Nebula	0.02	63	2015.1.01323.S
254	[GG2014] 230	3000**	Carina Nebula	0.02	63	2015.1.01323.S
255	HD 21997	70 ± 1	Columba Association	0.98	85	2011.0.00780.S
256	HD 100453	104 ± 1	DC296.27.9	0.03	25	2017.1.01424.S
257	HD 100546	110 ± 1	DC296.27.9	0.03	57	2015.1.00806.S
258	V* EH Cha	99 ± 1	η Chamaeleontis Association	0.42	122	2012.1.00350.S
259	V* EI Cha	100 ± 1	η Chamaeleontis Association	0.52	122	2012.1.00350.S
260	V* ET Cha	92 ± 3	η Chamaeleontis Association	0.40	184	2011.0.00133.S
261	S255IR SMA1	200000**	Gemini	0.4	42	2015.1.00500.S
262	V* V471 Tau	48 ± 1	Hydes	0.54	120	2015.1.00783.S
263	HG 7-85	42 ± 1	Hydes	0.54	69	2015.1.00783.S
264	EGGR 29	50 ± 1	Hydes	0.54	85	2015.1.00783.S
265	V* GW Ori[††]	402 ± 11	λOrionis Association	0.10	18	2017.1.00286.S
266	HD 121191	132 ± 1	Lower Centaurus Crux	0.50	37	2015.1.01243.S
267	HD 121617	117 ± 1	Lower Centaurus Crux	0.50	38	2015.1.01243.S
268	CD-40 8434	113 ± 1	Lower Centaurus Crux	0.05	30	2017.A.00006.S
269	SZ 66	157 ± 2	Lupus	0.28	236	2013.1.00220.S
270	2MASS J15445789-3423392	153 ± 3	Lupus	0.28	236	2013.1.00220.S
271	V* HW Lup	155 ± 2	Lupus	0.28	236	2013.1.00220.S
272	V* GW Lup	156 ± 1	Lupus	0.02	18	2016.1.00484.L
273	V* HM Lup	156 ± 1	Lupus	0.28	236	2013.1.00220.S
274	CD-35 10525	152 ± 1	Lupus	0.14	45	2013.1.00374.S
275	[L2013] J155140.32-214610.6	142 ± 2	Lupus	0.28	187	2013.1.00395.S
276	2MASS J15521088-2125372	168 ± 8	Lupus	0.28	187	2013.1.00395.S
277	[L2013] J155301.32-211413.7	146 ± 3	Lupus	0.28	187	2013.1.00395.S
278	NAME THA 15-10A	160 ± 2	Lupus	0.28	236	2013.1.00220.S
279	THA 15-12	158 ± 1	Lupus	0.39	59	2013.1.00226.S
280	V* RU Lup	160 ± 2	Lupus	0.02	16	2016.1.00484.L
281	SZ 84	153 ± 2	Lupus	0.28	236	2013.1.00220.S
282	WRAY 15-1400	162 ± 1	Lupus	0.03	15	2016.1.00484.L
283	2MASS J15592523-4235066	147 ± 2	Lupus	0.28	236	2013.1.00220.S

Table A1 – *continued*

ID #	Name[†]	Distance (pc)	Star-forming region	Resolution (arcsec)	Sensitivity (μJy beam^{-1})	ALMA project code
284	V∗ RY Lup	159 ± 2	Lupus	0.14	27	2017.1.00449.S
285	2MASS J16000060-4221567	161 ± 2	Lupus	0.28	236	2013.1.00220.S
286	2MASS J16000236-4222145	164 ± 2	Lupus	0.28	236	2013.1.00220.S
287	2MASS J16002612-4153553	164 ± 3	Lupus	0.60	152	2011.0.00733.S
288	SZ 130	160 ± 1	Lupus	0.28	236	2013.1.00220.S
289	V∗ MY Lup	157 ± 1	Lupus	0.60	152	2011.0.00733.S
290	SZ 131	160 ± 1	Lupus	0.28	236	2013.1.00220.S
291	V∗ MZ Lup	191 ± 4	Lupus	0.39	100	2012.1.00350.S
292	V∗ NO Lup	134 ± 1	Lupus	0.39	100	2012.1.00350.S
293	HD 143675	139 ± 1	Lupus	0.54	56	2015.1.01243.S
294	SZ 133	153 ± 13	Lupus	0.28	250	2013.1.00220.S
295	V∗ HO Lup A	158 ± 1	Lupus	0.28	236	2013.1.00220.S
296	2MASS J16070854-3914075	176 ± 13	Lupus	0.28	236	2013.1.00220.S
297	THA 15-21	160 ± 1	Lupus	0.28	236	2013.1.00220.S
298	THA 15-20	159 ± 2	Lupus	0.13	69	2013.1.00663.S
299	2MASS J16073773-3921388	174 ± 5	Lupus	0.28	236	2013.1.00220.S
300	SZ 95	158 ± 2	Lupus	0.60	174	2011.0.00733.S
301	2MASS J16080017-3902595	160 ± 3	Lupus	0.28	236	2013.1.00220.S
302	SZ 96	157 ± 1	Lupus	0.60	174	2011.0.00733.S
303	2MASS J16081497-3857145	146 ± 19	Lupus	0.28	236	2013.1.00220.S
304	V∗ V1279 Sco	156 ± 1	Lupus	0.28	236	2013.1.00220.S
305	THA 15-24	158 ± 2	Lupus	0.28	236	2013.1.00220.S
306	THA 15-25	159 ± 2	Lupus	0.28	236	2013.1.00220.S
307	THA 15-26	137 ± 3	Lupus	0.28	236	2013.1.00220.S
308	THA 15-30	165 ± 2	Lupus	0.28	236	2013.1.00220.S
309	IRAS 16051-3820	156 ± 1	Lupus	0.28	250	2013.1.00220.S
310	V∗ V856 Sco	161 ± 2	Lupus	0.47	124	2015.1.01600.S
311	V∗ V856 Sco	161 ± 2	Lupus	0.28	236	2013.1.00220.S
312	SZ 107	152 ± 3	Lupus	0.60	152	2011.0.00733.S
313	V∗ V1192 Sco	151 ± 14	Lupus	0.28	236	2013.1.00220.S
314	V∗ V1193 Sco	160 ± 1	Lupus	0.28	236	2013.1.00220.S
315	2MASS J16085373-3914367	134 ± 44	Lupus	0.28	236	2013.1.00220.S
316	THA 15-33	158 ± 1	Lupus	0.28	236	2013.1.00220.S
317	SZ 112	160 ± 2	Lupus	0.60	152	2011.0.00733.S
318	2MASS J16085529-3848481	158 ± 3	Lupus	0.28	236	2013.1.00220.S
319	THA 15-34	163 ± 2	Lupus	0.28	236	2013.1.00220.S
320	2MASS J16090141-3925119	164 ± 2	Lupus	0.60	174	2011.0.00733.S
321	THA 15-35	162 ± 1	Lupus	0.28	236	2013.1.00220.S
322	SZ 115	158 ± 2	Lupus	0.28	236	2013.1.00220.S
323	THA 15-37	159 ± 1	Lupus	0.28	236	2013.1.00220.S
324	SZ 118	164 ± 1	Lupus	0.28	236	2013.1.00220.S
325	SONYC Lup3-29	193 ± 7	Lupus	0.28	236	2013.1.00220.S
326	2MASS J16101307-3846165	145 ± 5	Lupus	0.28	236	2013.1.00220.S
327	2MASS J16101984-3836065	159 ± 3	Lupus	0.28	236	2013.1.00220.S
328	2MASS J16102955-3922144	163 ± 2	Lupus	0.60	181	2011.0.00733.S
329	2MASS J16104536-3854547	5435 ± 3072	Lupus	0.28	236	2013.1.00220.S
330	NAME THA 15-42B	1497 ± 323	Lupus	0.28	236	2013.1.00220.S
331	2MASS J16114865-3817580	1812 ± 263	Lupus	0.28	236	2013.1.00220.S
332	2MASS J16115979-3823383	165 ± 3	Lupus	0.28	236	2013.1.00220.S
333	2MASS J16120445-3809589	4630 ± 14168	Lupus	0.28	250	2013.1.00220.S
334	2MASS J16124373-3815031	160 ± 1	Lupus	0.28	250	2013.1.00220.S
335	2MASS J16134410-3736462	160 ± 2	Lupus	0.28	250	2013.1.00220.S
336	HD 145880	126 ± 1	Lupus	0.54	51	2015.1.01243.S
337	WRAY 15-1443	158 ± 1	Lupus	0.22	925	2011.0.00724.S
338	V1094 Sco	154 ± 1	Lupus	0.17	61	2016.1.01239.S
339	CPD-36 6759	136 ± 1	Lupus	0.35	108	2012.1.00870.S
340	NAME Lupus I	144∗∗	Lupus	0.28	250	2013.1.00220.S
341	2MASS J15450634-3417378	144∗∗	Lupus	0.28	236	2013.1.00220.S
342	[MHR2017] L1S2 9	144∗∗	Lupus	0.28	236	2013.1.00220.S
343	[DB2002b] G339.17+16.08	144∗∗	Lupus	0.28	236	2013.1.00220.S
344	DCld 339.0+15.0	144∗∗	Lupus	0.28	236	2013.1.00220.S
345	RX J1548.1-3515	144∗∗	Lupus	0.28	236	2013.1.00220.S
346	IRAS 15567-4141	144∗∗	Lupus	0.28	236	2013.1.00220.S
347	2MASS J16011549-4152351	144∗∗	Lupus	0.28	250	2013.1.00220.S
348	2MASS J16070384-3911113	144∗∗	Lupus	0.28	236	2013.1.00220.S
349	2MASS J16075475-3915446	144∗∗	Lupus	0.28	236	2013.1.00220.S
350	[G2006] 16	144∗∗	Lupus	0.28	236	2013.1.00220.S
351	2MASS J16080618-3912225	144∗∗	Lupus	0.28	236	2013.1.00220.S
352	[GMM2009] Lupus III 33	197∗∗	Lupus 3	0.28	236	2013.1.00220.S
353	THA 15-27	197∗∗	Lupus 3	0.60	152	2011.0.00733.S
354	[MJS2008] 52	197∗∗	Lupus 3	0.28	236	2013.1.00220.S

Table A1 – *continued*

ID #	Name†	Distance (pc)	Star-forming region	Resolution (arcsec)	Sensitivity (μJy beam⁻¹)	ALMA project code
355	2MASS J16083156-3847292	197∗∗	Lupus 3	0.60	174	2011.0.00733.S
356	[G2006] 72	197∗∗	Lupus 3	0.28	236	2013.1.00220.S
357	[SC95] ZET 14	197∗∗	Lupus 3	0.28	236	2013.1.00220.S
358	2MASS J16085834-3907491	197∗∗	Lupus 3	0.28	236	2013.1.00220.S
359	2MASS J16091644-3904438	197∗∗	Lupus 3	0.28	236	2013.1.00220.S
360	[BPB2012] Lup3 C3	197∗∗	Lupus 3	0.28	236	2013.1.00220.S
361	2MASS J16092032-3904015	197∗∗	Lupus 3	0.28	236	2013.1.00220.S
362	2MASS J16092317-3904074	197∗∗	Lupus 3	0.28	236	2013.1.00220.S
363	2MASS J16092697-3836269	197∗∗	Lupus 3	0.28	250	2013.1.00220.S
364	[MJS2008] 94	197∗∗	Lupus 3	0.28	236	2013.1.00220.S
365	[BPB2012] Lup3 C5	197∗∗	Lupus 3	0.28	236	2013.1.00220.S
366	2MASS J16095399-3923275	197∗∗	Lupus 3	0.60	181	2011.0.00733.S
367	2MASS J16095628-3859518	197∗∗	Lupus 3	0.28	236	2013.1.00220.S
368	2MASS J16102741-3902299	197∗∗	Lupus 3	0.28	236	2013.1.00220.S
369	2MASS J16121120-3832197	197∗∗	Lupus 3	0.28	236	2013.1.00220.S
370	2MASS J16122269-3713276	197∗∗	Lupus 3	0.28	250	2013.1.00220.S
371	WRAY 16-203	422 ± 96∗∗∗	Lupus	0.37	58	2012.1.00857.S
372	2MASS J16164198-3650456	38462 ± 178994∗∗∗	Lupus	0.77	35	2015.1.00791.S
373	2MASS J16232807-4015368	19231 ± 37721∗∗∗	Lupus	0.77	35	2015.1.00791.S
374	V∗ V1003 Oph	117 ± 1	Ophiuchus	0.52	305	2011.0.00531.S
375	Hen 3-1258	124 ± 1	Ophiuchus	0.03	16	2016.1.00484.L
376	EM∗ AS 209	121 ± 1	Ophiuchus	0.15	41	2015.1.00486.S
377	Haro 1-16	146 ± 1	Ophiuchus	0.23	64	2012.1.00158.S
378	2MASS J16230923-2417047	161 ± 1	Ophiuchus	0.13	261	2013.1.00157.S
379	EM∗ SR 21A	138 ± 1	Ophiuchus	0.23	64	2012.1.00158.S
380	[LMW2000] VLA 1623A	133∗∗	Ophiuchus	0.16	21	2015.1.00084.S
381	ROXs 12B	133∗∗	Ophiuchus	0.15	29	2015.1.00773.S
382	ROXs 12B	133∗∗	Ophiuchus	0.66	67	2016.1.01018.S
383	DoAr 26	133∗∗	Ophiuchus	0.30	217	2015.1.00637.S
384	EM∗ SR 24B	133∗∗	Ophiuchus	0.20	34	2013.1.00498.S
385	BKLT J162736-243020	133∗∗	Ophiuchus	0.13	51	2013.1.00100.S
386	[JJK2008] SMM J162740-24431††	133∗∗	Ophiuchus	0.10	48	2016.1.01042.S
387	WLY 2-55	133∗∗	Ophiuchus	0.39	100	2012.1.00350.S
388	GBS-VLA J163115.25-243313.8	133∗∗	Ophiuchus	0.49	45	2016.1.01018.S
389	2MASS J16313124-2426281	133∗∗	Ophiuchus	0.18	19	2016.1.00771.S
390	WSB 71	133∗∗	Ophiuchus	0.30	177	2015.1.00637.S
391	IRAS 16285-2355††	133∗∗	Ophiuchus	0.02	16	2015.1.01512.S
392	NAME IRAS 16293-2422B	133∗∗	Ophiuchus	0.20	21	2013.1.00393.S
393	EM∗ SR 24S	114 ± 5	Ophiuchus	0.14	23	2013.1.00091.S
394	V∗ V1366 Ori	312 ± 5	Orion	0.14	87	2013.1.00658.S
395	HD 36112	160 ± 2	Orion	0.29	87	2015.1.01600.S
396	V∗ V2377 Ori	912 ± 262	Orion	0.43	190	2011.0.00028.S
397	[HHM2007] 81	376 ± 37	Orion	0.24	281	2015.1.00089.S
398	2MASS J05375486-0241092	393 ± 19	Orion	0.24	281	2015.1.00089.S
399	[BZR99] S Ori 35	415 ± 58	Orion	0.24	281	2015.1.00089.S
400	[BZR99] S Ori 12	374 ± 29	Orion	0.24	281	2015.1.00089.S
401	Haro 5-7	236 ± 22	Orion	0.24	281	2015.1.00089.S
402	2MASS J05380097-0226079	349 ± 7	Orion	0.24	281	2015.1.00089.S
403	2MASS J05380552-0235571	354 ± 58	Orion	0.24	281	2015.1.00089.S
404	V∗ V1247 Ori	398 ± 10	Orion	0.01	42	2015.1.00986.S
405	Kiso A-0976 316	397 ± 10	Orion	0.24	281	2015.1.00089.S
406	Kiso A-0904 67	425 ± 8	Orion	0.24	281	2015.1.00089.S
407	HD 294268	374 ± 7	Orion	0.24	281	2015.1.00089.S
408	Kiso A-0976 326	392 ± 11	Orion	0.24	281	2015.1.00089.S
409	2MASS J05382119-0254110	344 ± 16	Orion	0.24	281	2015.1.00089.S
410	[W96] rJ053820-0234	343 ± 19	Orion	0.24	281	2015.1.00089.S
411	V∗ V2725 Ori	378 ± 16	Orion	0.24	281	2015.1.00089.S
412	V∗ V505 Ori	397 ± 6	Orion	0.24	281	2015.1.00089.S
413	V∗ V2728 Ori	339 ± 41	Orion	0.24	281	2015.1.00089.S
414	[BNM2013] 93.03 227	353 ± 18	Orion	0.24	281	2015.1.00089.S
415	Haro 5-9	415 ± 6	Orion	0.24	281	2015.1.00089.S
416	V∗ TX Ori	572 ± 85	Orion	0.24	281	2015.1.00089.S
417	[BNM2013] 93.03 29	402 ± 15	Orion	0.24	281	2015.1.00089.S
418	[W96] rJ053833-0236	385 ± 32	Orion	0.24	281	2015.1.00089.S
419	2MASS J05383902-0245321	428 ± 15	Orion	0.24	281	2015.1.00089.S
420	2MASS J05384053-0233275	372 ± 14	Orion	0.24	281	2015.1.00089.S
421	[BNM2013] 92.01 24	388 ± 12	Orion	0.24	281	2015.1.00089.S
422	2MASS J05384386-0237068	385 ± 13	Orion	0.24	281	2015.1.00089.S
423	V∗ V595 Ori A	212 ± 11	Orion	0.24	281	2015.1.00089.S
424	Mayrit 89175	395 ± 20	Orion	0.24	281	2015.1.00089.S
425	2MASS J05384818-0244007	428 ± 33	Orion	0.24	281	2015.1.00089.S

Table A1 – *continued*

ID #	Name†	Distance (pc)	Star-forming region	Resolution (arcsec)	Sensitivity (μJy beam⁻¹)	ALMA project code
426	∗∗ CAB 27B	502 ± 17	Orion	0.24	281	2015.1.00089.S
427	[BHM2009] SigOri-MAD-34	404 ± 8	Orion	0.24	281	2015.1.00089.S
428	[W96] pJ053847-0234	395 ± 14	Orion	0.24	281	2015.1.00089.S
429	[BZR99] S Ori 15	364 ± 28	Orion	0.24	281	2015.1.00089.S
430	2MASS J05384755-0227120	381 ± 15	Orion	0.24	281	2015.1.00089.S
431	2MASS J05385060-0242429	399 ± 22	Orion	0.24	281	2015.1.00089.S
432	2MASS J05384970-0234526	419 ± 20	Orion	0.24	281	2015.1.00089.S
433	V∗ V2737 Ori	412 ± 52	Orion	0.24	281	2015.1.00089.S
434	V∗ RU Ori	405 ± 5	Orion	0.24	281	2015.1.00089.S
435	2MASS J05385831-0216101	399 ± 7	Orion	0.24	281	2015.1.00089.S
436	ESO-HA 1693	371 ± 12	Orion	0.24	281	2015.1.00089.S
437	2MASS J05390297-0241272	410 ± 14	Orion	0.24	281	2015.1.00089.S
438	2MASS J05390193-0235029	336 ± 23	Orion	0.24	281	2015.1.00089.S
439	Mayrit 458140	450 ± 33	Orion	0.24	281	2015.1.00089.S
440	2MASS J05390387-0220081	347 ± 18	Orion	0.24	281	2015.1.00089.S
441	[BZR99] S Ori 7	332 ± 20	Orion	0.24	281	2015.1.00089.S
442	2MASS J05390878-0231115	335 ± 15	Orion	0.24	281	2015.1.00089.S
443	[BZR99] S Ori 30	339 ± 57	Orion	0.24	281	2015.1.00089.S
444	Haro 5-20	411 ± 7	Orion	0.24	281	2015.1.00089.S
445	[BNM2013] 90.02 146	381 ± 15	Orion	0.24	281	2015.1.00089.S
446	Haro 5-21	402 ± 9	Orion	0.24	281	2015.1.00089.S
447	V∗ BG Ori	384 ± 7	Orion	0.24	281	2015.1.00089.S
448	2MASS J05392633-0228376	370 ± 19	Orion	0.24	281	2015.1.00089.S
449	2MASS J05392935-0227209	387 ± 10	Orion	0.24	281	2015.1.00089.S
450	Haro 5-25	392 ± 5	Orion	0.24	281	2015.1.00089.S
451	V∗ RW Ori	383 ± 20	Orion	0.24	281	2015.1.00089.S
452	V∗ V603 Ori	368 ± 16	Orion	0.24	281	2015.1.00089.S
453	Haro 5-27	395 ± 5	Orion	0.24	281	2015.1.00089.S
454	V∗ RV Ori	398 ± 4	Orion	0.24	281	2015.1.00089.S
455	2MASS J05394318-0232433	363 ± 13	Orion	0.24	281	2015.1.00089.S
456	[BZR99] S Ori 10	413 ± 37	Orion	0.24	281	2015.1.00089.S
457	Haro 5-32	388 ± 10	Orion	0.24	281	2015.1.00089.S
458	Haro 5-30	401 ± 17	Orion	0.24	281	2015.1.00089.S
459	Haro 5-34	407 ± 5	Orion	0.24	281	2015.1.00089.S
460	Mayrit 1045094	435 ± 74	Orion	0.24	281	2015.1.00089.S
461	2MASS J05395421-0227326	382 ± 21	Orion	0.24	281	2015.1.00089.S
462	V∗ V605 Ori B	397 ± 15	Orion	0.24	281	2015.1.00089.S
463	Haro 5-36	373 ± 12	Orion	0.24	281	2015.1.00089.S
464	Mayrit 1196092	635 ± 212	Orion	0.24	281	2015.1.00089.S
465	2MASS J05400525-0230522	354 ± 28	Orion	0.24	281	2015.1.00089.S
466	V∗ V608 Ori	403 ± 6	Orion	0.24	281	2015.1.00089.S
467	2MASS J05400933-0225067	380 ± 21	Orion	0.24	281	2015.1.00089.S
468	Haro 5-38	416 ± 6	Orion	0.24	281	2015.1.00089.S
469	[DRS2009] 2091	450∗	Orion	0.43	190	2011.0.00028.S
470	∗ tet01 Ori F	450∗	Orion	0.43	190	2011.0.00028.S
471	HH 520††	450∗	Orion	0.07	34	2017.1.01478.S
472	[KPM2006] 139	450∗	Orion	0.43	190	2011.0.00028.S
473	ESO-HA 1656	440∗∗	Orionis	0.24	281	2015.1.00089.S
474	2MASS J05381189-0245568	440∗∗	Orionis	0.24	281	2015.1.00089.S
475	2MASS J05381319-0226088	440∗∗	Orionis	0.24	281	2015.1.00089.S
476	2MASS J05381778-0240500	440∗∗	Orionis	0.24	281	2015.1.00089.S
477	V∗ V2726 Ori	440∗∗	Orionis	0.24	281	2015.1.00089.S
478	2XMM J053826.4-023428	440∗∗	Orionis	0.24	281	2015.1.00089.S
479	Mayrit 803197	440∗∗	Orionis	0.24	281	2015.1.00089.S
480	Haro 5-11	440∗∗	Orionis	0.24	281	2015.1.00089.S
481	[W96] rJ053831-0235	440∗∗	Orionis	0.24	281	2015.1.00089.S
482	2MASS J05383976-0232203	440∗∗	Orionis	0.24	281	2015.1.00089.S
483	[BZR99] S Ori 74	440∗∗	Orionis	0.24	281	2015.1.00089.S
484	[BHM2009] SigOri-MAD-2	440∗∗	Orionis	0.24	281	2015.1.00089.S
485	2MASS J05385911-0247133	440∗∗	Orionis	0.24	281	2015.1.00089.S
486	GSC2 S02003215312	440∗∗	Orionis	0.24	281	2015.1.00089.S
487	2MASS J05391427-0221458	440∗∗	Orionis	0.24	281	2015.1.00089.S
488	[HHM2007] 1242	440∗∗	Orionis	0.24	281	2015.1.00089.S
489	2MASS J05395804-0237402	440∗∗	Orionis	0.24	281	2015.1.00089.S
490	IRAS 03292+3039	300∗∗	Perseus	0.15	38	2015.1.01053.S
491	2MASS J17112317-2724315††	130∗∗	Pipe Nebula	0.03	17	2016.1.01186.S
492	HD 98363	139 ± 1	Scorpius-Centaurus Association	0.67	65	2015.1.01243.S
493	HD 131835	134 ± 4	Scorpius-Centaurus Association	0.30	40	2013.1.01166.S
494	CPD-36 6759	136 ± 1	Scorpius-Centaurus Association	0.26	108	2012.1.00870.S
495	HD 139614	135 ± 1	Scorpius-Centaurus Association	0.54	90	2015.1.01600.S
496	HD 141569	111 ± 1	Scorpius-Centaurus Association	0.53	115	2015.1.01600.S

Table A1 – *continued*

ID #	Name†	Distance (pc)	Star-forming region	Resolution (arcsec)	Sensitivity (μJy beam⁻¹)	ALMA project code
497	HD 95086	86 ± 1	Scorpius-Centaurus Association	0.91	14	2013.1.00773.S
498	CD-40 8434	113 ± 1	Scorpius-Centaurus Association	0.08	30	2017.A.00006.S
499	SH 2-68 N	193**	Serpens	0.51	37	2015.1.01478.S
500	[B96] Serpens 2	193**	Serpens	0.13	16	2015.1.00354.S
501	2MASS J18295766+0113045	193**	Serpens	0.51	37	2015.1.01478.S
502	SSTc2d J182959.5+011159	193**	Serpens	0.51	37	2015.1.01478.S
503	[ETC2005] 19	193**	Serpens	0.51	37	2015.1.01478.S
504	IRAS 04158+2805	90 ± 5	Taurus	0.06	92	2016.1.00460.S
505	HD 32297	133 ± 1	Taurus	0.46	21	2015.1.00633.S
506	IRAS 04113+2758	140***	Taurus	0.47	103	2011.0.00150.S
507	IP Tau	131 ± 1	Taurus	0.09	75	2016.1.01164.S
508	MHO 2	133 ± 4	Taurus	0.14	51	2013.1.00498.S
509	2MASS J04141188+2811535	131 ± 3	Taurus	0.25	174	2012.1.00743.S
510	V* FM Tau	132 ± 1	Taurus	0.13	55	2013.1.00426.S
511	[BCG93] 1	136 ± 2	Taurus	0.42	154	2011.0.00259.S
512	V* FP Tau	128 ± 1	Taurus	0.23	113	2012.1.00743.S
513	V* CX Tau	128 ± 1	Taurus	0.13	55	2013.1.00426.S
514	V* FO Tau	157 ± 9	Taurus	0.14	90	2013.1.00105.S
515	2MASS J04161210+2756385	137 ± 2	Taurus	0.23	113	2012.1.00743.S
516	V* CY Tau	129 ± 1	Taurus	0.14	51	2013.1.00498.S
517	2MASS J04181710+2828419	124 ± 5	Taurus	0.23	113	2012.1.00743.S
518	2MASS J04182147+1658470	181 ± 1	Taurus	0.64	150	2012.1.00350.S
519	V* V892 Tau	117 ± 2	Taurus	0.14	51	2013.1.00498.S
520	2MASS J04190110+2819420	119 ± 2	Taurus	0.23	113	2012.1.00743.S
521	WK81 1	132 ± 1	Taurus	0.64	150	2012.1.00350.S
522	2MASS J04202555+2700355	170 ± 5	Taurus	0.23	113	2012.1.00743.S
523	2MASS J04213459+2701388	167 ± 4	Taurus	0.23	113	2012.1.00743.S
524	IRAS 04187+1927	149 ± 2	Taurus	0.92	142	2013.1.00105.S
525	V* DE Tau	127 ± 1	Taurus	0.13	55	2013.1.00426.S
526	2MASS J04230607+2801194	134 ± 2	Taurus	0.25	174	2012.1.00743.S
527	IRAS 04200+2759	139 ± 3	Taurus	0.06	91	2016.1.00460.S
528	[XCR2012] TrES J042423+265008	155 ± 2	Taurus	0.64	150	2012.1.00350.S
529	[BLH2002] KPNO-Tau 3	156 ± 6	Taurus	0.25	174	2012.1.00743.S
530	2MASS J04263055+2443558	119 ± 10	Taurus	0.92	142	2013.1.00105.S
531	CoKu FV Tau c	140 ± 3	Taurus	0.47	159	2011.0.00150.S
532	V* DG Tau††	121 ± 2	Taurus	0.02	12	2015.1.01268.S
533	2MASS J04295950+2433078	131 ± 3	Taurus	0.14	90	2013.1.00105.S
534	V* ZZ Tau	134 ± 5	Taurus	0.92	142	2013.1.00105.S
535	V* HK Tau	133 ± 2	Taurus	0.47	159	2011.0.00150.S
536	V* V710 Tau B	145 ± 1	Taurus	0.14	93	2013.1.00105.S
537	Haro 6-13	130 ± 3	Taurus	0.11	48	2016.1.01042.S
538	2MASS J04321606+1812464	145 ± 2	Taurus	0.14	93	2013.1.00105.S
539	2MASS J04322210+1827426	142 ± 2	Taurus	0.23	113	2012.1.00743.S
540	2MASS J04322415+2251083	155 ± 3	Taurus	0.92	142	2013.1.00105.S
541	V* FZ Tau	130 ± 1	Taurus	0.13	55	2013.1.00426.S
542	JH 112	165 ± 2	Taurus	0.47	108	2011.0.00150.S
543	2MASS J04324938+2253082	165 ± 7	Taurus	0.92	142	2013.1.00105.S
544	V* V1321 Tau	147 ± 1	Taurus	0.64	150	2012.1.00350.S
545	V* V807 Tau	113 ± 8	Taurus	0.14	90	2013.1.00105.S
546	2MASS J04330945+2246487	149 ± 9	Taurus	0.92	142	2013.1.00105.S
547	IRAS 04303+2240	148 ± 6	Taurus	0.92	142	2013.1.00105.S
548	V* GK Tau	129 ± 1	Taurus	0.47	108	2011.0.00150.S
549	V* IS Tau	133 ± 5	Taurus	0.14	90	2013.1.00105.S
550	V* HN Tau	137 ± 3	Taurus	0.47	108	2011.0.00150.S
551	V* DL Tau	159 ± 1	Taurus	0.20	61	2015.1.01207.S
552	2MASS J04334465+2615005	173 ± 6	Taurus	0.24	138	2012.1.00743.S
553	V* DM Tau	145 ± 1	Taurus	0.02	17	2017.1.01460.S
554	V* CI Tau	159 ± 1	Taurus	0.07	52	2017.A.00014.S
555	V* AA Tau	137 ± 2	Taurus	0.19	58	2015.1.01017.S
556	V* HO Tau	161 ± 1	Taurus	0.47	108	2011.0.00150.S
557	V* DN Tau	128 ± 1	Taurus	0.26	57	2015.1.01207.S
558	2MASS J04361030+2159364	118 ± 8	Taurus	0.92	142	2013.1.00105.S
559	2MASS J04362151+2351165	115 ± 2	Taurus	0.92	142	2013.1.00105.S
560	HD 283759	163 ± 2	Taurus	0.64	150	2012.1.00350.S
561	ITG 3	145 ± 15	Taurus	0.25	174	2012.1.00743.S
562	V* GM Tau	138 ± 3	Taurus	0.25	174	2012.1.00743.S
563	V* DO Tau	139 ± 1	Taurus	0.23	41	2015.1.01207.S
564	2MASS J04385859+2336351	127 ± 2	Taurus	0.24	138	2012.1.00743.S
565	2MASS J04390163+2336029	128 ± 1	Taurus	0.24	138	2012.1.00743.S
566	2MASS J04390396+2544264	144 ± 4	Taurus	0.25	175	2012.1.00743.S
567	EM* LkCa 15	159 ± 1	Taurus	0.17	68	2012.1.00870.S

Table A1 – *continued*

ID #	Name[†]	Distance (pc)	Star-forming region	Resolution (arcsec)	Sensitivity (μJy beam^{-1})	ALMA project code
568	V∗ VY Tau	152 ± 3	Taurus	0.14	93	2013.1.00105.S
569	2MASS J04393364+2359212	127 ± 2	Taurus	0.24	138	2012.1.00743.S
570	IRAS F04366+2555	137 ± 2	Taurus	0.24	138	2012.1.00743.S
571	2MASS J04400067+2358211	121 ± 2	Taurus	0.24	138	2012.1.00743.S
572	2MASS J04403979+2519061	152 ± 11	Taurus	0.64	150	2012.1.00350.S
573	NAME JH 223B	141 ± 3	Taurus	0.14	95	2013.1.00105.S
574	ITG 33A	141 ± 4	Taurus	0.14	95	2013.1.00105.S
575	ITG 34	157 ± 6	Taurus	0.14	95	2013.1.00105.S
576	2MASS J04414489+2301513	120 ± 5	Taurus	0.14	95	2013.1.00105.S
577	2MASS J04414825+2534304	136 ± 4	Taurus	0.25	174	2012.1.00743.S
578	V∗ V999 Tau	123 ± 6	Taurus	0.64	150	2012.1.00350.S
579	EM∗ LkHA 332	160 ± 12	Taurus	0.14	93	2013.1.00105.S
580	V∗ GO Tau	145 ± 1	Taurus	0.10	45	2016.1.01164.S
581	Haro 6-36	171 ± 4	Taurus	0.14	95	2013.1.00105.S
582	IRAS S04414+2506	141 ± 3	Taurus	0.42	154	2011.0.00259.S
583	V∗ DR Tau	196 ± 2	Taurus	0.16	107	2016.1.00158.S
584	V∗ DS Tau	159 ± 1	Taurus	0.09	44	2016.1.01164.S
585	V∗ UY Aur	156 ± 1	Taurus	0.47	105	2011.0.00150.S
586	V∗ GM Aur	160 ± 2	Taurus	0.02	15	2017.1.01151.S
587	2MASS J04554535+3019389	155 ± 2	Taurus	0.14	95	2013.1.00105.S
588	V∗ AB Aur	163 ± 2	Taurus	0.14	51	2012.1.00303.S
589	2MASS J04554801+3028050	165 ± 5	Taurus	0.14	95	2013.1.00105.S
590	2MASS J04554969+3019400	156 ± 5	Taurus	0.14	95	2013.1.00105.S
591	2MASS J04560118+3026348	159 ± 9	Taurus	0.14	95	2013.1.00105.S
592	V∗ SU Aur	158 ± 1	Taurus	0.13	55	2013.1.00426.S
593	HD 31648	162 ± 2	Taurus	0.10	45	2016.1.01164.S
594	2MASS J05062332+2432199	151 ± 10	Taurus	0.14	95	2013.1.00105.S
595	2MASS J05075496+2500156	165 ± 2	Taurus	0.24	138	2012.1.00743.S
596	V∗ CQ Tau	163 ± 2	Taurus	0.21	31	2013.1.00498.S
597	HD31648	162 ± 2	Taurus	0.11	45	2016.1.01164.S
598	LDN 1489	140∗∗	Taurus	0.65	116	2011.0.00210.S
599	V∗ CZ Tau	140∗∗	Taurus	0.14	90	2013.1.00105.S
600	V∗ FQ Tau	140∗∗	Taurus	0.47	159	2011.0.00150.S
601	2MASS J04202144+2813491	140∗∗	Taurus	0.06	90	2016.1.00460.S
602	2MASS J04220069+2657324	140∗∗	Taurus	0.06	89	2016.1.00460.S
603	V∗ FS Tau	140∗∗	Taurus	0.14	90	2013.1.00105.S
604	V∗ FV Tau	140∗∗	Taurus	0.47	159	2011.0.00150.S
605	2MASS J04270266+2605304	140∗∗	Taurus	0.11	44	2016.1.01042.S
606	2MASS J04284263+2714039	140∗∗	Taurus	0.23	113	2012.1.00743.S
607	IRAS F04262+2654	140∗∗	Taurus	0.25	174	2012.1.00743.S
608	V∗ DH Tau B	140∗∗	Taurus	0.14	30	2015.1.00773.S
609	V∗ UX Tau	140∗∗	Taurus	0.14	93	2013.1.00105.S
610	V∗ FX Tau	140∗∗	Taurus	0.47	159	2011.0.00150.S
611	V∗ DK Tau	140∗∗	Taurus	0.47	103	2011.0.00150.S
612	V∗ V1213 Tau[††]	140∗∗	Taurus	0.02	13	2017.1.01701.S
613	V∗ HL Tau[††]	140∗∗	Taurus	0.09	36	2013.1.00355.S
614	V∗ XZ Tau	140∗∗	Taurus	0.14	93	2013.1.00105.S
615	NAME HK Tau B	140∗∗	Taurus	0.06	88	2016.1.00460.S
616	V∗ V710 Tau	140∗∗	Taurus	0.47	108	2011.0.00150.S
617	V∗ GG Tau	140∗∗	Taurus	0.14	93	2013.1.00105.S
618	V∗ GH Tau	140∗∗	Taurus	0.14	90	2013.1.00105.S
619	IRAS 04302+2247	140∗∗	Taurus	0.06	86	2016.1.00460.S
620	V∗ IT Tau	140∗∗	Taurus	0.47	108	2011.0.00150.S
621	NAME CoKu Tau 3	140∗∗	Taurus	0.47	162	2011.0.00150.S
622	Haro 6-28	140∗∗	Taurus	0.14	93	2013.1.00105.S
623	V∗ HV Tau C	140∗∗	Taurus	0.06	91	2016.1.00460.S
624	V∗ GN Tau	140∗∗	Taurus	0.14	93	2013.1.00105.S
625	IRAS 04365+2535	140∗∗	Taurus	0.75	89	2011.0.00210.S
626	[BCK99] HCl 2 NW-7a	140∗∗	Taurus	0.42	154	2011.0.00259.S
627	LDN 1527	140∗∗	Taurus	0.75	89	2011.0.00210.S
628	ITG 40	140∗∗	Taurus	0.14	95	2013.1.00105.S
629	V∗ DP Tau	140∗∗	Taurus	0.14	93	2013.1.00105.S
630	Haro 6-37	140∗∗	Taurus	0.14	93	2013.1.00105.S
631	2MASS J04555605+3036209	140∗∗	Taurus	0.24	138	2012.1.00743.S
632	IRAS 05022+2527	140∗∗	Taurus	0.47	45	2011.0.00150.S
633	HD 282276	492 ± 12∗∗∗	Taurus	0.64	150	2012.1.00350.S
634	V∗ V1322 Tau	463 ± 13∗∗∗	Taurus	0.64	150	2012.1.00350.S
635	RY Tau	442 ± 47∗∗∗	Taurus	0.02	44	2017.1.01460.S
636	2MASS J10455263-2819303	84 ± 1	TW Hya Association	1.04	50	2013.1.00457.S
637	V∗ TW Hya	60 ± 1	TW Hya Association	0.04	11	2017.1.00520.S
638	2MASS J11064461-3715115	101 ± 4	TW Hya Association	1.03	29	2013.1.00457.S

Table A1 – *continued*

ID #	Name†	Distance (pc)	Star-forming region	Resolution (arcsec)	Sensitivity (μJy beam⁻¹)	ALMA project code
639	TWA 37	50 ± 1	TW Hya Association	1.04	50	2013.1.00457.S
640	TWA 30	48 ± 1	TW Hya Association	1.04	51	2013.1.00457.S
641	TWA 30B	46 ± 1	TW Hya Association	1.04	51	2013.1.00457.S
642	TWA 33	49 ± 1	TW Hya Association	1.03	29	2013.1.00457.S
643	TWA 38	80 ± 1	TW Hya Association	0.99	39	2013.1.00457.S
644	TWA 31	81 ± 1	TW Hya Association	1.04	51	2013.1.00457.S
645	TWA 27	64 ± 1	TW Hya Association	0.28	36	2013.1.01016.S
646	TWA 40	67 ± 4	TW Hya Association	0.99	39	2013.1.00457.S
647	HD 109573	72 ± 1	TW Hya Association	0.17	39	2015.1.00032.S
648	HD 109832	108 ± 1	TW Hya Association	0.67	60	2015.1.01243.S
649	TWA 29	83 ± 3	TW Hya Association	0.92	39	2013.1.00457.S
650	2MASS J12474428-3816464	85 ± 3	TW Hya Association	0.99	39	2013.1.00457.S
651	2MASS J12520989-4948280	116 ± 4	TW Hya Association	0.92	39	2013.1.00457.S
652	2MASS J13265348-5022270	107 ± 7	TW Hya Association	0.92	39	2013.1.00457.S
653	EC 13436-1335	88 ± 1	TW Hya Association	0.69	43	2015.1.00783.S
654	HE 1350-1612	109 ± 2	TW Hya Association	0.69	43	2015.1.00783.S
655	TWA 32	50**	TW Hya Association	0.99	39	2013.1.00457.S
656	HD 98800††	50**	TW Hya Association	0.10	33	2016.1.01042.S
657	TWA 34	61 ± 1	TW Hya Association	1.04	50	2013.1.00457.S
658	V∗ V419 Hya	22 ± 1	TW Hya Association	0.40	29	2016.1.00104.S
659	V∗ CE Ant††	34 ± 1	TW Hya Association	0.10	33	2015.1.01015.S
660	∗ eps Eri	3 ± 1	Ursa Major Moving Group	1.04	30	2013.1.00645.S
661	Haro 1-5	140**	Upper Scorpius	0.30	172	2015.1.00637.S
662	UCAC2 23646111	136 ± 3	Upper Scorpius	0.30	204	2013.1.00395.S
663	ScoPMS 8b	125 ± 2	Upper Scorpius	0.28	187	2013.1.00395.S
664	HD 142506	144 ± 1	Upper Scorpius	0.28	186	2013.1.00395.S
665	DENIS J155556.0-204518	146 ± 5	Upper Scorpius	0.37	161	2012.1.00743.S
666	UScoCTIO 113	140 ± 5	Upper Scorpius	0.37	161	2012.1.00743.S
667	[PBB2002] USco J155624.8-222555	141 ± 2	Upper Scorpius	0.46	392	2011.0.00526.S
668	HD 142666	148 ± 1	Upper Scorpius	0.20	34	2013.1.00498.S
669	[PBB2002] USco J155706.4-220606	158 ± 3	Upper Scorpius	0.46	254	2011.0.00526.S
670	CD-23 12602	143 ± 1	Upper Scorpius	0.28	186	2013.1.00395.S
671	RX J155829.5-231026	148 ± 3	Upper Scorpius	0.46	392	2011.0.00526.S
672	HD 143006	166 ± 4	Upper Scorpius	0.40	62	2015.1.00964.S
673	2MASS J15584772-1757595	139 ± 1	Upper Scorpius	0.30	204	2013.1.00395.S
674	UScoCTIO 128	140 ± 7	Upper Scorpius	0.37	161	2012.1.00743.S
675	2MASS J16001330-2418106	146 ± 1	Upper Scorpius	0.28	186	2013.1.00395.S
676	UCAC3 135-174588	149 ± 2	Upper Scorpius	0.28	186	2013.1.00395.S
677	[PBB2002] USco J160018.4-223011	138 ± 8	Upper Scorpius	0.28	186	2013.1.00395.S
678	2MASS J16014157-2111380	145 ± 2	Upper Scorpius	0.30	204	2013.1.00395.S
679	RX J1602.0-2221	145 ± 2	Upper Scorpius	0.28	186	2013.1.00395.S
680	[PBB2002] USco J160207.5-225746	140 ± 1	Upper Scorpius	0.28	186	2013.1.00395.S
681	EPIC 204607034	142 ± 3	Upper Scorpius	0.29	188	2013.1.00395.S
682	UScoCTIO 45	96 ± 3	Upper Scorpius	0.37	161	2012.1.00743.S
683	RX J1602.8-2401B	144 ± 1	Upper Scorpius	0.28	186	2013.1.00395.S
684	UScoCTIO 59	144 ± 3	Upper Scorpius	0.29	188	2013.1.00395.S
685	2MASS J16031329-2112569	143 ± 2	Upper Scorpius	0.29	188	2013.1.00395.S
686	2MASS J16032225-2413111	144 ± 3	Upper Scorpius	0.28	186	2013.1.00395.S
687	2MASS J16035767-2031055	143 ± 1	Upper Scorpius	0.50	246	2011.0.00526.S
688	[PGZ2001] J160357.9-194210	158 ± 2	Upper Scorpius	0.30	204	2013.1.00395.S
689	EPIC 205037578	161 ± 2	Upper Scorpius	0.30	204	2013.1.00395.S
690	2MASS J16042165-2130284	150 ± 1	Upper Scorpius	0.16	46	2015.1.00888.S
691	[PGZ2001] J160439.1-194245	151 ± 2	Upper Scorpius	0.30	204	2013.1.00395.S
692	2MASS J16050231-1941554	158 ± 3	Upper Scorpius	0.30	204	2013.1.00395.S
693	2MASS J16052459-1954419	153 ± 2	Upper Scorpius	0.30	204	2013.1.00395.S
694	[PGZ2001] J160525.5-203539	143 ± 3	Upper Scorpius	0.46	254	2011.0.00526.S
695	[PGZ2001] J160532.1-193315	154 ± 3	Upper Scorpius	0.46	254	2011.0.00526.S
696	[PGZ2001] J160545.4-202308	145 ± 2	Upper Scorpius	0.30	204	2013.1.00395.S
697	2MASS J16055863-1949029	149 ± 2	Upper Scorpius	0.30	204	2013.1.00395.S
698	DENIS J160603.9-205644	137 ± 5	Upper Scorpius	0.37	161	2012.1.00743.S
699	2MASS J16061330-2212537	140 ± 2	Upper Scorpius	0.29	188	2013.1.00395.S
700	[PGZ2001] J160622.8-201124	151 ± 2	Upper Scorpius	0.43	135	2011.0.00526.S
701	2MASS J16063539-2516510	139 ± 3	Upper Scorpius	0.28	186	2013.1.00395.S
702	2MASS J16064115-2517044	149 ± 2	Upper Scorpius	0.28	186	2013.1.00395.S
703	2MASS J16064102-2455489	152 ± 3	Upper Scorpius	0.28	186	2013.1.00395.S
704	[PGZ2001] J160643.8-190805	144 ± 7	Upper Scorpius	0.50	246	2011.0.00526.S
705	[PGZ2001] J160700.1-203309	139 ± 2	Upper Scorpius	0.30	199	2013.1.00395.S
706	1RXS J160708.6-192737	146 ± 2	Upper Scorpius	0.30	199	2013.1.00395.S
707	[PGZ2001] J160719.7-202055	164 ± 3	Upper Scorpius	0.30	199	2013.1.00395.S
708	EPIC 203889938	143 ± 2	Upper Scorpius	0.28	186	2013.1.00395.S
709	[PGZ2001] J160739.4-191747	137 ± 1	Upper Scorpius	0.30	199	2013.1.00395.S

Table A1 – *continued*

ID #	Name†	Distance (pc)	Star-forming region	Resolution (arcsec)	Sensitivity (μJy beam⁻¹)	ALMA project code
710	EPIC 204830786	198 ± 8	Upper Scorpius	0.29	188	2013.1.00395.S
711	2MASS J16080555-2218070	143 ± 1	Upper Scorpius	0.29	188	2013.1.00395.S
712	2MASS J16081566-2222199	140 ± 2	Upper Scorpius	0.29	188	2013.1.00395.S
713	[T64] 3	138 ± 1	Upper Scorpius	0.50	246	2011.0.00526.S
714	2MASS J16083455-2211559	136 ± 3	Upper Scorpius	0.29	188	2013.1.00395.S
715	2MASS J16084894-2400045	145 ± 2	Upper Scorpius	0.28	186	2013.1.00395.S
716	[PGZ2001] J160900.7-190852	138 ± 1	Upper Scorpius	0.43	135	2011.0.00526.S
717	[PBB2002] USco J160900.0-190836	139 ± 3	Upper Scorpius	0.43	135	2011.0.00526.S
718	[PBB2002] USco J160935.6-182822	165 ± 3	Upper Scorpius	0.30	199	2013.1.00395.S
719	2MASS J16094098-2217594	146 ± 1	Upper Scorpius	0.29	188	2013.1.00395.S
720	[PBB2002] USco J160953.6-175446	158 ± 5	Upper Scorpius	0.30	199	2013.1.00395.S
721	[PGZ2001] J160954.4-190654	137 ± 1	Upper Scorpius	0.30	199	2013.1.00395.S
722	[PGZ2001] J160959.4-180009	136 ± 2	Upper Scorpius	0.46	392	2011.0.00526.S
723	DENIS J161005.4-191936	150 ± 7	Upper Scorpius	0.37	161	2012.1.00743.S
724	K2-33	140 ± 2	Upper Scorpius	0.30	199	2013.1.00395.S
725	EPIC 203756600	156 ± 4	Upper Scorpius	0.28	186	2013.1.00395.S
726	ScoPMS 42b	134 ± 1	Upper Scorpius	0.30	199	2013.1.00395.S
727	[PBB2002] USco J161028.1-191043	151 ± 3	Upper Scorpius	0.30	199	2013.1.00395.S
728	[PGZ2001] J161039.5-191652	159 ± 2	Upper Scorpius	0.30	199	2013.1.00395.S
729	GSC 06213-01459	140 ± 1	Upper Scorpius	0.29	188	2013.1.00395.S
730	2MASS J16104636-1840598	143 ± 3	Upper Scorpius	0.30	199	2013.1.00395.S
731	UCAC2 23893922	155 ± 2	Upper Scorpius	0.30	199	2013.1.00395.S
732	1RXS J161115.1-175741	137 ± 1	Upper Scorpius	0.30	199	2013.1.00395.S
733	ScoPMS 45	137 ± 1	Upper Scorpius	0.30	199	2013.1.00395.S
734	2MASS J16115091-2012098	152 ± 4	Upper Scorpius	0.30	199	2013.1.00395.S
735	2MASS J16122737-2009596	147 ± 4	Upper Scorpius	0.30	199	2013.1.00395.S
736	[T64] 6	139 ± 2	Upper Scorpius	0.30	199	2013.1.00395.S
737	[PBB2002] USco J161248.9-180052	158 ± 2	Upper Scorpius	0.30	199	2013.1.00395.S
738	HD 145655	152 ± 1	Upper Scorpius	0.29	188	2013.1.00395.S
739	EPIC 205165965	137 ± 2	Upper Scorpius	0.30	199	2013.1.00395.S
740	HD 145718	153 ± 2	Upper Scorpius	0.72	79	2015.1.01600.S
741	[T64] 7	143 ± 3	Upper Scorpius	0.43	135	2011.0.00526.S
742	EPIC 205188906	141 ± 2	Upper Scorpius	0.30	199	2013.1.00395.S
743	[PGZ2001] J161433.6-190013	142 ± 2	Upper Scorpius	0.30	199	2013.1.00395.S
744	RX J1614.6-1858	101 ± 1	Upper Scorpius	0.39	100	2012.1.00350.S
745	2MASS J16145918-2750230	149 ± 1	Upper Scorpius	0.28	186	2013.1.00395.S
746	EPIC 203770673	159 ± 3	Upper Scorpius	0.29	188	2013.1.00395.S
747	EPIC 203938167	154 ± 3	Upper Scorpius	0.29	188	2013.1.00395.S
748	GSC 06209-00747	132 ± 2	Upper Scorpius	0.30	199	2013.1.00395.S
749	EPIC 203664569	163 ± 1	Upper Scorpius	0.29	188	2013.1.00395.S
750	2MASS J16181904-2028479	138 ± 2	Upper Scorpius	0.29	188	2013.1.00395.S
751	2MASS J16214199-2313432	139 ± 2	Upper Scorpius	0.37	161	2012.1.00743.S
752	GSC 06214-00210	109 ± 1	Upper Scorpius	0.29	188	2013.1.00395.S
753	2MASS J16220961-1953005	138 ± 2	Upper Scorpius	0.64	152	2011.0.00733.S
754	2MASS J16223757-2345508	137 ± 1	Upper Scorpius	0.39	100	2012.1.00350.S
755	CD-22 11523	140 ± 1	Upper Scorpius	0.29	188	2013.1.00395.S
756	HD 147594	134 ± 1	Upper Scorpius	0.29	188	2013.1.00395.S
757	2MASS J16251469-2456069	136 ± 1	Upper Scorpius	0.39	100	2012.1.00350.S
758	GSS 31	138 ± 2	Upper Scorpius	0.30	177	2015.1.00637.S
759	BKLT J162620-240854	136 ± 1	Upper Scorpius	0.30	217	2015.1.00637.S
760	Elia 2-24	136 ± 2	Upper Scorpius	0.20	34	2013.1.00498.S
761	GSS 39	116 ± 13	Upper Scorpius	0.20	34	2013.1.00498.S
762	[GY92] 204	142 ± 3	Upper Scorpius	0.42	295	2011.0.00259.S
763	2MASS J16270942-2148457	140 ± 3	Upper Scorpius	0.29	188	2013.1.00395.S
764	YLW 58	137 ± 3	Upper Scorpius	0.10	48	2016.1.01042.S
765	2MASS J16303390-2428062	151 ± 3	Upper Scorpius	0.29	188	2013.1.00395.S
766	HD 163296	101 ± 1	Upper Scorpius	0.17	138	2015.1.00847.S
767	DoAr 25	138 ± 1	Upper Scorpius	0.03	18	2016.1.00484.L
768	Elia 2-20††	138 ± 4	Upper Scorpius	0.02	15	2016.1.00484.L
769	EM∗ SR 4	135 ± 1	Upper Scorpius	0.02	15	2016.1.00484.L
770	V∗ V1094 Sco	154 ± 1	Upper Scorpius	0.24	61	2016.1.01239.S
771	UScoCTIO 13	140∗∗	Upper Scorpius	0.46	392	2011.0.00526.S
772	[PBB2002] USco J160140.8-225810	140∗∗	Upper Scorpius	0.28	186	2013.1.00395.S
773	[PBB2002] USco J160202.9-223613	140∗∗	Upper Scorpius	0.28	186	2013.1.00395.S
774	2MASS J16052661-1957050	140∗∗	Upper Scorpius	0.30	204	2013.1.00395.S
775	[PGZ2001] J160600.6-195711	140∗∗	Upper Scorpius	0.43	135	2011.0.00526.S
776	ScoPMS 31	140∗∗	Upper Scorpius	0.50	246	2011.0.00526.S
777	[PGZ2001] J160702.1-201938	140∗∗	Upper Scorpius	0.46	254	2011.0.00526.S
778	2MASS J16072747-2059442	140∗∗	Upper Scorpius	0.29	188	2013.1.00395.S
779	[PGZ2001] J160827.5-194904	140∗∗	Upper Scorpius	0.43	135	2011.0.00526.S
780	RX J1609.5-2105B	140∗∗	Upper Scorpius	0.15	29	2015.1.00773.S

Table A1 *– continued*

ID #	Name[†]	Distance (pc)	Star-forming region	Resolution (arcsec)	Sensitivity (μJy beam^{-1})	ALMA project code
781	ScoPMS 42a	140**	Upper Scorpius	0.30	199	2013.1.00395.S
782	V* V866 Sco	140**	Upper Scorpius	0.52	305	2011.0.00531.S
783	UCAC2 24372422	140**	Upper Scorpius	0.39	100	2012.1.00350.S
784	EPIC 203750883	140**	Upper Scorpius	0.28	186	2013.1.00395.S
785	2MASS J16135434-2320342	140**	Upper Scorpius	0.29	188	2013.1.00395.S
786	CD-22 11432	140**	Upper Scorpius	0.43	135	2011.0.00526.S
787	V* VV Sco	140**	Upper Scorpius	0.29	188	2013.1.00395.S
788	DENIS J161816.2-261908	140**	Upper Scorpius	0.29	188	2013.1.00395.S
789	WSB 4	140**	Upper Scorpius	0.30	217	2015.1.00637.S
790	DENIS J161939.8-214535	140**	Upper Scorpius	0.37	161	2012.1.00743.S
791	WSB 18	140**	Upper Scorpius	0.30	221	2015.1.00637.S
792	GSS 26[††]	140**	Upper Scorpius	0.10	48	2016.1.01042.S
793	* zet02 Ret	12 ± 1	ζ Herculis Moving Group	2.74	167	2017.1.00786.S

Notes.

[†]The name of each object given here can be queried in data bases such as *SIMBAD*. An alternative name for each object may have been used on the ALMA Archive, in which case the project code should also be used to find the object.

[††]These observations meet both the resolution and sensitivity limits to justify having substructure (See Section 7.1). Some were discarded from our sample due to our selection criteria (see Section 2).

*These sources have no associated *Gaia* distances and their distance was obtained from literature measurements. V* RW Aur, HD 98800, * Alf PsA and* Bet Leo (van Leeuwen 2007), EM* AS 220 (Gaia Collaboration 2016), 2MASS J18191220−2047297 (Maud et al. 2015), IRAS 13481−6124 (Fontani et al. 2005).

**These sources have no associated *Gaia* distance, nor individual distance estimate. Therefore, we approximate the distance by using the distance to its association.
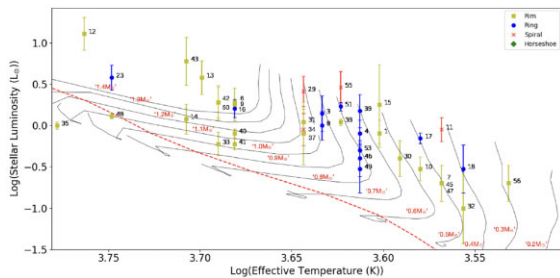
***These sources have been attributed to belonging to the associated star-forming region. The updated *Gaia* distances, however, put this into question.
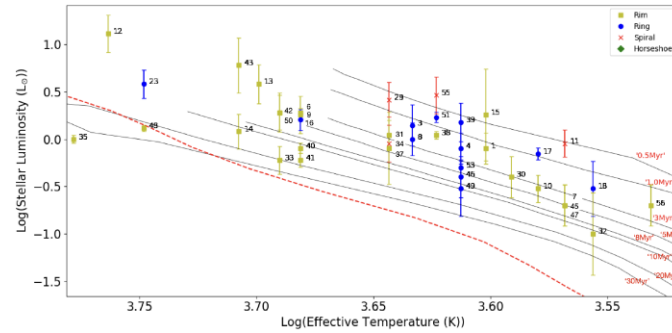
Figure B1. An HR diagram of the low-mass ($<1.4M_\odot$) sources studied in this work. The red dashed line marks the ZAMS using the model of Siess et al. (2000). Stellar tracks for a range of ages have been overplotted as black lines from the models of Baraffe et al. (2015). The discs have been labelled and their identities can be found in Table 1.

## APPENDIX B: STELLAR MASS AND AGE DETERMINATIONS

Figs B1 to B4 display the HR diagram shown in Fig. 4 with the addition of stellar tracks from the models of Baraffe et al. (2015) and Siess et al. (2000). These evolutionary diagrams have been used to determine the stellar masses and ages of the sources in our sample, the values of which can be found in Tables 1 and 2, respectively. The following plots and tables can be found online.

We compare the derived ages to the average age of the star-forming region each object belongs to. The ages of each star-forming region can be found online in Table B1.

Figure B2. An HR diagram of the low-mass ($<1.4M_\odot$) sources studied in this work. The red dashed line marks the ZAMS using the model of Siess et al. (2000). Stellar tracks for a range of masses have been overplotted as black lines from the models of Baraffe et al. (2015). The discs have been labelled and their identities can be found in Table 1.
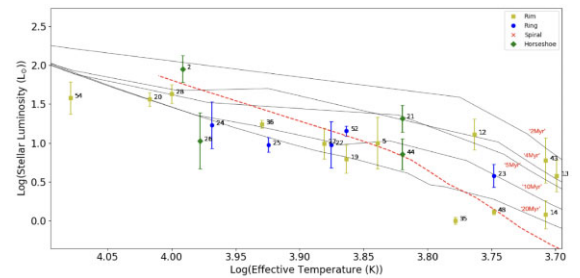
Figure B3. An HR diagram of the high-mass ($>1.4M_\odot$) sources studied in this work. The red dashed line marks the ZAMS using the model of Siess et al. (2000). Stellar tracks for a range of ages have been overplotted as black lines from the models of Siess et al. (2000). The discs have been labelled and their identities can be found in Table 1.
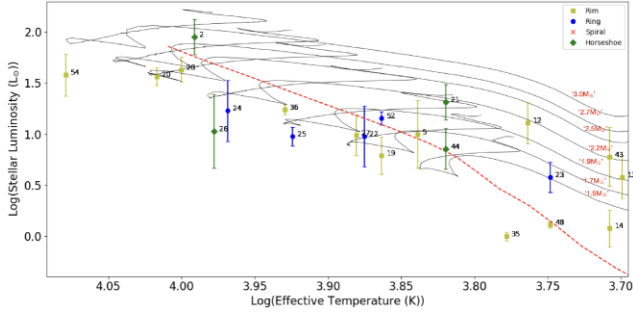
Figure B4. An HR diagram of the high-mass ($>1.4M_\odot$) sources studied in this work. The red dashed line marks the ZAMS using the model of Siess et al. (2000). Stellar tracks for a range of masses have been overplotted as black lines from the models of Siess et al. (2000). The discs have been labelled and their identities can be found in Table 1.

**Table B1.** Average age of nearby star-forming regions used to compare the ages derived in Section 4.1.

SFR	Age (Myr)	Reference
Beta Pic	22 ± 3	(1)
Chamaeleon	3–4	(2)
Corona Australis	9 ± 4	(3)
Lower Centaurus Crux	16	(4)
Lupus	3	(5)
Ophiuchus	2–5	(6)
Orion A	1–3	(7)
Orion OB1	5	(8)
Taurus	1–5	(9)
TW Hya	10 ± 3	(10)
Upper Scorpius	5	(4)

Note. References: (1) Mamajek & Bell (2014), (2) Luhman (2007), (3) James et al. (2006), (4) Preibisch & Mamajek (2008), (5) Alcalá et al. (2017), (6) Wilking, Gagné & Allen (2008), (7) Da Rio et al. (2010), (8) Caballero & Solano (2008), (9) Kraus & Hillenbrand (2009), (10) Bell, Mamajek & Naylor (2015)

APPENDIX C: CATALOGUE OF PROTOPLANETARY DISCS STUDIED

Figs C1 to C4 display the full catalogues of discs investigated in this work. Figs C1 to C4, respectively, show the rim, ring, horseshoe, and spiral class discs, with the discs within each class ordered by their stellar age. These images were discussed in Section 6.2. All figures in Appendix C can be found online.

Figs C5 to C8, respectively, show the rim, ring, horseshoe, and spiral class discs, with the discs within each class ordered by their stellar mass.
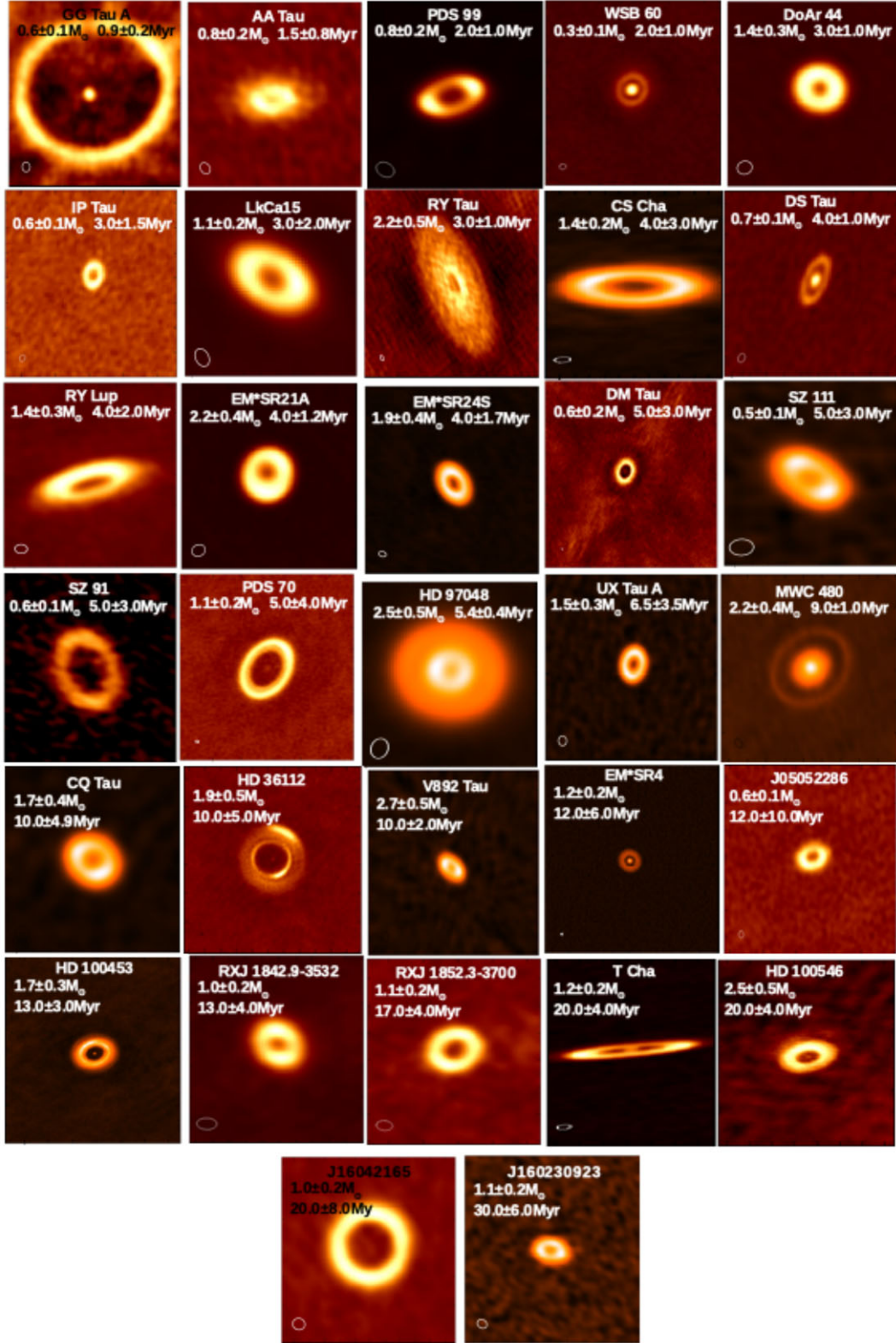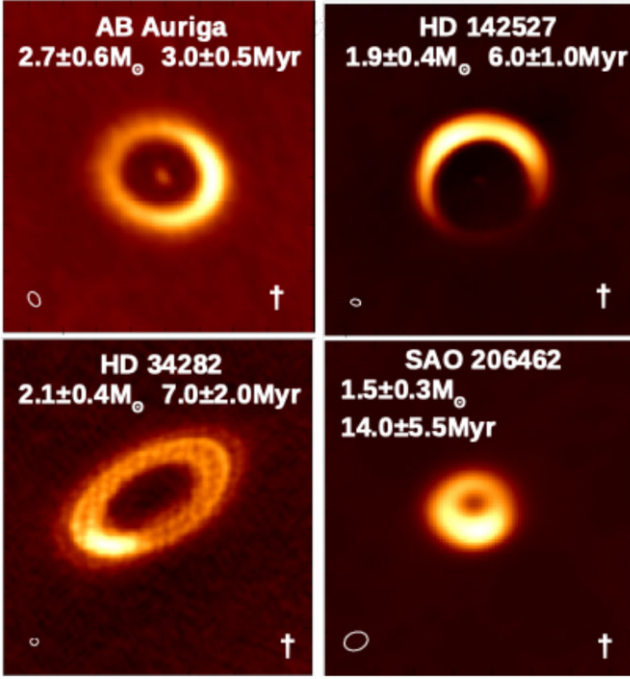
Figure C1. Images of the protoplanetary discs classified as Rims in this study. The discs are ordered by age with the top left (Elias 2-20) being the youngest and the lower right (J160230923) showing the oldest. The beam sizes used in each observation can be seen in the lower left of each image. All discs have been scaled to 500 × 500 au with the exception of the discs labelled with a † in the lower right. These discs have been scaled to 1000 × 1000 au.
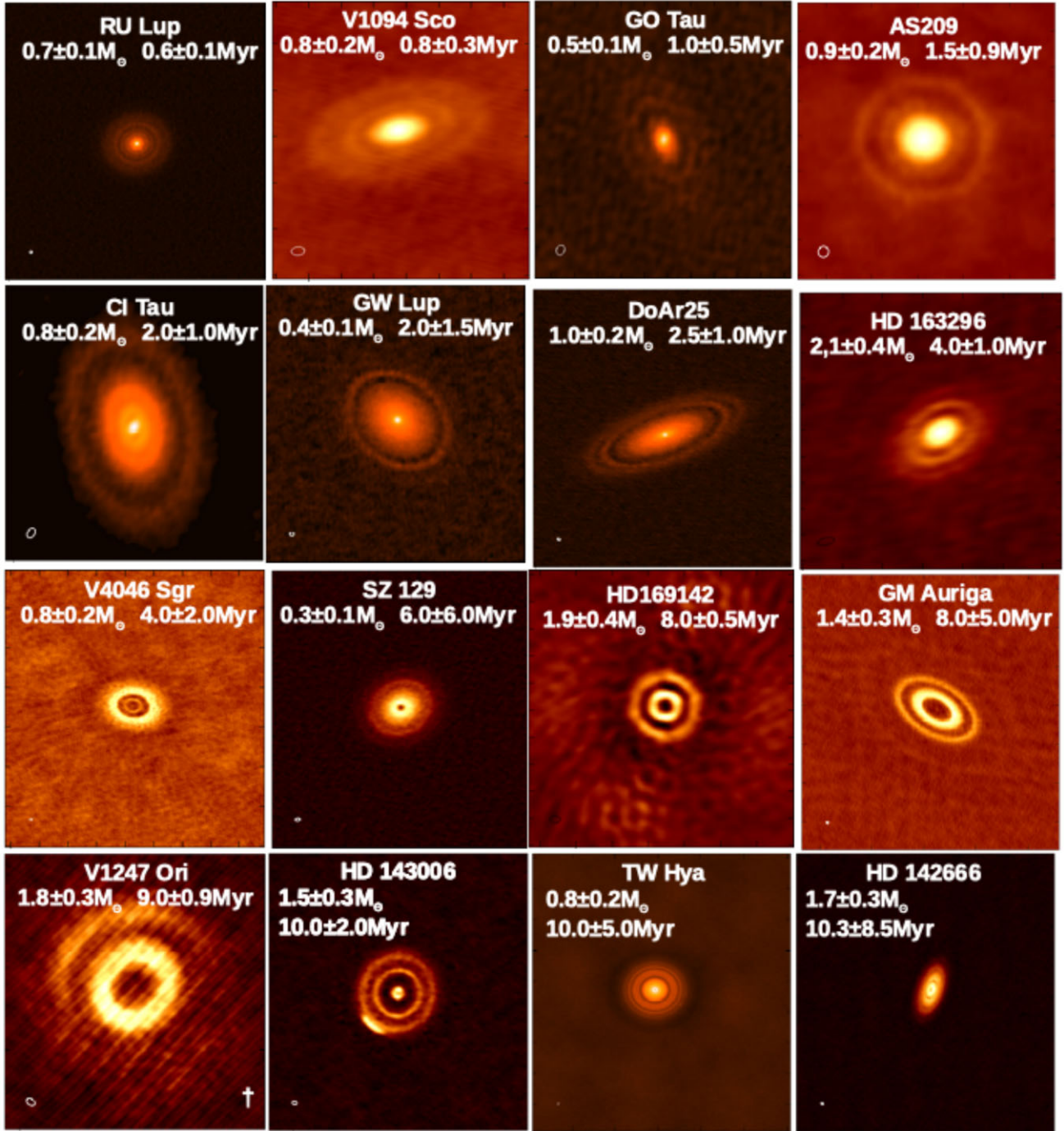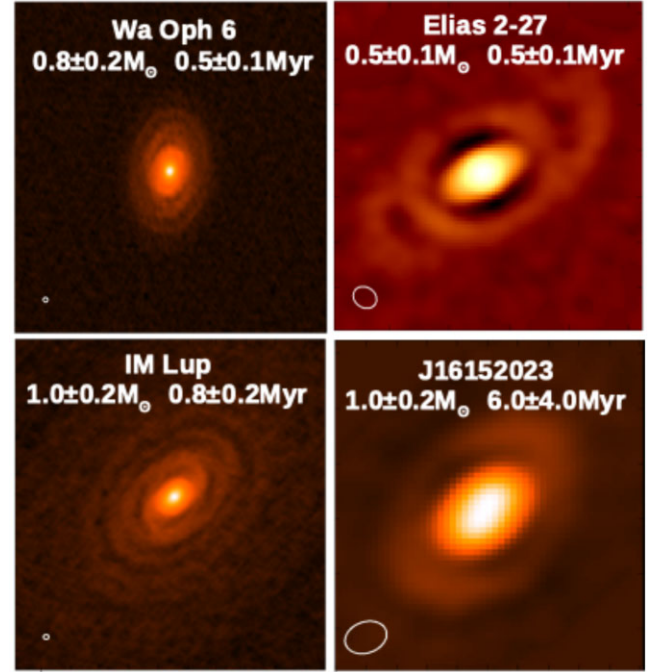
**Figure C2.** Images of the protoplanetary discs classified as Rings in this study. The discs are ordered by age with the top left (RU LUP) being the youngest and the lower right (HD 142666) showing the oldest. The beam sizes used in each observation can be seen in the lower left of each image. All discs have been scaled to 500 × 500 au with the exception of the discs labelled with a † in the lower right. These discs have been scaled to 1000 × 1000 au.

Figure C3. Images of the protoplanetary discs classified as Horseshoe in this study. The discs are ordered by age with the top left (AB Auriga) being the youngest and the lower right (HD100546) showing the oldest. The beam sizes used in each observation can be seen in the lower left of each image. The discs with the † in the lower right have been scaled to 1000 × 1000 au.


Figure C4. Images of the protoplanetary discs classified as Spiral in this study. The discs are ordered by age with the top left (Wa Oph 6) being the youngest and the lower right (J16152023) showing the oldest. The beam sizes used in each observation can be seen in the lower left of each image.
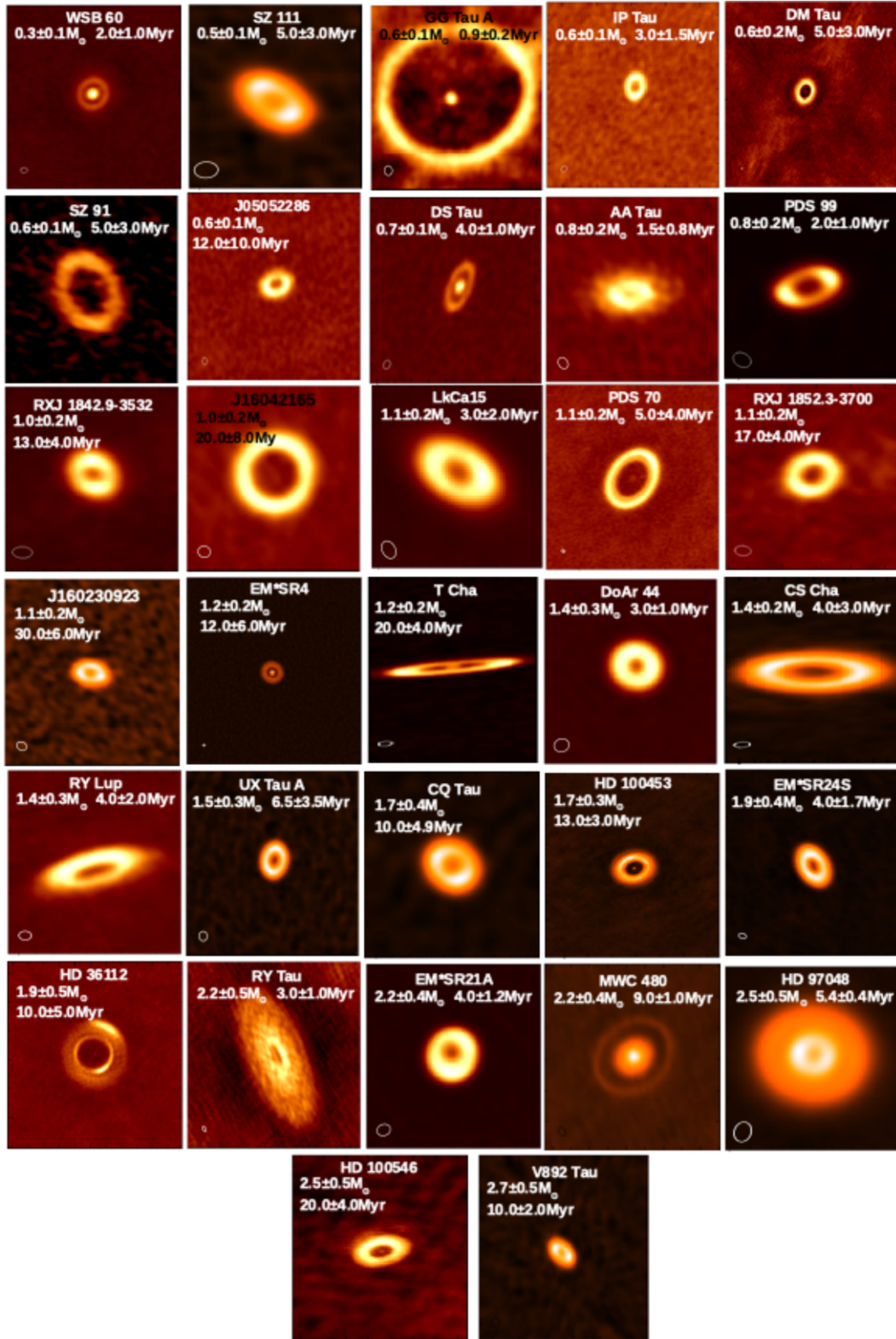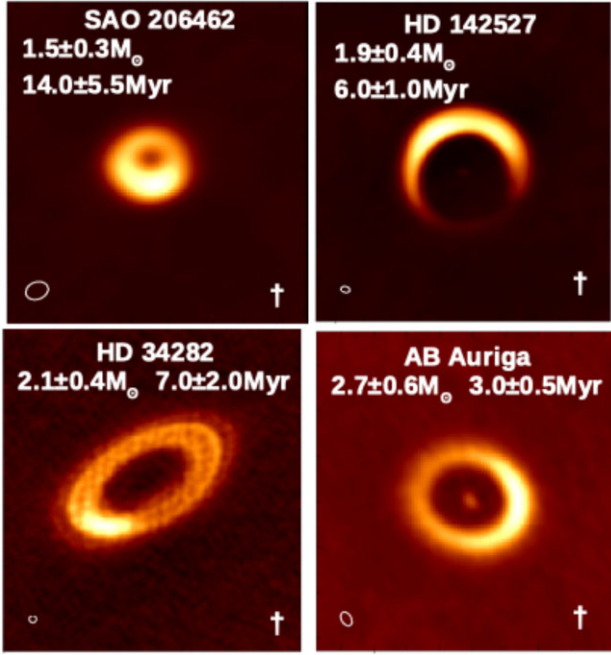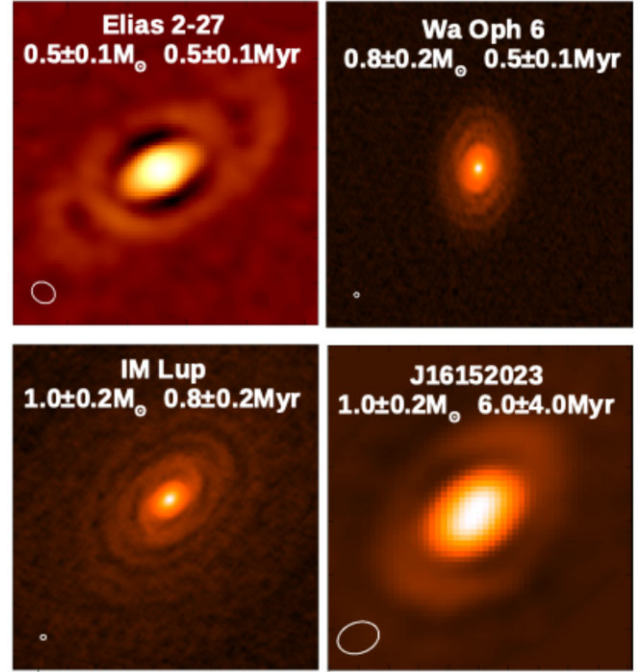
Figure C5. The Rim protoplanetary discs have been ordered according to stellar mass. WSB 60 has the lowest stellar mass of $M_* = 0.3_{\odot}$, while RY Tau has a stellar mass of $M_* \, 3.0_{\odot}$. All discs have been scaled to 500×500 au. The discs with the † in the lower right have been scaled to 1000×1000 au.
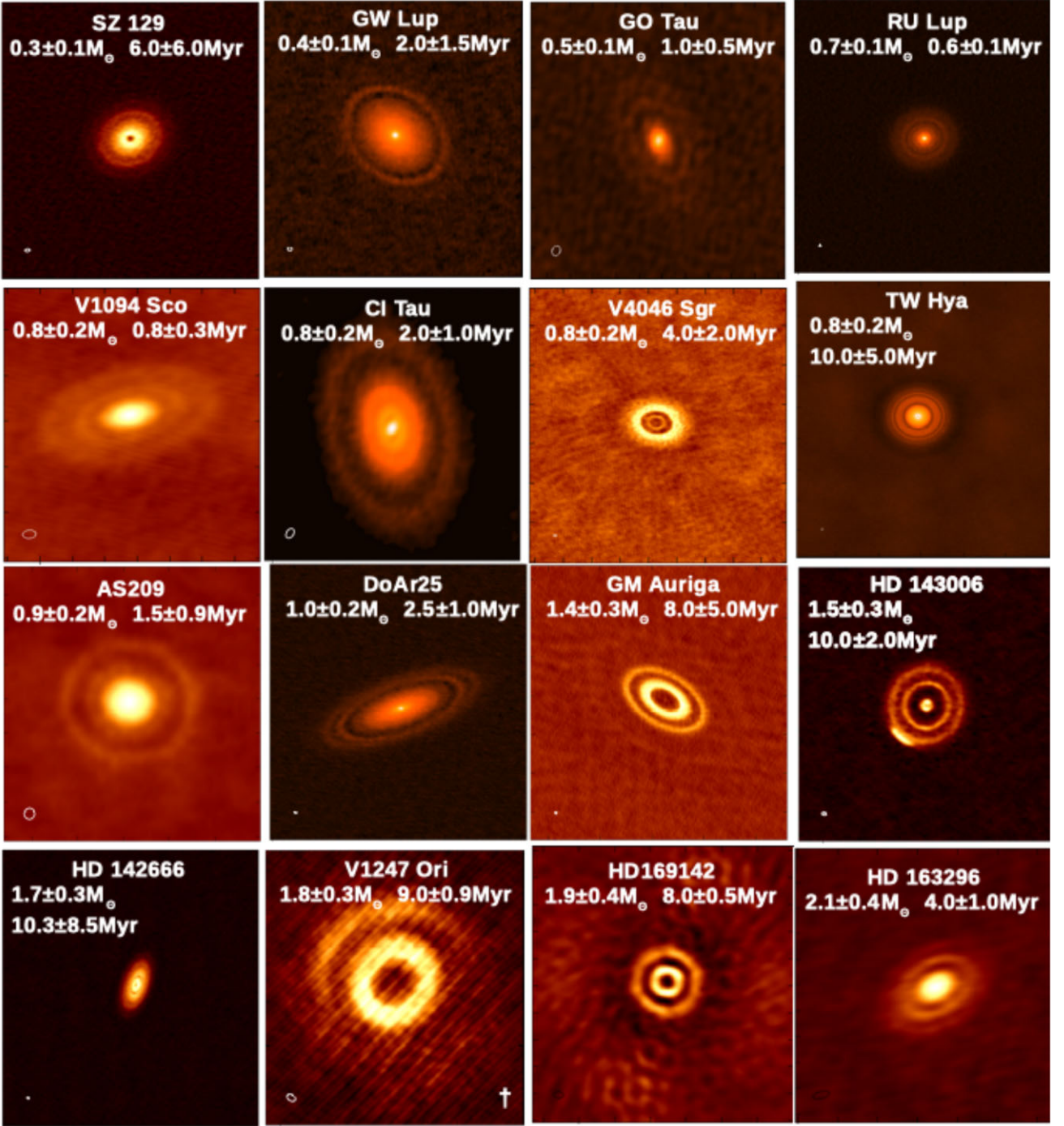
Figure C6. The Ring protoplanetary discs have been ordered according to stellar mass. SZ 129 has the lowest stellar mass of $M_* = 0.3 M_\odot$, while HD163296 has a stellar mass of $M_* = 2.1_\odot$. All discs have been scaled to 500×500 au. The discs with the † in the lower right have been scaled to 1000×1000 au.

Figure C7. The Horseshoe protoplanetary discs have been ordered according to stellar mass. SAO206462 has the lowest stellar mass of $M_* = 1.5M_\odot$, while AB Auriga has a stellar mass of $M_* = 2.7_\odot$. The discs with the † in the lower right have been scaled to 1000×1000 au.

Figure C8. The Spiral protoplanetary discs have been ordered according to stellar mass. Elias 2-27 has the lowest stellar mass of $M_* = 0.5$ $M_\odot$, while J16152023 has a stellar mass of $M_* = 1.0_\odot$. The discs have been scaled to 500×500 au.

This paper has been typeset from a TEX/LATEX file prepared by the author.